BIOENGINEERING A THREE-DIMENSIONAL CARDIAC LEFT VENTRICLE

A Dissertation

Presented to

the Faculty of the Department of Biomedical Engineering

University of Houston

In Partial Fulfillment

of the Requirements for the Degree

Doctor of Philosophy

in Biomedical Engineering

by

Nikita M. Patel

May 2015

BIOENGINEERING A THREE-DIMENSIONAL CARDIAC LEFT VENTRICLE

_____

(Nikita M. Patel)

Approved:

_____

Chair of the Committee
Dr. Ravi K. Birla, Associate Professor,
Department of Biomedical Engineering

Committee Members:

_____

Dr. Yu Liu, Assistant Professor,
Department of Biology and Biochemistry

_____

Dr. Elebeoba E. May, Associate Professor, Department of Biomedical Engineering

_____

Dr. Bradley K. McConnell, Associate Professor of Pharmacology, Department of Pharmacological and Pharmaceutical Sciences

_____

Dr. Ahmet Omurtag, Associate Professor, Department of Biomedical Engineering

_____

Dr. Suresh K. Khator,
Associate Dean,
Cullen College of Engineering

_____

Dr. Metin Akay, Founding Chair,
John S. Dunn Cullen Endowed Professor,
Department of Biomedical Engineering

ACKNOWLEDGEMENTS

I would like to express my appreciation and thanks to my advisor Professor Dr. Ravi Birla, you have been a tremendous mentor to me. I would like to thank you for encouraging my research and for allowing me to grow as a research scientist. Your advice on both research, as well as on my career, have been invaluable. I would like to thank Dr. Yu Liu, Dr. Elebeoba May, Dr. Bradley McConnell, and Dr. Ahmet Omurtag for serving as my committee members. I want to thank you for making my defense an enjoyable experience, and for your insightful comments and suggestions. I would especially like to thank my lab colleagues. It has been a pleasure to work with you and learn from you.

A special thanks to my family. Words cannot express how grateful I am to my mother, father, and brother for their unwavering guidance, support and encouragement; I dedicate my dissertation work to you. My success and achievement is our success and achievement. I would also like to thank all of my friends for their support throughout my PhD.

BIOENGINEERING A THREE-DIMENSIONAL CARDIAC LEFT VENTRICLE

An Abstract

Of a

Dissertation

Presented to

the Faculty of the Department of Biomedical Engineering

University of Houston

In Partial Fulfillment

of the Requirements for the Degree

Doctor of Philosophy

in Biomedical Engineering

by

Nikita M. Patel

May 2015

ABSTRACT

Hypoplastic left heart syndrome (HLHS) is a congenital condition characterized by an underdeveloped left ventricle (LV). The current treatment options are surgery and/or heart transplant. Current tissue engineering strategies focus on graft models. The development of an engineered 3D cardiac LV would provide a therapeutic option to overcome current treatment limitations. A series of five models, to understand the ideal LV platform, fabricate and optimize a bioengineered open ventricle chamber and complete the chamber with a trileaflet valve, were produced in this research. Models were designed to emulate the human neonate LV geometry; molds were used to produce chitosan scaffolds. Functional models were fabricated by culturing rat neonatal primary cardiac cells on the chitosan scaffold. Chitosan was shown to be biocompatible with suitable material properties. An open chamber model was designed and optimized with respect to cellularization efficiency and function, using a novel seeding strategy and bioreactor, respectively; cellularized constructs demonstrated cardiac myocyte biopotential activity with contractions and pressure generation. Trileaflet valves were engineered and fitted into the open chamber to complete the bioengineered ventricle. The outcome of this research is the production of a complete bioengineered 3D cardiac LV.

TABLE OF CONTENTS

LIST OF FIGURES

LIST OF TABLES

CHAPTER 1

INTRODUCTION

Tissue engineering is defined as an interdisciplinary field of research, aimed at developing three-dimensional bioartificial tissues and organs, to augment, repair or replace damaged or diseased tissues and organs [1, 2]. The processes involved in tissue engineering may be organized into eight categories: cell sourcing, biomaterial synthesis, genetic manipulation, cellularization, embedded sensors, vascularization and *in vivo* assessment [2]. These fundamental processes can be applied in any sequence to engineer any mammalian tissue. The focus of this research is cardiovascular tissue engineering; more specifically, the development of a three-dimensional bioengineered cardiac left ventricle.

1.1 Tissue Engineering

1.1.1 What is Tissue Engineering?

Tissue engineering utilizes cellular, biomaterial and bioreactor components for the development of three-dimensional (3D) bioartificial tissues [2]. There are eight fundamentals processes involved in the fabrication of an artificial tissue; these are discussed in this section.

The sourcing of cells provides the functional component of the tissue; options include animal cell lines and stem cells. Biomaterials provide the 3D structural support platforms and replicate the role of extracellular matrix (ECM) during culture. Biomaterials may be natural (e.g., decellularized ECM), polymeric, metal or ceramic. The genetic composition of cells may be adapted prior to scaffold cellularization to improve cell

function and/or survival, or to eliminate/augment a particular component for analysis. Scaffold cellularization is the process by which cells are seeded and cultured in a 3D environment; cell seeding is pivotal in 3D tissue engineered constructs, as efficient cellularization supports tissue formation and the longevity of the bioartificial tissue. In order to monitor cell behaviours, tissue development and maturation during fabrication, sensors may be used. Bioreactors are developed to simulate the *in vivo* environment *in vitro*, exposing the tissue to numerous physiological stimuli, including chemical, electrical, mechanical and fluid stresses; this facilitates the maturation of the bioartificial tissue. The incorporation of blood vessels, through artificial vessels or neovascularization is essential in any 3D tissue, to ensure oxygen and nutrient delivery, and support metabolic activity. *In vivo* assessment of the bioartificial tissue determines its potential to repair and/or replace damaged and diseased tissue; it is the precursor to clinical application [2].

1.1.2 Seminal Papers in Tissue Engineering

Two papers published by Dr Robert Langer have been considered seminal in the field of tissue engineering. They have served to establish the foundation principles of scaffold synthesis and cellularization, as well as bringing recognition to the present role of tissue engineering and its future application.

The first paper described the culture of primary hepatocytes in 3D polymeric matrices, composed of polyglactin, polyorthoesters or polyanhydride; matrices were fabricated using solvent casting, compression molding and filament drawing. Cells were plated onto the polymeric matrix, cultured in an incubated environment for three to four days and the construct was implanted *in vivo*. The outcome analysis showed cell engraftment into polymeric scaffolds during *in vitro* culture and cell survival on implantation *in vivo* [3].

The second seminal work is a review of tissue engineering. The work provides a current overview of the field and in addition, describes and envisions the potential future impact of tissue engineering. Within this work, Langer et al., [1] provide one of the most widely accepted definitions describing tissue engineering "*Tissue Engineering is an interdisciplinary field that applies the principles of engineering and the life sciences toward the development of biological substitutes that restore, maintain, or improve tissue formation"*[1]. The authours went on to outline the application of tissue engineering in different systems, such as cartilage, bone and skin [1].

Collectively, these seminal works defined tissue engineering, providing the foundation principles for the field. They outlined the potential clinical applications of tissue engineered technologies.

1.1.3 Applications of Tissue Engineering

Bioengineered 3D artificial tissues have numerous applications, from being *in vitro* models to clinical applications. The use of tissue engineered constructs as basic research models allows for the development of knowledge relating to cell biology; cell-cell and cell-matrix interaction processes. Additionally, 3D tissue engineered models allow for more accurate modelling of outcomes in simulated environments; the 3D aspect better replicates a physiological tissue to provide comparative models to develop an understanding of the environment on tissues. Similarly, one of the most promising *in vitro* applications of tissue engineering is in high-throughput screening for pharmacological assays; as above, the 3D structure provides a more accurate and comparable physiologically intermediate simulative model between two-dimensional and *in vivo* testing. As a result, the need to utilize animal models and the number of animal models may be significantly reduced.

Long term, the ideal application of tissue engineering is in a clinical setting. Currently, examples of tissue engineering in clinical settings include dental implants and wound dressings. Cardiac tissue engineering represents a future prospective application of tissue engineering, both in the short and long term; this area of tissue engineering is discussed further, with regards to the context of the current statistics in cardiac disorders and the applicability of cardiac tissue engineering.

Annually, millions of Americans experience cardiovascular conditions resulting in tissue loss and/or end-stage organ failure [4]. As a result, over five million in-patient surgeries are performed [5]; the typical treatment options for tissue loss and/or organ failure include the implantation of mechanical assist devices, such as left ventricular assist devices (LVADs), or heart transplant. These therapies improve the prognoses and quality of life for many patients however, they remain insufficient long-term solutions. Mechanical assist devices cannot completely recreate the function of a tissue or organ, with diminishing functional efficiency over time. Additional limitations include biocompatibility, thrombogenicity and risk of infection. Heart transplant is considered the "gold standard" of treatment in many cases, but organ donor availability is severely limited; in 2014, in the U.S., approximately 2700 heart transplants were carried out and almost 4000 patients still remain on the waiting list, with waiting times of at least several months [6].

Short term, tissue engineering could be applied as an interface between the tissue and mechanical device both to anchor the device and promote functional coupling, as well as to alleviate immediate limitations including infection risk, biocompatibility and thrombogenicity. Long term, the ideal would be to produce bioengineered tissue to supersede LVADs and reduce the need for transplantation.

1.2 The Heart

The heart is a muscular organ, located in the middle of the central thoracic cavity, or mediastinum, of the chest. It is enclosed in a protective fluid filled sac; the pericardium. The heart is composed of four chambers; the upper left and right atria and the lower left and right ventricles. The right atria and ventricle constitute the right heart, and the left atria and ventricle constitute the left heart. Heart valves between chambers and in vessels ensure the one-way flow of blood. The wall of the heart is composed of the epicardium, myocardium and endocardium layers [7]. The heart pumps blood through both circulatory systems to provide the body with oxygen and nutrients, as well as removing metabolic waste products.

Figure 1.1 represents the passage of blood flow through the heart.

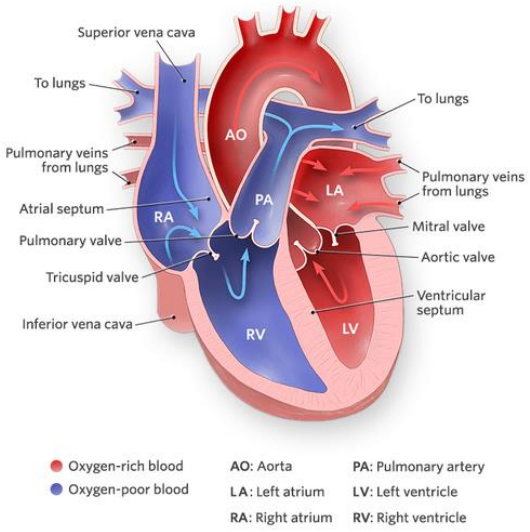

Figure 1.1: Healthy Human Heart [8]

The systemic circulation returns deoxygenated blood to the heart. De-oxygenated blood enters the right atrium from the superior and inferior vena cava, passes in the right ventricle and moves to the lungs via the pulmonary circulation, for oxygenation. Oxygenated blood is returned to left atrium, passes into the left ventricle and is pumped

out into the systemic circulation via the aorta. The volume of blood pumped from the right ventricle into the lungs is equal to that pumped out to the body by the left ventricle, for each heartbeat; at rest, the average heartbeat is 72 beats per minute (bpm). Venous blood flow is at a low pressure, compared to arterial blood flow; veins carry blood back to the heart and arteries carry blood from the heart [9].

1.2.1 Embryonic Development

Within three weeks of embryogenesis, the heart starts to beat and pump blood; it is the first functional organ to develop. The initial heart beat begins at 22days in embryogenesis, at a rate of approximately 75 to 80bpm, or equivalent to the mother's heart rate. The embryonic heart rate accelerates by approximately 10bpm every three days, for an increase in heart rate of up to 100bpm, to a peak of 165-185bpm by week seven. The heart rate decelerates at the foetal stage, after week nine, for a birth heart rate of approximately 145bpm [10].

The heart is derived from the splitting of the embryo mesodermal layer in the neural plate to form the cardiogenic region. The tubular heart is formed here; two endocardial tubes to form a primitive heart tube. The tubular heart differentiates into five regions; the truncus arteriosus divides to form the pulmonary artery and aorta; the bulbus cordis develops into the right ventricle; the primitive LV forms the LV; the primitive atrium becomes the front of the left and right atria and their appendages; the sinus venosus develops into the posterior part of the right atrium, the sinoatrial node and the coronary sinus.

During the initial stages of development, all venous blood flows into the sinus venosus with contractions propelling blood to the truncus arteriosus. At weeks three to four, the tubular heart lengthens and then folds into an S-shape within the pericardium; this ensures the correct alignment of the heart chambers and vessels for development.

The heart continues to develop with the formation of septa, and valves and chambers are remodelled; at week five, the septa are complete, and at week nine, the heart valves are complete [11].

1.2.2 Structure

An adult heart has a mass of 250-350g and is typically the size of a fist; 12cm long, 8cm wide and 6cm thick [12]. The heart is situated in the mediastinum, in the chest, behind the breastbone; the largest part of the heart is typically offset to the left. As such, the left lung is smaller to accommodate the heart. The heart has a broad base that tapers to the apex. The base is the upper surface of the heart, wherein the vena cavae, aorta and pulmonary trunk are attached. The apex is the lower tip of the heart and is located to the left of the sternum. The heart is oriented right side forwards and left side backwards.

1.2.2.1 Chambers

The atria are the receiving chambers of the heart; they are separated by the interatrial septum. The atria are connected to the ventricles by the atrioventricular valves; they are separated from the ventricles by the coronary sulcus, which contains the trunks of the nutrient delivery vessels of the heart. The right atrium receives deoxygenated blood from the body and the left atrium receives oxygenated blood from the lungs. Contraction of the atria pushes the blood into the ventricles.

The ventricles are the discharging chambers of the heart; they are separated by the interventricular septum. The interventricular septum is thicker than the interatrial septum, as the ventricles generate greater pressure on contraction. The choridae tendinae are anchored in the ventricles and attach to the cusps of the atrioventricular valve.

The underlying structure of the heart is composed of dense collagen; it acts as a

skeleton to maintain the shape of the heart. Additionally, it forms the atrioventricular septum to separate the left and right heart, as well as the fibrous valve ring bases.

1.2.2.2 Valves

Valves ensure unidirectional blood flow in the heart, and prevent backflow. There are four valves in the heart (**Figure 1.2**); these valves lie along the same plane. The atrioventricular valves are the tricuspid and mitral valves; the aortic and pulmonary valves are present at the base of the major vessels of the heart [11].

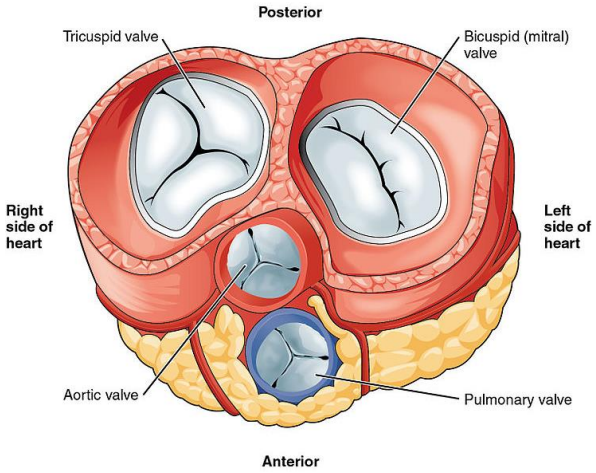

Figure 1.2: Healthy Human Heart Valves [11]

The tricuspid valve is situated between the right atrium and the right ventricle; blood flows through the valve from the right atrium into the right ventricle. The three cusps or leaflets of the tricuspid valves are composed of endocardium, with additional connective tissue. Cusps are connected to the papillary muscle, which emanates from the lower ventricle surface, by the choridae tendinae. The choridae tendinae are fibres composed predominantly of collagen, with elastic fibres and endothelium, which are connect to leaflets and papillary muscle. Papillary muscles control the opening and closing of valves; the anterior, posterior and septal muscles correspond to the three positions of the valve leaflets.

The mitral valve is situated between the left atrium and ventricle. It is a bicuspid valve, with only two leaflets; the anterior and posterior. As per the tricuspid valves, the two cusps are attached to two papillary muscles projecting from the ventricle wall, via the choridae tendinae.

During the relaxation phase of the cardiac cycle, papillary muscles are relaxed with minimal tension on the choridae tendinae. On ventricular contraction, papillary muscles contract applying tension to the choridae tendinae. As a result, the atrioventricular valve cusps remain in place, as opposed to being pushed back into the atria, by the pressure generated on ventricular contraction.

The pulmonary and aortic valves, or the semilunar valves, are not attached to choridae tendinae; both valves have three cusps. The pulmonary valves close on ventricle relaxation, to seal the pulmonary artery from the right ventricle, thus preventing back flow. Similarly, the aortic valve closes to the pressure generated by ventricular contraction to ensure unidirectional blood flow.

1.2.2.3 The Right Heart

The right heart consists of the right atrium and ventricle. The right atrium collects deoxygenated blood from the body, pumping it through to the pulmonary circulation via the right ventricle and pulmonary artery; carbon dioxide and oxygen exchange occurs by passive diffusion in the lungs.

The atrium receives continuous venous blood flow from the superior (above the diaphragm) and inferior (below the diaphragm) vena cavae. Atrial relaxation allows for blood flow through the tricuspid valve for ventricular filling. The atria contracts immediately prior to ventricular contraction.

Ventricular contraction ejects blood via the pulmonary trunk into the left and right pulmonary arteries. Concurrent papillary muscle contraction occurs, to close the

tricuspid valve and prevent backflow into the atrium. The pulmonary trunk valve prevents backflow on ventricular relaxation. The thin walls of the right ventricle are lined with ridges of cardiac muscle and a band of cardiac muscle for structural reinforcement and cardiac conduction, respectively.

1.2.2.4 The Left Heart

The left heart consists of the left atrium and ventricle. The pulmonary veins return oxygenated blood to the left atrium, wherein it is pumped into the systemic circulation via the LV and aorta. Systemic capillaries are present throughout the body and deliver oxygen and nutrients to tissues and cells; oxygen and nutrients are taken up for utilization in cellular metabolic processes, and carbon dioxide and waste products enter the blood.

Oxygenated blood flows passively from the pulmonary veins into the left atrium, through the mitral valve and into the LV during atrial and ventricular relaxation. At the end of the ventricular relaxation phase of the cardiac cycle, the left atrium contracts to further fill the ventricle. The volume of blood pumped by the left and right ventricles is the equal however the LV wall is thicker, as a greater force needs to be generated for systemic circulation through the aorta. As per the right ventricle, the LV is composed of ridges of cardiac muscle in the ventricle wall however there is no cardiac muscle band.

1.2.2.5 Heart Wall Layers

The pericardium is the membrane that surrounds the heart. It is a two layered membrane; the outer layer is composed of dense fibrous connective tissue for protection, and the second layer reduces contraction friction through pericardial fluid secretion and enables the heart to respond to lung and diaphragm movement [13]. Within and on the surface of the heart, fissures are observable; these grooves accommodate blood vessels and separate the ventricle. The heart wall is composed of three layers;

the epicardium, myocardium and endocardium [11]. The pericardial and heart wall layers are shown in **Figure 1.3**.

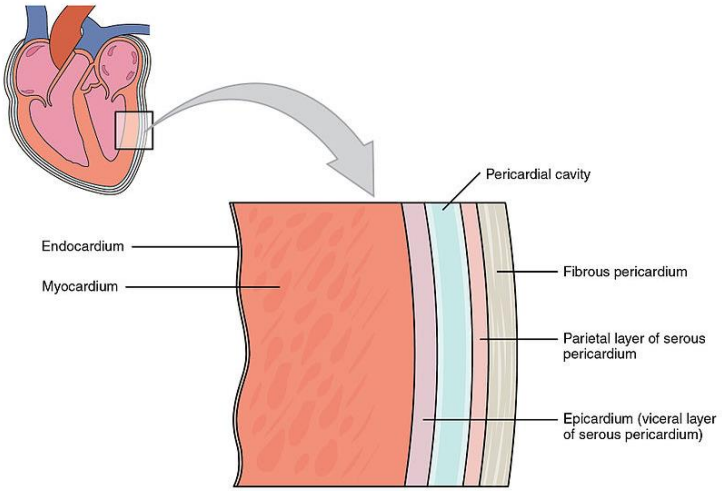

Figure 1.3: Pericardial and Heart Wall Layers [11]

The epicardium is the outermost layer of the heart wall. It is the inner visceral pericardium, and is fused to the heart. The pericardial cavity lies between the epicardium and pericardium; pericardial fluid is present in this cavity.

The myocardium is the middle layer of the heart wall; it is the thickest layer and is largely composed of cardiac cells. The underlying structure of the myocardium includes collagen fibres, blood vessels and nerve fibres for regulation. Myocardial contraction mediates the pumping of blood through the heart and into the arteries. The arrangement of the myocardium is unique; it spirals around the chambers of the heart as shown in **Figure 1.4**. The spiral pattern ensures more efficient pumping of the blood compared to a linear muscle arrangement. The muscle pattern is organized in a figure eight configuration around each atrium and within the deeper muscles of each ventricle, proceeding towards the apex; superficial muscle layers wrap around both ventricles.

The endocardium is the innermost layer of the heart wall; it lines the heart chambers and valves. It is linked to the myocardium by a thin layer of connective tissue. It is

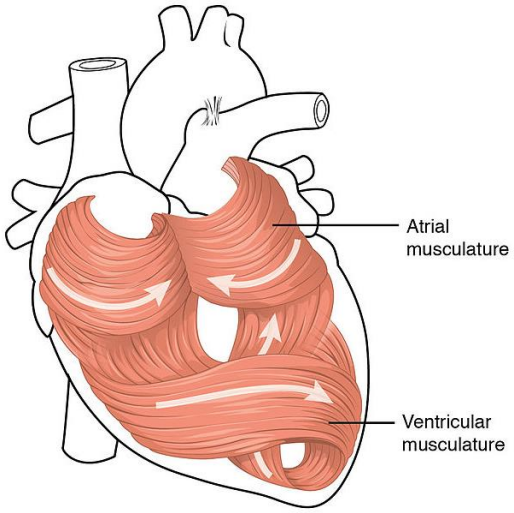

Figure 1.4: Myocardium Arrangement in the Heart [11]

composed of endothelium, which regulates the growth of cardiac muscle cells and secretes endothelins to regulate contractility.

1.2.3 Physiology

Cardiac physiology refers to understanding heart function. Heart function involves blood flow, cardiac muscle, membrane potentials and ion movement in cardiac cells and the cardiac cycle.

1.2.3.1 Blood Flow

The function of the heart is to act as a pump, to circulate blood throughout the body; the pulmonary circulation oxygenates blood in the lungs and the systemic circulation transports oxygenated blood around the body, to deliver oxygen and nutrients to tissues and cells. Blood flow is unidirectional, as mediated by the presence of vales, flowing from the atria to the ventricles and into the arteries. The right heart is responsible for the pulmonary circulation and the left heart is responsible for systemic circulation.

1.2.3.2 Cardiac Muscle

Cardiac muscle tissue initiates cardiac action potentials at a fixed rate, for rapid impulse propagation from cell to cell, triggering contraction of the heart. This autorhytmicity is modulated by the nervous and endocrine systems. Cardiac muscle is composed of two cell types; contractile cardiac myocytes and conductive pacemaker cells. Approximately 99% of atrial and ventricular cells are cardiac myocytes; these cells have a single nucleus and mediate heart contraction in response to pacemaker cell action potential impulses [11]. Pacemaker cells constitute the remainder of cells and function as the conduction system of the heart.

Myofibrils and myofilaments are organized and arranged in the sarcomere along the length of the cardiac myocyte cells, as shown in **Figure 1.5**; as a result, cardiac muscle appears striated. On action potential initiation of contraction, the cardiomyocyte sarcoplasmic reticulum releases calcium ions, to initiate the sliding of actin and myosin fibrils to potentiate contraction.

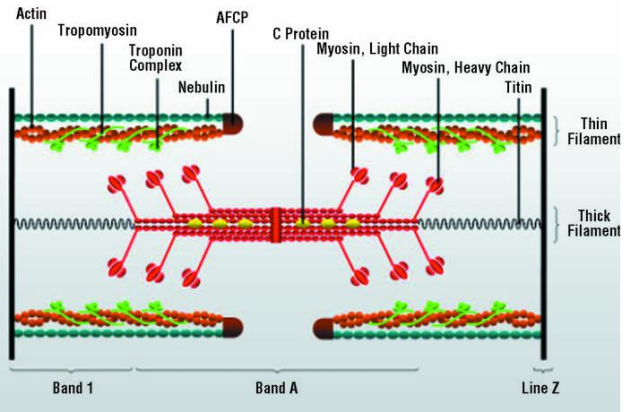

Figure 1.5: Cardiac Sarcomere Structure [14]

Muscle contraction is synchronized through the branching of cardiac myocytes to form intercalated disc connection junctions (**Figure 1.6**). Adjacent cells bind together at intercalated discs via adjoining cell membranes. Intercalated discs consist of

desmosomes, specialized proteoglycans, tight and gap junctions; these allow ion passage to facilitate the synchronization of contraction. Cardiac myocytes undergo twitch-type contractions; the associated refractive period is lengthy, with a brief relaxation period during heart filling for the next cardiac cycle [14].

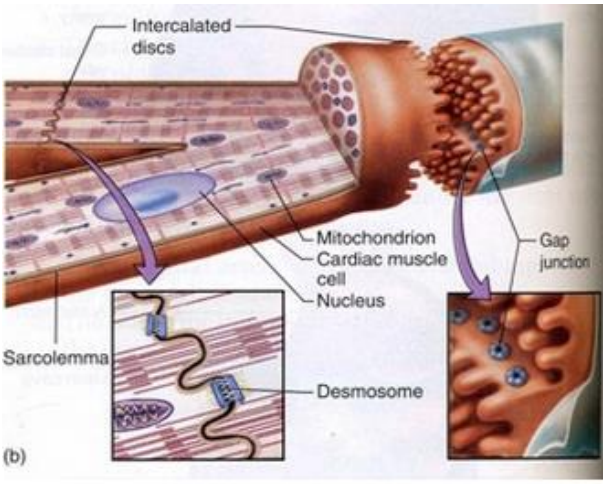

Figure 1.6: Cardiac Myocytes and Intercalated Discs [15]

1.2.3.3 Membrane Potentials

The resting potential of cardiac conductive pacemaker cells is not stable. Pacemaker cells contain sodium ion channels; sodium influx into the cell is slow, causing the membrane potential to rise slowly from -60mV (millivolts) to -40mV, to initiate spontaneous depolarization. Further rapid depolarization occurs due to the concurrent influx of calcium ions through open calcium channels; the final depolarization value reaches approximately +5mV. This maximum initiates repolarization; calcium channels close, and potassium ions are effluxed through potassium channels to return the membrane potential to -60mV. At -60mV, potassium channels close and sodium channels reopen to repeat the process. This process constitutes the autorhythmicity of cardiac muscle [16].

The entire action potential process lasts 250 to 350msecs (milliseconds) in cardiomyocytes. The components of the action potential are very similar to that of the pacemaker cells; there is rapid depolarization, a plateau phase and repolarization. The resting potential of cardiomyocytes is stable; -80mV in the atria and -90mV in the ventricles. Rapid depolarization occurs to produce a membrane potential of +30mV within 3-5msecs. The plateau phase accounts for the long refractory period associated with cardiac myocytes; slow calcium channels and few potassium channels are open to moderate ion efflux rates. The plateau phase lasts 175msecs. At 0mV, repolarization to the resting state is quicker, at 75msecs. The extended refractory periods in cardiac myocytes prevents premature heart contractions [16].

Calcium ions ensure the proper function of the myocardium, through two roles. In contractile myocytes, calcium ions influx through slow calcium channels to produce the plateau phase and long refractory period, regulating cardiac contractions. Additionally, calcium ions form a complex with the regulatory protein troponin, to trigger cardiac muscle contraction.

Troponin is a component of filaments consisting of actin and tropomyosin. It is attached to the protein, tropomyosin, which is situated in the groove between actin filaments in the muscle tissue. In the relaxation phase, contraction is prevented as tropomyosin blocks the myosin cross-bridge attachment site. On action potential stimulation and calcium ion influx, calcium binds to troponin to induce a conformational change, exposing the myosin binding sites on actin filaments; myosin binds actin for cross-bridge formation and contraction. Troponin is a complex of three regulatory proteins; troponin C (TnC), troponin T (TnT) and troponin I (TnI). TnC has three calcium binding sites in cardiac muscle, and on binding with calcium ions, induces a conformational change in TnI. TnT binds tropomyosin to form the troponin-tropomyosin

complex. TnI binds to actin in myofilaments, to hold the troponin-tropomyosin complex in place [17].

1.2.3.4 Cardiac Cycles

Initially, both the atria and ventricles are in diastole, a relaxed state; blood flows into the right atrium from the vena cavae and into the left atrium from the pulmonary veins. The atrioventricular valves are open, therefore, blood flows through the atria into the ventricles; the pulmonary and aortic valves are closed to prevent backflow into the right and left ventricles, respectively. The electrocardiogram (ECG) phases corresponding to the phases of the cardiac cycle are shown in **Figure 1.7**.

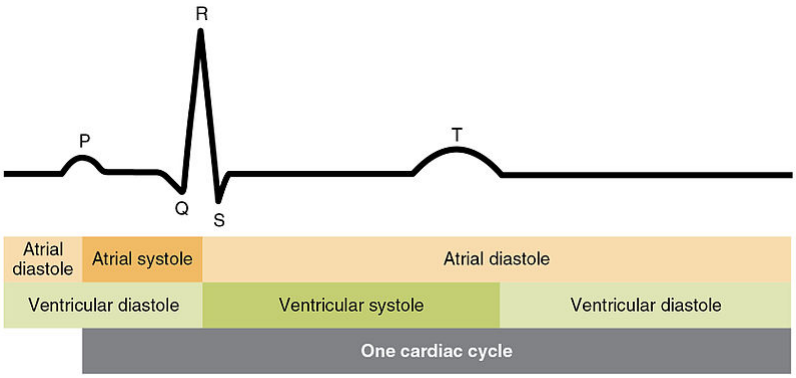

Figure 1.7: ECG and the Cardiac Cycle [11]

Depolarization occurs in cardiomyocytes, resulting in atrial contraction, or systole (P wave in ECG). Systole increases atrial pressure and blood is pumped into the ventricles through the open atrioventricular valve; it accounts for 20-30% of ventricular filling. The atrial muscle returns to diastole prior to ventricular systole [11].

Ventricular systole (QRS complex in ECG) can be divided into two phases; isovolumetric contraction and the ventricular ejection phase. Isovolumetric contraction refers to the initial stages of ventricular contraction; pressure in the ventricle rises to close in tricuspid and mitral valves, however blood is not ejected. Blood is pumped from

the heart during the ventricular ejection phase, as ventricular contraction generates pressures greater than that in the aorta and pulmonary trunk. The same volume of blood is ejected from both ventricles; the LV generates a greater pressure. The end diastolic volume refers to the volume of blood remaining in the ventricle following contraction [11].

Ventricular diastole (T wave of ECG) occurs in two phases; isovolumetric relaxation and late ventricular diastole. Isovolumetric ventricular relaxation is early phase diastole, wherein chamber pressure drops causing pulmonary and aortic valves to close, whilst the atrioventricular valves remain closed. In late ventricular diastole, the pressure continues to drop, allowing the atrioventricular valves to open and blood to flow through from the atria. Both chambers return to diastole, with the atrioventricular valves open and the pulmonary and aortic valves closed; the cardiac cycle is completed [11].

1.3 Congenital Heart Defects

Congenital heart defects (CHDs) develop *in utero* and are present at birth. CHDs affect the structure and function of the heart; they are the most common type of birth defect. CHDs can be categorized, ranging from mild (e.g., septal defects) to severe (e.g., missing/underdeveloped components of the heart). In the U.S., CHDs have a prevalence of approximately 1%, and occur in 47,000 births per year [18]. Critical CHDs account for 25% of all CHD cases; critical CHDs are conditions requiring surgical procedures within the first year of life [19]. Ventricular septal defects are the most commonly observed CHD [20].

CHDs are one of the foremost birth-defect associated causes of infant illness and mortality; from 2003-2006, 4.2% of all neonatal deaths (deaths within the first 28days of birth), were due to CHDs [20]. Infant survival is dependent on CHD severity, diagnosis and treatment. Survival to one year of age is 97% and 75% in non-critical and critical

CHDs, respectively; expected survival to 18years of age is 95% and 69% [20]. The complexity of CHD is dependent on the presence and severity of concurrent conditions; over 15% of CHDs are associated with genetic disorders [21] and 20-30% of patients with CHDs have physical, developmental and cognitive disorders [22].

In 2004, the hospital costs associated with CHD care in the U.S., approximated $1.4billion; severe CHD cases accounted for $511million, or 37% of the total cost of care. The estimated private cost of care in the U.S., for an infant (from age one month to 12months) with any CHD, was approximated to be $23,000; the cost associated with severe CHDs was higher [23].

1.4 Hypoplastic Left Heart Syndrome

Hypoplastic left heart syndrome (HLHS) is a critical CHD affecting the normal flow of blood through the heart. The left side of the heart does not develop and form completely, *in utero*; sections of the foetal heart are abnormally underdeveloped during the first eight weeks of pregnancy [24]. Numerous structures in the left heart are affected.

1.4.1 Epidemiology

The cause of HLHS is unknown however it is postulated to be caused by genetic or chromosomal defects, as per other CHDs. HLHS affects two to three of all 10,000 live births in the U.S. and accounts for two to three percent of all CHDs; it is the most common form of functional single ventricle heart disease [24]. HLHS has a low incidence, however if left untreated, it accounts for 25-40% of all neonatal cardiac deaths [25].

1.4.2 Anatomy

In HLHS, multiple structures in the left heart are small and underdeveloped, as shown in **Figure 1.8**. The LV cavity is very small, with thickening of the endocardium. The mitral valve is atretic (closed), hypoplastic (small) or stenotic (narrowed); the

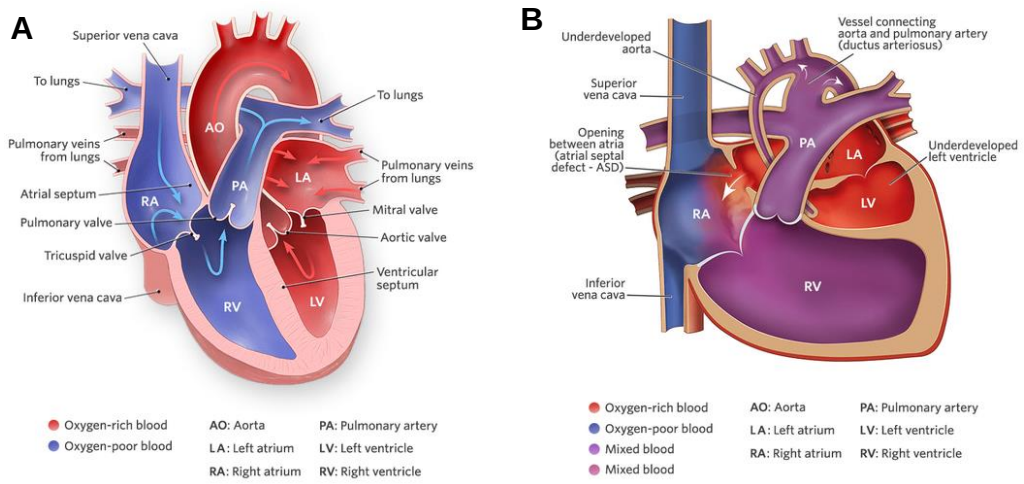

Figure 1.8: Cardiac Anatomy of **A:** Normal Heart and **B:** HLHS [8]

valves are thick and rigid, as opposed to thin and flexible. Additionally, the valve annulus, leaflets, papillary muscle and choridae tendinae are underdeveloped. The aortic valve is atretic or stenotic; the aorta itself is severely hypoplastic with a diameter of two to three millimetres as opposed to three centimetres [26]. During pregnancy, the patent ductus arteriosus, the blood vessel connecting the aorta and the pulmonary artery and the patent foramen ovale, the opening between the left and right upper chambers of the heart, are present; in the normal heart, these structures close shortly after birth. In HLHS, these do not close, resulting in the aorta and pulmonary artery remaining connected after birth and the presence of an atrial septal defect.

1.4.3 Pathophysiology

In HLHS, the left side of the heart cannot properly pump oxygen rich blood to the body. The outcome varies in severity, based on three major factors; interatrial adequacy, the open or closed state of the ductus arteriosus and the level of pulmonary vascular resistance. **Figure 1.8** indicates the pathophysiological impact of each of these factors.

Oxygenated blood is returned to the left atrium, however in cannot pass through the LV due to mitral valve atresia or stenosis. As the patent foramen ovale remains present after birth, the oxygenated blood flow is redirected across the atrial septum and into the right atrium. In the right atrium, oxygenated blood mixes with deoxygenated blood [27].

The right heart pumps blood to both the lungs and the body. The mixed oxygenated and deoxygenated blood in the right atrium passes into the right ventricle, and is pumped into both the pulmonary and systemic circulation. Blood exits the right ventricle to the lungs via the pulmonary artery and to the body via the ductus arteriosus. The presence of the ductus arteriosus results in these circulations being connected in parallel, as opposed to in series. The volume of blood flowing into each circulation is dependent on the relative resistance [28].

In general, the relationship between resistance and blood flow is inversely proportional; as blood vessel resistance decreases, blood flow through the vessel increases. In HLHS, a balance must be maintained between the pulmonary and systemic circulations, to ensure adequate blood oxygenation and tissue perfusion. Typically in HLHS, after birth, the pulmonary vascular resistance decreases, thus a greater proportion blood output from the right ventricle is delivered to the lungs; systemic blood flow is decreased resulting in inadequate tissue perfusion. Additionally, myocardial and cerebral complications may occur due to lack of blood flow into the ductus arteriosus and aorta [29].

The combination of anatomy and pathophysiology in HLHS, leads to several presenting symptoms, observable 24-48hours after birth. Cyanosis, or bluing of the skin, occurs due to the mixing of oxygenated and deoxygenated blood. Breathing problems, pounding heart and weak pulse also occur as a result of underdevelopment of the left heart.

1.4.4 Current Treatments

There are currently two main options to treat HLHS; staged reconstruction surgery and heart transplant. Both options have associated benefits and risks. The treatment strategy utilized is case dependent.

1.4.4.1 Staged Reconstruction Surgery

The purpose of surgical reconstruction in HLHS, is to separate the systemic and pulmonary circulations; the heart functions as a one-sided pump, with two chambers. Deoxygenated blood no longer flows into the heart, but rather directly into the lungs. The right ventricle remains the systemic ventricle. This is called the Fontan circulation. Reconstruction is a three stage surgical process; the Norwood procedure (Stage I), the bidirectional Glenn or Hemi-Fontan procedure (Stage II) and the Fontan procedure (Stage III).

The Norwood procedure is carried out within the first few weeks of birth. The procedure is intended to ensure controlled blood flow, wherein damage to the heart and lungs is prevented; it establishes systemic circulation without the ductus arteriosus and ensures sufficient pulmonary blood flow for adequate blood oxygenation [30]. The outcome of the Norwood procedure is shown in **Figure 1.9**.

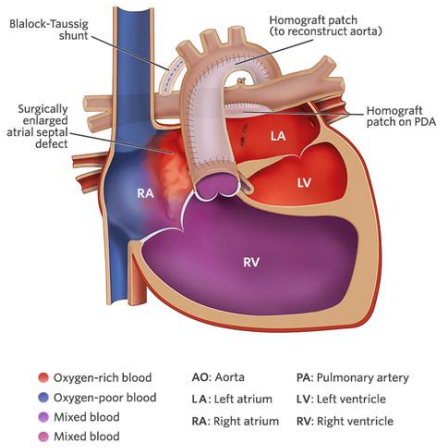

Figure 1.9: The Norwood Procedure [8]

The atrial septum is enlarged to allow unrestricted blood flow across the atria. The ductus arteriosus is closed off and a connection, or anastomosis, is created between the pulmonary artery and aorta, for systemic blood flow. The aorta is widened and an aorta-to-pulmonary artery shunt is placed to produce the pulmonary circulation. Without treatment, HLHS is fatal within the first two weeks of birth. The overall success rate of the Stage I procedure is approximately 75% [31].

The bidirectional Glenn procedure is performed approximately six months after Stage I surgery. The outcome of the procedure is shown in **Figure 1.10**.

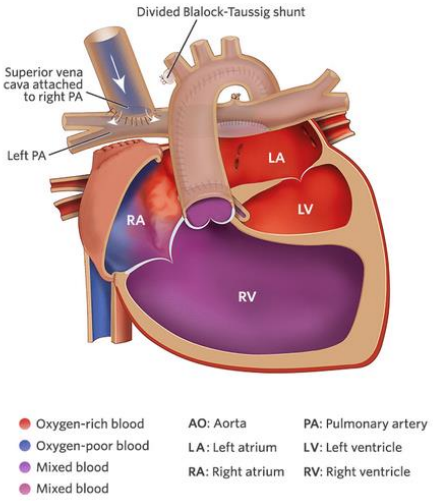

Figure 1.10: The Bidirectional Glenn Procedure [8]

An anastomosis is created between the superior vena cava and the right pulmonary artery, to allow blood returning from the upper body to flow directly into the lungs. The connection is configured with the end of the vena cava being attached to the side of the pulmonary artery. The prior junction, between the superior vena cava and the right atrium, is temporarily closed off until Stage III surgery. The shunt between the aorta and pulmonary artery, placed in Stage I surgery, is closed off. The right atrium continues to receive blood from the inferior vena cava. The overall success rate of Stage II surgery is approximately 95% [32].

The Fontan procedure is performed when the child is aged between one-and-a-half to three years or 12 months after Stage II surgery. The final outcome of staged reconstruction, to establish Fontan circulation is shown in **Figure 1.11**.

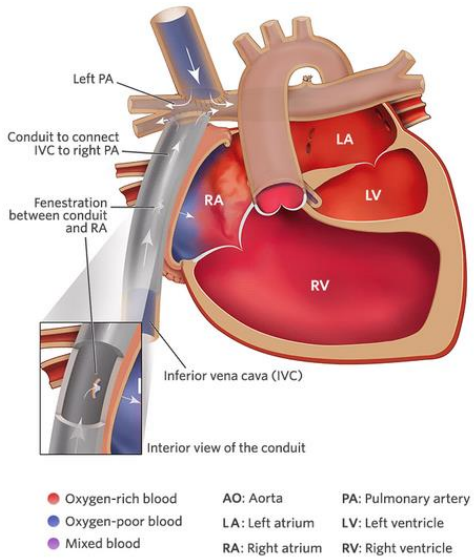

Figure 1.11: The Fontan Procedure [8]

The inferior vena cava is detached from the heart and attached to the right pulmonary artery, by means of extracardiac conduit. Blood flow from the systemic circulation is returned to the lungs passively, and no longer passes through the ventricle. The overall success rate of Stage III surgery is approximately 90% [32].

The survival rate five years after stage reconstruction surgery is 55% [32]. In the short-term, complications may occur with each stage of surgery. Stage I complications include blocking of the aorta and cyanosis due to limited blood flow through the fitted shunt. The potential complications of Stage II and III surgeries are predominantly excess fluid accumulation around the tissue lining of the lungs and chest and/or the heart. Long term care includes the numerous medications to maintain blood pressure and thin the blood, further corrective surgeries and catheter interventions following the initial three step staged reconstruction process [32].

1.4.4.2 Heart Transplant

Heart transplant is the alternative treatment option in HLHS; in cases where surgery proves ineffective, it remains the only viable treatment option. The time taken to find a suitable organ donor can be lengthy due to a shortage of donor organs, and during the waiting period, medications are required to keep the ductus arteriosus patent, or open. Almost 20% of infants listed for transplants die whilst waiting for a suitable donor organ [6]. On successful transplantation, long term immunosuppression therapy is required to prevent rejection. The five year survival rate following transplant is 70% [32].

1.4.5 Tissue Engineering

Current tissue engineering research in HLHS focusses on developing graft-type models, designed to be utilized as left ventricle augments, through redefinition of the myocardial wall, or septation of the single ventricle [33-39]. Only one complete LV model has been developed; it is a spherical Matrigel high-throughput screening model [40].

1.5 Motivation for the Work

Both current surgical treatment and tissue engineering research in HLHS do not repair, reconstruct or replace the underdeveloped left ventricle. Surgical staged reconstruction focusses on re-functionalizing the right ventricle. Transplant is a severely limited treatment option due to a chronic shortage of donor organs. Tissue engineered models are grafts, developed to for use as augments, as opposed to a functional LV chamber replacement; the singular existing 3D LV model, is designed for *in vitro* drug development screening.

The purpose of this work is to bioengineer a 3D cardiac LV. The tissue engineered ventricle may be used to either replace the underdeveloped LV, or as structural or reparative implant within the ventricle, around which the existing tissue may be remodelled. The concept and potential application of this work is completely novel, both

in HLHS and in the field of tissue engineering. In HLHS, this study provides an initial step towards the development of a less invasive and more efficient long term treatment. In the field of tissue engineering, it demonstrates progress towards the future of the field; the development of functional substitutes for damaged tissue, superseding the need for transplant [1].

1.6 Dissertation Overview

We hypothesize that we can bioengineer a 3D cardiac LV, as a replacement construct for use in HLHS. Initially, we will study the ideal system and explore the efficacy of culturing on an ideal platform, the LV ECM, in static culture conditions. We will design and engineer a closed LV model using biocompatible and biomimetic materials to reproduce the LV geometry. These constructs will be cellularized using a novel two-stage strategy and cultured in custom bioreactors. At each stage of model development, viability will be assessed through functional, electrical and histological characterization.

1.7 Summary

This chapter defines the key concepts of tissue engineering and provides an overview of the physiology and complexity of both the normal heart and in HLHS. It provides a reference with regards to the aim of this study and the considerations associated with bioengineering a 3D LV.

The proposed study addresses the gap in current HLHS treatment and research; the repair, reconstruction and/or replacement of the underdeveloped LV. In Chapter 2, we further review current tissue engineering strategies in HLHS and establish that bioengineering a three-dimensional LV is a novel concept.

CHAPTER 2

LITERATURE REVIEW

Surgical repair in HLHS is palliative. Heart transplant remains the gold standard of treatment however it is severely limited due to a chronic shortage of donor organs. Tissue engineering presents the potential to develop an alternative treatment for biological repair.

Current tissue engineering strategies in HLHS focus on the development of biocompatible, non-immune graft-type myocardial tissue augments, to emulate the morphological and functional properties of natural heart muscle. Technologies can be categorized into four sections; the bioengineering approach, the bioassembly approach the cell-sheet approach and the decellularization-recellularization approach [41]. This review serves to list examples of each of these technologies, and further review the most pertinent study within those fields.

2.1 The Bioengineering Approach

This approach involves cardiac cells being seeded on a preformed scaffold. Scaffolds are either chemically engineered or derived from biological sources. Constructs are cultured in a 3D format, following cell seeding.

2.1.1 Chemically Engineered Scaffolds

Chemically engineered cardiac tissue engineered scaffold materials include polylactic acid (PLA), polyglycolic acid (PGA) and polyglycerol sebacate (PGS) [42- 44].

Bursac et al., [42] studied the feasibility of PGA scaffolds, to produce artificial cardiac muscle, with physiologically simulative structural and electrophysiological properties.

Rat neonatal cardiac myocytes were isolated, passively seeded on a PGA scaffold, of mesh-like constitution and cultured with media mixing at 50 rotations per minute (rpm). It was observed that cardiac myocytes demonstrated cardiac tissue properties at the periphery of the construct, with cell differentiation and 3D attachment to the polymer and between cells. The constructs were reported to have electrophysiological activity however it was significantly lower than that of the native ventricle. Additionally, construct characterization showed diminished cell proliferation and, due to material thickness, the survival rate of cardiac myocytes was also low. The study establishes the development of specific cardiac features in an engineered 3D tissue; structural and electrophysiological function was observed.

The study discussed presents the application of a chemically engineered material scaffold in the development of a structurally and electrophysiologically simulative cardiac patch. It is intended for application as a myocardial augment in HLHS. The work provides a platform in understanding the complexities associated with cell culture and material properties to produce cardiac features, such as electrophysiological activity. However, the gap in knowledge that our work aims to address is the creation of a complete tissue engineered LV with regards to architecture, as opposed to a cardiac patch and with cell culture to elucidate electrophysiological properties, as a function of novel cellularization methods and geometric complexity. Additionally, to ensure future biocompatibility, our work focuses on the use of a naturally-derived polymeric scaffold material.

2.1.2 Biosourced Material Scaffolds

Cardiac tissue engineering scaffold materials derived from biological sources include alginates from seaweed, collagen from tendons, silk from silkworms and spiders and chitosan from crustacean exoskeletons and fungi cell walls [34, 45- 47].

Blan et al., [47] describe the evaluation of a porous chitosan polymer-based scaffold, as a feasible technology to engineer functional heart muscle *in vitro*. Scaffolds were produced at varying chitosan concentrations (0.5-3% in 0.5% increments) and thicknesses (200-1000µm in 200µm increments). Chitosan solutions were produced at the desired concentration in 1% glacial acetic acid, pre-frozen at -80°C and lyophilized. The porous lyophilized scaffolds were rehydrated prior to cellularization, to neutralize the acid. Scaffold material properties were assessed at different concentrations and thicknesses, to determine morphology, using scanning electron microscopy (SEM) and degradation kinetics. Rat neonatal cardiac myocytes were isolated and seeded, at varying densities, on rehydrated porous scaffolds using either direct cell injection (DCI) or fibrin gel; constructs were cultured for up to 11days. Cellularized constructs were evaluated for contractile function, using an optimized force transducer and histologically, using haematoxylin and eosin (H&Es) staining.

The optimal chitosan concentration to tissue engineer functional cardiac muscle was derived to be between 1-2.5%w/v. As a function of force and degradation kinetics, cell seeding densities of $1x10^6$ to $5x10^6$ cells per construct generated measurable force with favourable degradation kinetics. Active force increased to a peak over 8-11days, after which a decline was observed. The material degradation kinetics were shown to be controllable, to increase or decrease time to complete degradation. Constructs seeded using DCI elicited no measureable contraction, whereas those seeded with fibrin gel did; additionally, the fibrin acted as a scaffold support matrix.

This study provides a foundation for our research, with regards to the use of chitosan as a biologically sourced biomaterial scaffold and cell seeding strategies. It identifies initial biocompatibility and material properties which may be amenable to tissue

engineering cardiac constructs. However, the development of a complete 3D LV is not addressed in this work; the construct is a cuboid chitosan section.

2.1.3 Overview

All of the listed bioengineered cardiac tissue engineering models are focused on the development of 3D planar cardiac patches; the gap in current knowledge is identified to be the development of a 3D LV-shaped closed model. The proposed applications are as tissue augments, as opposed to replacement constructs. The predominant limitations associated with these bioengineered models include material thickness and relative oxygen and nutrient diffusion, as well as biocompatibility to support cardiac myocyte attachment, particularly in chemically engineered scaffolds. Additionally, in synthetic scaffolds, material degradation remains a limiting property. The model proposed by Blan et al., [47] provides a foundation for our work to develop a complete bioengineered 3D cardiac LV.

2.2 The Bioassembly Approach

This approach generates cardiac micro-tissues based on the inherent properties of cardiac myocytes when they are cultured at high seeding densities. Cells are suspended in casting molds, to define a 3D structure. The casts contain mixtures of ECM materials or naturally occurring products. Cardiac tissue formation can be guided using biophysical stimuli to produce optimized contracting heart equivalents.

2.2.1 ECM Materials

ECM materials used in casting molds to suspend cardiac cells include collagen, laminin, fibronectin and Matrigel [36, 40, 48, 49]. These materials are purported to provide 3D structural support whilst promoting the self-aggregation of cardiac myocytes.

Lee et al., [40] describe the development of a cardiac organoid; an autonomous living engineered cardiac tissue chamber. The work provides a step towards developing a "functional biological ventricle model" as a platform for *in vitro* studies and high-throughput screening applications.

An agarose cup-shaped cast was developed to create the outer wall of the organoid chamber and a silicone balloon catheter was inflated and positioned concentrically within the outer chamber, to produce the inner wall. Rat neonatal cardiac cells were mixed into a gel composed of collagen and Matrigel, at a ratio of 8:1:1, with the further addition of neonatal cardiac fibroblasts to promote gel compaction. The composite gel was loaded into the cast and incubated at 37°C and 5% carbon dioxide (CO_2) for two hours to initiate polymerization of the collagen gel. The outer cast was removed after 24hours and the gel structure was cultured for a further seven to ten days to allow for the contraction of the myocytes and fibroblast matrix remodelling. Pump function was evaluated by replacing the inner silicone balloon catheter with a modified Langendorff system. Residual stress was assessed using a cross-section of the organoid chamber. Acute myocardial infarction modelling potential of the organoid was assessed using an experimental cryoinjury technique.

The chambers produced were spherical with a spontaneous contraction rate of 180-300bpm. Histological analysis showed a cell structure resembling that of the early stages of cardiac development in an embryonic rat heart; myofilaments, f-actin, sarcomeres and connexin 43 (Cx43) gap junctions were observed. Organoids were able to generate pressures of 1.2mmH_2O, with a volumetric ejection fraction of 3-5%; these are significantly lower than that of the associated embryonic development stage of the mouse heart. Organoids elicited a Frank-Starling response to increased extracellular calcium concentration; contractile strength increased with load. In the zero stress state,

the organoid cross-section residual stress opening angle was within the mature rat left ventricle range of 45-90°. Following induced cryoinjury, the organoid model demonstrated reduced total function and local sites of injury, with damaged tissue being stretched by contraction of adjacent myocytes; similar ventricular deformation is observed in animal models.

This study provides a foundation for our research with regards to the 3D aspect of developing a complete tissue engineered LV. It identifies the initial method to create a hollow 3D chamber structure for cell culture and the niches associated with ensuring LV-type function, such as maintaining chamber structure and eliciting contractile function and pressure. Lee et al., [40] identify the importance of incorporating valves to further simulate the isovolumic phases of the cardiac cycle. The development of a self-supporting, geometrically simulative, complete 3D LV, for use *in vivo* to treat HLHS is not addressed in this work; this remains an unaddressed gap in current knowledge.

2.2.2 Naturally Occurring Products

Naturally occurring products used in the bioassembly approach are derived from the blood. Fibrin is present in the blood and has been used in cardiac tissue engineering [50].

Huang et al., [50] describe a method to engineer functional 3D heart muscle using biodegradable fibrin gel. Two methods were implemented to produce the bioengineered heart muscle; the layering approach and the embedding approach. Isolated rat neonatal cardiac myocytes were used as the cell type in both approaches. Thirty-five millimetre tissue culture plates were coated with 1.5ml of polydimethylsiloxane (PDMS) elastomer and silk sutures were pinned into the PDMS, 12mm apart, to provide anchor points. In the layering approach, 0.5ml of thrombin (10U/ml) was plated on the PDMS surface, followed by 200µl of fibrinogen (20mg/ml). The solution was mixed and fibrin gel was

formed within 10-15mins. Differential cell quantities of 0.5, 1, 2 and $4x10^6$ were seeded on the fibrin gel. In the embedding approach, the differential cell densities were incorporated into the thrombin solution, plated onto the PDMS and fibrinogen was added for gel formation as per the layering approach. Contractile force was measured using a customized optical force transducer; function was measured for spontaneous, electrically stimulated, calcium induced and isoproterenol treated patch models. H&Es and immunohistochemistry were used to assess engineered heart muscle and histology.

Overall, the layering approach was more favourable in promoting myotubule formation. Cells plated on the surface of the fibrin gel produced an entire cell monolayer within 48hours with observable regular contractions; the observation can be explained by the potential formation of intercellular connections between cardiac myocytes and cell interaction with the fibrin gel. Conversely, embedded constructs only showed patches of contraction. The layered model showed increasing force with an increased cell seeding density, unlike embedded models, wherein the fibrin gel limited cell spreading. Engineered constructs were able to generate maximum specific forces of up to $15kN/m^2$. Histological analysis showed evidence of initial intercellular functional coupling with Cx43 and N-cadherin and tissue level organization with collagen type-I and F-actin. Constructs did have reduced sensitivity to extracellular calcium levels compared to native tissues. Low concentrations of isoproterenol were required to elicit an increase in contraction rate, thus postulating the presence of β-adrenergic receptors in constructs. At low frequencies, electrical pacing showed construct recovery to baseline rates; the limitations at higher frequencies may be due to architectural components such as tissue organization and ECM components.

This study shows the potential to develop functional artificial heart muscle using a naturally occurring product. It highlights the benefits of fibrin gel with respect to

controllable degradation kinetics and producing customisable patches which can generate considerable force, with a physiological response to both electrical and chemical variables. However, the gap in knowledge of developing a complete engineered 3D LV remains unaddressed by this study.

2.2.3 Overview

The discussed bioassembly approaches focus on the development of a functional cardiac organoid model and bioengineered heart muscle patches, respectively, using biocompatible, physiologically simulative biomaterial platforms. The proposed applications of these technologies, is as *in vitro* models. The limitations associated with these approaches includes the development of an appropriate casting mold or anchorage setup, as these variables determine the shape and size of the tissue, as opposed to the matrix itself. Additionally, oxygen and nutrient diffusion based on material thickness remains a limitation, as per the bioengineered approach. The gap in knowledge can be more clearly defined based on the model produced by Lee et al. [40]; produce a 3D complete LV, with a self-supporting structure and the incorporation of valves for application *in vivo*, in HLHS. The cardiac organoid model [40] is the only 3D tissue engineered LV produced to date and as such, provides a platform for our work to develop a complete 3D engineered LV.

2.3 The Cell Sheet Approach

The cell sheet approach is based on the assembly of cell monolayers; it is a scaffold-free technology. Cells are cultured on temperature-sensitive polyisopropylacrylamide (PIPAAm)-coated dishes. At 37°C, or physiological temperature, PIPAAm facilitates cell attachment by hydrophobic surface properties, but at temperatures below 20°C, PIPAAm becomes hydrophilic, therefore cell layers rapidly detach [37,51].

2.3.1 PIPAAm Culture Surface

Shimizu et al., [37] describe the use of overlaid neonatal rat cardiac myocyte monolayer sheets to produce cardiac grafts. Isolated neonatal rat cardiac myocytes were cultured on PIPAAm surfaces for four days at 37°C to form a monolayer cell sheet, after which they were detached at 20°C and transferred and attached to a culture surface. The process was repeated and cell sheets were placed directly on top of each other on the culture surface. Additionally, pulsatile grafts were produced using the same method, with transfer to a hollow collagen frame, with the edges of the sheet in contact with the frame and an unsupported central region. Cell sheet grafts were assessed histologically and for force and electrical potential activity.

Cell sheets transferred from PIPAAm to the culture surface underwent some shrinkage due to cytoskeletal tensile rearrangement, but retained their square shape; spontaneous beating was present on both surfaces. Electrical communication was measureable between sheets. Macroscopic contractions were observable in the frame-mounted pulsatile grafts *in vitro*; collagen frame deformation occurred several days after initiation of contraction. Cell sheets were tested as *in vivo* grafts; grafts were cultured *in vivo* for three weeks. The graft shape remained square, with contraction occurring one week after transplant; microvasculature was observed in the graft following transplant. Transplanted grafts demonstrated extensive cardiac hypertrophy with reduced fibroblastic tissues on histological analysis.

2.3.2 Overview

This study shows the biocompatibility and functional potential of cell-sheet engineered pulsatile cardiac tissue grafts. The proposed application of this technology is as an *in vitro* heart model and an *in vivo* tissue patch for cardiac tissue repair. The approach, as per the two previous approaches, is diffusion limited. Additionally,

producing macroscopic function requires multiple sheets and is a lengthy process; transfer and handling of the graft results in a short delay period of no function. The gap in knowledge to engineer a complete 3D LV is not addressed within this study; the final cell sheet is a planar square.

2.4 The Decellularization-Recellularization Approach

Decellularization is utilized to remove all cells and potentially immunogenic material from the heart, whilst retaining the underlying ECM structure. The heart tissue is decellularized using a series of detergents and DNAase treatments. Cells are reseeded back into the ECM by direct injection and/or transfusion through vascular channels [38].

2.4.1 Perfusion Decellularization and Injection-Perfusion Recellularization

Ott et al., [38] describe the perfusion decellularization of a whole adult rat heart with cardiac and endothelial cell reseeding. The rat heart was excised and perfusion decellularized using detergent solutions and antibiotic phosphate buffer solution (PBS), over a five day period. Decellularized hearts were mounted onto a working heart bioreactor and a flow loop was established. Isolated neonatal rat cardiac myocytes were injected into the anterior of the LV. Isolated rat endothelial cells were perfusion seeded into the aorta. Contractile force, pressure and the histology of the recellularized heart was assessed.

The perfusion decellularization approach was histologically validated to show complete removal of cellular and immunogenic materials, with preservation of the underlying ECM and heart structure. Eight days after recellularization with cardiac myocytes, heart constructs showed electrical and contractile function. Recellularization by injection showed increased cell retention at the injection site, with increasing confluence throughout the construct, over time. Histological analysis showed the

expression of α-actin and cardiac myosin heavy chain in the LV. Increased Cx43 expression was observed after eight to ten days of culture; this validated observed contractions to show functional connections. Seven days after endothelial cell perfusion, single cell layers were formed throughout the walls of the large and small coronary vessels, with further re-endothelialisation of ventricle cavities.

2.4.2 Overview

This study shows the potential to engineer a complete heart using the decellularization-recellularization approach. The proposed application is for use as an alternative to donor organs in transplant. The limitations associated with this approach include whole heart and cell sourcing, and the long term effects of detergent decellularization, both on the longevity of the ECM and *in vivo*. The study addresses the importance of the 3D structure in tissue-engineering, however, its limitations mean that the gap in knowledge is not addressed. In the context of this study, an additional consideration in the current gap in knowledge is identifiable; sourcing biocompatible and "off-the shelf" available scaffold biomaterials.

2.5 Conclusion

Based on the review of current tissue engineering solutions applicable to HLHS, a gap in knowledge is observed and validated. The current gap in knowledge is to develop a complete 3D engineered LV, to be utilised as an implantable system in HLHS. Particulars to consider in this knowledge gap have been derived based on the reviewed literature; producing an LV of accurate size and shape, with a self-supporting structure, using a biocompatible, easily sourced biomaterial scaffold with the addition of valves to complete the system.

Current work in the field does not address this gap, with technologies focusing on the development of graft-type augments and/or *in vitro* models. Aspects of the reviewed literature provide a platform on which to develop our research. Blan et al., [47] present both a potentially biocompatible material platform, with the use of chitosan and a viable cellularization strategy. The work of Lee et al., [40] and Ott et al., [38] highlights the complexities associated with 3D tissue engineering in developing an *in vitro* bioengineered LV and the importance of inherent physiological properties and structures, respectively, when engineering a complete 3D cardiac LV.

Tissue engineering provides a strategy to both treat HLHS and address the issue of donor shortage. Engineering a 3D LV would provide a treatment modality to directly correct one of the defining pathological features of HLHS. Bioengineering this construct provides a more physiologically replicative model for implant, in terms of cellular, mechanical and functional attributes. Based on the reviewed literature, our work presents a completely novel approach to addressing HLHS.

2.6 Summary

The reviewed literature outlines current tissue engineering strategies applicable to HLHS. The development of a bioengineered complete 3D LV has been validated as an area of research yet to be addressed, and provides a completely novel potential treatment modality both to directly address the problem and supersede the need for donor organs, as identified in Chapter 1. The conclusions elucidated from this review provide a platform for the research design to bioengineer a 3D cardiac LV.

CHAPTER 3

RESEARCH DESIGN

3.1 Overview

This research focuses on the overall aim of bioengineering a 3D cardiac LV, as a replacement construct for use in HLHS. Particular considerations include understanding the ideal platform, the design and fabrication of biocompatible and biomimetic LV components, reproducing LV geometry, cellularization, culture and ensuring functional, electrical and histological viability.

The study emanates from several motivations. Current treatment strategies in HLHS include either multiple surgeries to re-functionalize the right ventricle or heart transplant. The surgeries are highly invasive and yield an inefficient solution with many associated risks and long-term complications. Heart transplant is severely limited due to a chronic shortage of donor organs. Current strategies in cardiac tissue engineering for HLHS are predominantly designed to be graft-type myocardial augments with a planar 3D structure; the singular 3D cardiac organoid model has been developed exclusively for *in vitro* applications. Bioengineering a 3D cardiac LV would provide a treatment modality to directly correct one of the defining pathophysiological features of HLHS and supersede the limitations associated with existing treatment options. Bioengineering this construct provides a more physiologically replicative model for implant in terms of cellularization, mechanical and functional attributes. This is a completely novel approach to addressing HLHS.

In the context of tissue engineering, the process to bioengineer a 3D cardiac LV can be summarized as shown in **Figure 3.1**.

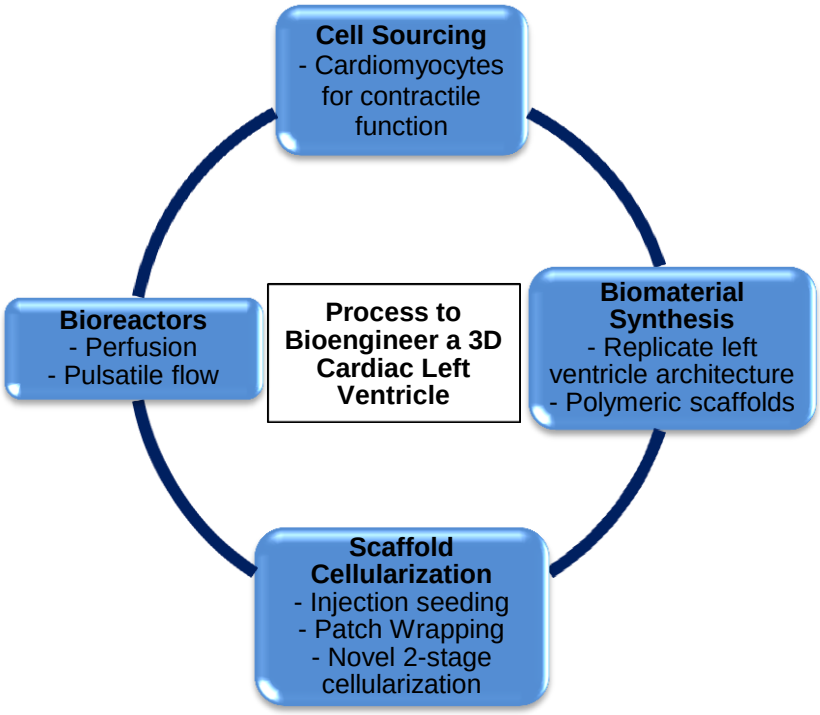

Figure 3.1: Process to Bioengineer a 3D cardiac LV

Considerations accompanying these listed processes include the use of autologous or alternative cell sources, natural or synthetic biomaterials, differential cell delivery methods to improve cell retention and bioreactors designed to recreate physiological stimuli.

3.2 Research Questions

From this general aim and the overview of the tissue engineering processes involved in bioengineering a 3D cardiac LV, a number of specific questions emerged to develop the research design. The main questions are summarized overleaf:

1. Can we develop a better understanding of the ideal LV material platform, the LV itself?
2. Is it possible to design and fabricate a 3D cardiac LV? Does it function when cellularized?
3. How can we improve cell retention in our fabricated LV?
4. Can we develop a custom pulsatile flow stretch bioreactor to condition our fabricated LV?
5. Is it possible to design and fabricate trileaflet valves to produce a complete bioengineered 3D cardiac LV?

3.3 Research Design

The research design is completely novel and utilizes aspects of the bioengineering approach proposed by Blan et al., [47] the bioassembly approach proposed by Lee et al., [40] and the decellularization-recellularization approach explored by Ott et al., [38] to develop a model to address each research question. Models sequentially build on each other to address the overall aim of developing a complete bioengineered 3D cardiac LV. The specific models are shown in **Figure 3.2** and will be discussed further with respect to experimental design.

3.4 AVEM

The AVEM is the acellular ventricular extracellular matrix model. This work addresses the research question: Can we develop a better understanding of the ideal LV material platform, the LV itself? Secondary questions addressed by this model include deriving the efficacy of culture on the ECM under static conditions, the ability to produce a functional tissue and assessing the details of the microscopic structure which make it amenable to cardiac cell infiltration.

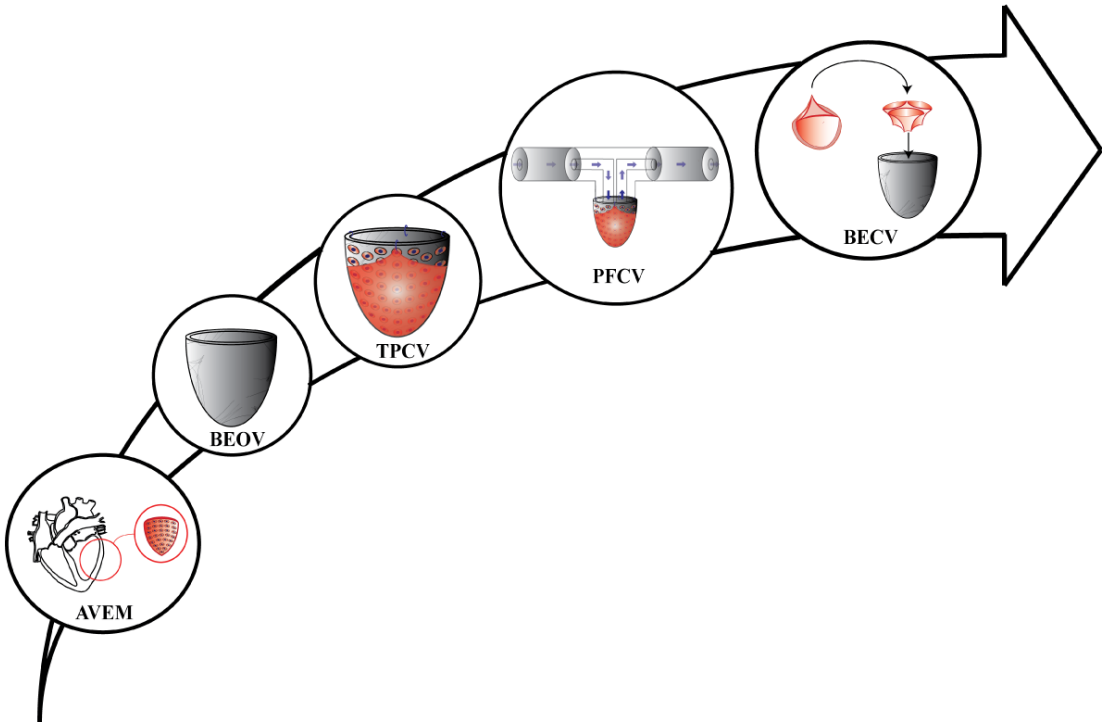

Figure 3.2: Research design to bioengineer a 3D cardiac LV.

An adult rat heart was decellularized using a series of detergent solutions, over a 14day period. Acellular ventricular tissues were excised and utilized as scaffolds. Scaffolds were washed with PBS, for 48hours, prior to cellularization. Primary rat neonatal cardiac cells were isolated and passively seeded into the scaffold; half of the total cell load was seeded for 24hours, the scaffold was rotated to expose the posterior surface and the seeding process was repeated with the remaining cell load. Multiple cell seeding densities were assessed; the total cell number resulting in optimal contractile frequency and cell retention was defined as the AVEM. AVEM were cultured under static conditions, for 14days, in an incubator maintained at 37°C and 5%CO_2. The twitch force and Frank-Starling relationship of the AVEM was assessed using an isometric force transducer. Histological analysis was utilized to validate AVEM characteristics, including pore size and the presence of specific cardiac factors identifying cell-matrix interactions, cell organization and the definitive presence of cardiac myocytes.

This study provides us with a platform of ideal material properties to emulate when designing and fabricating a 3D left ventricle. Specifically, we can determine the efficacy of passive cell seeding, and the outcome function of our model.

3.5 BEOV

The BEOV is the bioengineered open ventricle model. This work addresses the research question: Is it possible to design and fabricate a 3D LV? Does it function when cellularized? Secondary questions addressed by this model include characterizing the scaffold material properties, both in terms of geometry and in manipulation for cellularization and cell viability.

Three-dimensional LV molds were developed using Solidworks computer-aided design (CAD) modelling and 3D printing, based on the geometry of the human neonatal LV. A 2.5%w/v chitosan in 0.2M acetic acid solution was used as the scaffold biomaterial; after mixing for 24hours at room temperature, the solution was loaded into molds, frozen at -80°C for 24hours and lyophilized for 24hours. The outcome porous scaffolds were rehydrated in 0.1M sodium hydroxide (NaOH) solution and sterilized prior to cellularization. Primary rat neonatal cardiac cells were isolated and directly injected into the scaffold and the construct was cultured under static conditions, oriented open face down, in an incubator maintained at 37°C and 5%CO_2, for four days. The cellularized constructs are defined as the BEOV. The consistency in geometry was assessed between CAD models, 3D printed molds, lyophilized and rehydrated scaffolds, by material surface area and volume. Scaffold composition was assessed using Fourier Transform Infrared spectroscopy (FTIR), surface morphology was assessed using SEM and Atomic Force microscopy (AFM) was used to determine surface topology and the Young's modulus; these material tests were used to assess lyophilized, rehydrated and cellularized constructs. BEOV biopotential activity was assessed to evaluate cardiac

myocyte electrophysiological activity using a 32 electrode biopotential sensor. Cellularization efficiency and cell retention were assessed using 3-(4, 5-dimethylthiazol-2-yl) 2, 5-diphenyltetrazolium bromide (MTT) assay. Histological analysis was used to evaluate the presence of contractile, sarcomeric and gap-junction cardiac specific factors in the BEOV.

This study provides an initial proof-of-concept in our ability to develop a 3D LV model. One of the key aspects for any tissue engineered construct is cellularization; improving cell retention inherently improves the function of an engineered tissue.

3.6 TPCV

The TPCV is the two-stage perfusion cellularized ventricle model. This work addresses the research question: How can we improve cell retention in our fabricated LV? Secondary questions addressed by this model include the effect of perfusion culture on cell retention, construct function and material properties.

Chitosan scaffolds were prepared as outlined in the BEOV model and a novel two-stage cellularization process was implemented. In stage one isolated primary rat neonatal cardiac cells were directly injected into the scaffold, as per the BEOV model. In stage two, a 3D artificial heart muscle (AHM) patch was wrapped around the outer side of the scaffold. The cardiac patch was loaded with primary rat neonatal cardiac cells and was attached with the cell-loaded side oriented to be facing inward, onto the scaffold surface. Positive controls with only one stage of the cellularization process were also assessed. All cellularized variants were culture in both static and perfusion conditions, for four days, in an incubated environment, at 37°C and 5%CO_2. The perfusion cultured two-stage cellularized constructs were defined as the TPCV. TPCV biopotential activity and morphology were evaluated using a 32 electrode biopotential sensor and SEM,

respectively. Histological analysis was used to determine the presence of cardiac specific sarcomeric organization, contractile and gap-junction factors.

This study optimizes the cellularization of the open ventricle model. The function of the TPCV can be further improved using a bioreactor to simulate the mechanical stretch of the cardiac LV chamber.

3.7 PFCV

The PFCV is the pulsatile flow conditioned ventricle model. This work addresses the research question: Can we develop a custom pulsatile flow stretch bioreactor to condition our fabricated LV? Secondary questions addressed by this model include the ability to further improve biopotential activity, as well as assessing the pressure generation capability of the fabricated ventricles.

Chitosan scaffolds were prepared as per the BEOV model and cellularized as per Stage II of the TPCV model, by AHM patch wrapping. A custom pulsatile flow stretch bioreactor was fabricated. Following cellularization, constructs were incorporated into the pulsatile flow loop to close the system, and conditioned for 20hours, in an incubated environment maintained at 37°C and 5%CO_2. The pulsatile flow rate was 16ml/min per scaffold. Pressure output was evaluated using a Mikro-Tip catheter transducer. Biopotential activity was assessed using a 32 electrode biopotential sensor.

This study emulates the physiological mechanical stretch which the LV chamber undergoes *in vivo* and acts to further optimize our engineered LV. The engineered LV chamber has been studied in detail to determine biocompatibility, improving cell retention and bioreactor conditioning. The PFCV identifies the need to complete our LV model in a more physiologically simulative manner; developing a tissue engineered valve to fit the existing model presents a viable solution.

3.8 BECV

The BECV is the bioengineered complete ventricle. This work addresses the research question: Is it possible to design and fabricate trileaflet valves to produce a complete bioengineered 3D cardiac LV? Secondary questions addressed by this model include identifying an appropriate valve scaffold material, producing a geometrically appropriate valve and completing the BEOV.

The BEOV chitosan scaffold was produced as per the outlined method. Three-dimensional trileaflet valve molds were developed using Solidworks CAD modelling and computer-numerical code (CNC) machining based on the geometry of the human infant aortic valve. As per the BEOV model, a 2.5%w/v chitosan in 0.2M acetic acid solution was used as the scaffold biomaterial; the process to produce the scaffold is as per that of the BEOV scaffold. The porous BEOV and bioengineered trileaflet valve (BETV) structures were sutured together to seal and complete the model. The consistency of the valve geometry and internal cavity volume were assessed for the assembled CAD models, CNC valve molds, lyophilized and rehydrated BECV scaffolds.

This study is an initial proof-of-concept in the design and fabrication of a complete bioengineered 3D cardiac LV. It assembles our initial work on the BEOV LV chamber and the concept of valve design and tissue engineering.

3.9 Summary

The research design is divided into five specific models, with each study building on the previous to achieve the overall aim of bioengineering a 3D cardiac LV. We begin by studying the ideal platform, in the AVEM model.

CHAPTER 4

ENGINEERING 3D BIO-ARTIFICIAL HEART MUSCLE: THE ACELLULAR VENTRICULAR EXTRACELLULAR MATRIX MODEL

Current therapies in left ventricular systolic dysfunction and end stage heart failure include mechanical assist devices and/or transplant. The development of a tissue-engineered integrative platform would present a therapeutic option which overcomes the limitations associated with current treatment modalities. This study provides a foundation for the fabrication and preliminary viability of the Acellular Ventricular Extracellular Matrix (AVEM) model. AVEM were fabricated by culturing four million rat neonatal cardiac cells around an excised acellular ventricular segment. AVEM generated a maximum spontaneous contractile force of 388.3μN and demonstrated a Frank-Starling relationship at varying pretensions. Histological assessment displayed cell cohesion and adhesion within the AVEM as a result of passive cell seeding.

4.1 Introduction

Left ventricular systolic dysfunction (LVSD) is a primary component of end-stage heart failure (ESHF), which most commonly occurs in conjugation with ischemic heart disease and myocardial infarction. Resultant physiological outcomes include heart wall thinning, ventricular dilation and cardiac remodelling. These outcomes are irreversible due to the nominal reparative capacity within myocardial tissues [52].

Current drug therapies aim to maintain cardiac output by reducing the decline in myocardial function. They are often unable to sustain declining ESHF heart function, and are, therefore, coupled or replaced with cardiac assist devices [53]. Mechanical left

ventricular assist devices (LVADs) pump blood from the LV to the aorta [53]. Biocompatibility presents the predominant limitation in mechanical device therapy applications. Additional limitations include lack of functional interaction and coupling with host tissue, thrombogenicity, risk of infection, device control complexity and long-term durability [54]. Transplant remains the precedent treatment option for ESHF, however, a shortage of donor hearts and the accompanying need for long term immunosuppression, presents a major limitation.

Cell-based cardiac tissue engineering strategies may provide regenerative therapeutic options of equivalent function to mechanical devices. If these strategies utilized autologous cells and ECM, surmounting biocompatibility and biomimetic considerations would be more feasible. This natural alternative encourages functional coupling and interaction with native tissue.

Previous research has focussed on characterizing acellular platform feasibility to bioengineer functional cardiac constructs. Ott et al., [38] utilized native rat acellular cardiac tissue matrices, onto which cardiac cells may be loaded, to promote functional differentiation. Eitan et al., [55] characterized acellular porcine ventricle ECM mechanical properties, and its propensity to functionally couple cardiac cells as measured by protein expression. Potpova et al., [56] and Godier-Furnemont et al., [57] characterized acellular urinary bladder matrices as potential cardiac cell delivery platforms. These cited studies provide platforms to develop cardiac-tissue specific engineered models in the treatment of ESHF.

Hydrogels [58-60], alginates [61, 62] and collagen gels [35, 36, 63] have also been reported to be appropriate self-organizing scaffolds with ECM properties. Constraints associated with synthetic ECM platforms emanate around biocompatibility and biomimetic

considerations. Use of acellular ECM as a cell delivery platform alleviates these considerations.

We propose the use of a cardiac patch as a treatment method to either replace damaged native tissue or facilitate regeneration in LVSDs and ESHF, as a viable alternative to LVADs and transplant. This study focuses on re-cellularization of Acellular Ventricular Extracellular Matrix (AVEM) constructs to provide a foundational assessment of applicability. The rationale for the use of ventricular ECM as the biomaterial platform is derived from the whole heart study carried out by Ott et al [38]. Ott et al., [38] demonstrated the retention of collagen structure in the acellularized whole heart, with the preservation of ECM fibre orientation and composition. Ventricular ECM was chosen as the decellularized scaffold material for the AVEM model, to utilize the complex cardiac ECM architecture. The inherent bioactivity and mechanical integrity of the ECM may better promote the viability of the transplanted cells. The suitability of the optimal loading density was determined to be the cell loading quantity at which macroscopic contractions were observable. The rationale for this study develops the whole heart study carried out by Ott et al [38]. The aim of this study is to provide a model to determine the potential of cell loading acellular ventricular tissue to yield function and cell-scaffold integration.

Rat hearts were detergent decellularized to produce an acellular total organ. Excised ventricles were repopulated with rat neonatal cardiac cells. Construct functionality and cell distribution of the AVEM was characterized by twitch force measurements and histology. The particulars of the presented concept are novel, with the potential to have a significant impact in both the field of tissue engineering and to be developed into a therapeutic option in the treatment of LVSDs and ESHF.

4.2 Materials and Methods

All protocols were approved by the Institutional Animal Care and Use Committee (IACUC) in accordance with the "Guide for the Care and Use of Laboratory Animals" (NIH publication 86-23, 1986).

4.2.1 Decellularization of Rat Hearts

The decellularization protocol for rat hearts has been adapted from previously described methods [64]. Rat hearts were obtained from three to six month old Sprague-Dawley rats. The hearts were washed with PBS to remove extraneous debris and blood. The whole hearts were then detergent decellularized as described in **Table 4.1**, over a 14 day period.

Table 4.1: Decellularization Protocol.

Solution/Properties	Components	Schedule
Solution 1: Fixing agent/Detergent	80% Glycerol (by volume) 0.9% NaCl 0.05% NaN_3 25 mM EDTA	Day 0-2
Solution 2: Detergent	4.2% sodium deoxycholate 0.05% NaN_3	Day 2-4
Solution 3: Detergent	1% SDS 0.05% NaN_3	Day 4-6 Day 8-10
Solution 4: Detergent	0.05% NaN_3	Day 12-14
Solution 5: Detergent	3% Triton X-100 (by volume) 0.05% NaN_3	Day 6-8 Day 10-12

Components of Decellularization Key: Glycerol: Solvent; NaCl: Isotonic component; NaN_3: Bacteriostatic**;** EDTA: Ionic surfactant for celly lysis and membrane/cellular component solubilisation; SDS: Denaturing agent for non-covalent protein bonds to make tissue quasi-transparent**;** Triton-X 100: non-ionic surfactant for membrane solubilisation and cell lysis.

4.2.2 Ventricular Scaffold Excision and Preparation

Acellular ventricular tissue segments were excised (**Figure 4.1**). To circumferentially isolate the left, right and septal myocardium, an incision was made along the longitudinal direction of the decellularized heart and continued along the pulmonary axis, symmetrically about the apex.

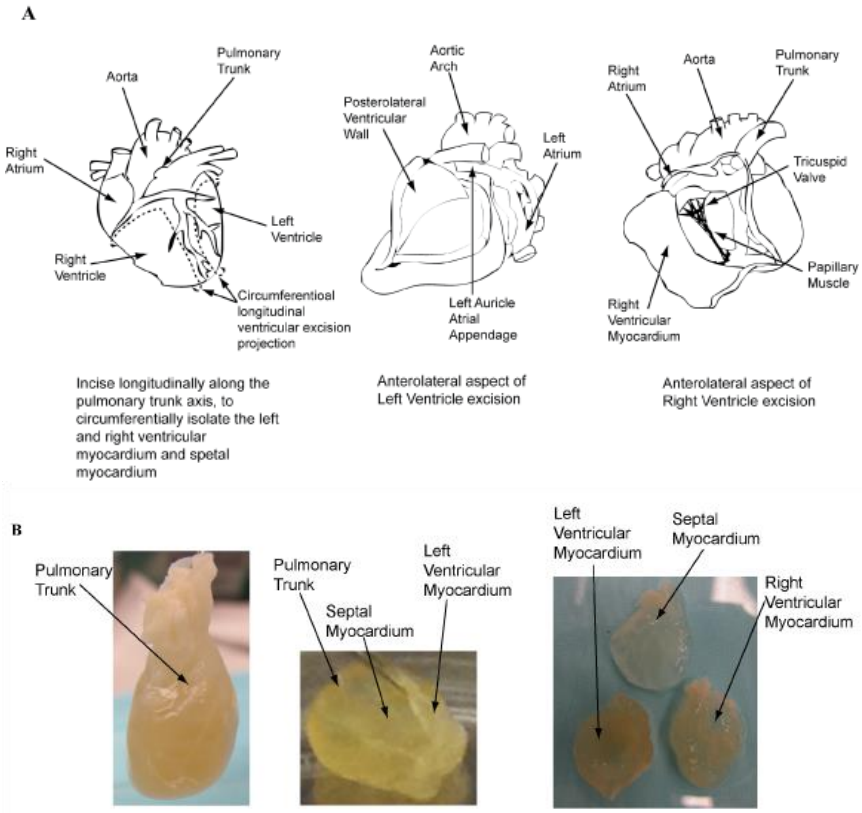

Figure 4.1: A: Schematic of ventricular scaffold; **B:** Ventricular scaffold excision from acellular heart constructs.

Acellular ventricular ECM constructs were passive-seeded in conical tubes to increase the surface area in contact with the cell solution. Natural cell migration populates the interior of the AVEM constructs. A 50ml conical was trimmed to a volume of 5ml, coated with 2ml of SYLGARD (PDMS, type 184 silicone elastomer) (Dow Chemical Corporation, Midland, MI) and air dried for two weeks. The conical was sterilized with 80% ethanol, exposed to UV light for 20 minutes and air dried in a laminar flow hood prior to scaffold transference. Scaffolds were pinned, using four minutien pins of 0.1mm diameter (Fine Science Tools, Foster City, CA), sterilized in 80% ethanol and air dried, as shown in **Figure 4.1B and 4.2**.

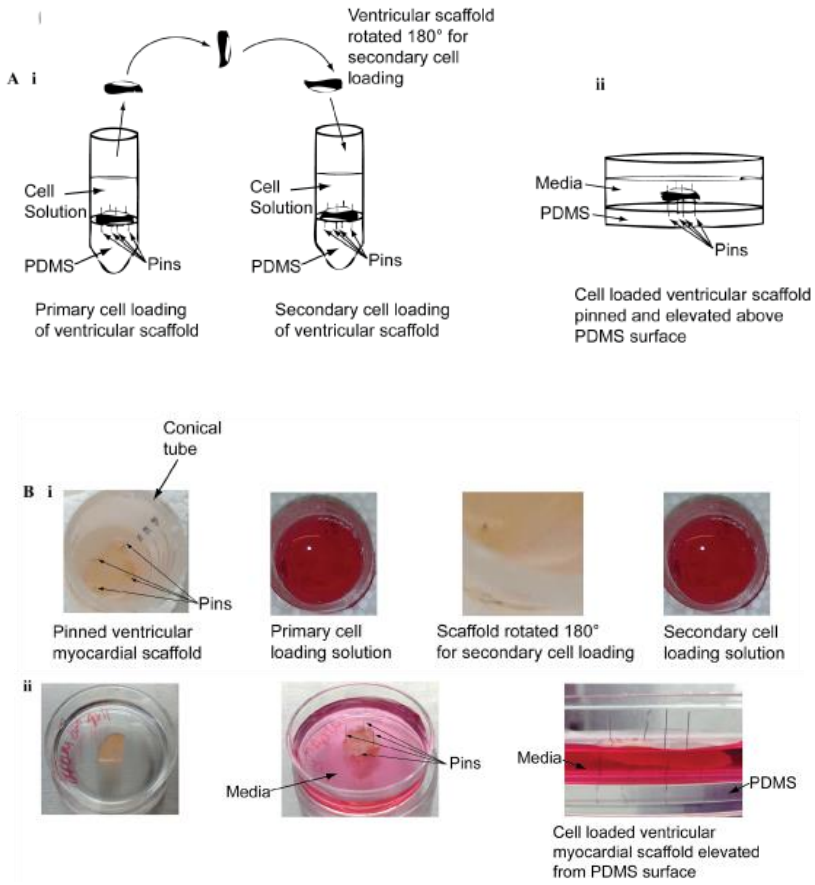

Figure 4.2: **A: i)** Surface-anterior cell loading of ventricular scaffold; **ii)** Cell culture with elevated suspended cellularized ventricular construct; **B: i)** Primary-secondary anterior surface cellularization; **ii)** Cell culture.

Pinned scaffolds were washed three times in sterile PBS to remove residual decellularization detergents and preservatives. Scaffolds were then submerged in 3ml of culture medium, composed of M199 (Life Technologies, Grand Island, NY), with 20% F12k (Life Technologies, Grand Island, NY), 10% foetal bovine serum, 5% horse serum, 1% antibiotic-antimycotic, 40 ng/ml hydrocortisone and 100 ng/ml insulin. Culture medium was renewed at 24hour intervals over a 48hour period, in preparation for cell loading. Throughout the preparatory scaffold media wash step, pinned constructs were incubated at 37ºC supplied with 5% CO_2.

4.2.3 Isolation of Primary Cardiac Myocytes

Cardiac cells were isolated from the hearts of two to three day old neonatal Sprague-Dawley rats using an established method [50]. Each heart was cut into three to four pieces in an ice-cold PBS phosphate buffer. The pieces were gently rinsed in order to remove blood cells and transferred to a secondary phosphate buffer solution for further mincing. Tissues were minced into $1mm^2$ pieces and transferred to a dissociation solution consisting of 0.32 mg/ml collagenase type 2-filtered (Worthington Biochemical Corporation, Lakewood, NJ) and 0.6 mg/ml pancreatin in phosphate buffer. A 50ml conical tube containing 15ml of dissociation solution and the minced tissues was placed in an orbital shaker and maintained at 37^oC for 30mins at 60rpm. At the end of the digestion process, the supernatant was collected in 3ml of horse serum to neutralize the enzyme and centrifuged at 1000 rpm for five minutes at $4^\circ C$. The cell pellet was re-suspended in 5ml horse serum and kept in an incubator at $37^\circ C$ supplied with 5% CO_2. Fresh dissociation solution was added to the partially-digested tissue and the digestion process was repeated an additional two to three times. Cells from all the digests were pooled, centrifuged and suspended in culture medium. Cell viability was analyzed by Trypan blue (4%) staining according to the manufacturer's protocol.

4.2.4 Determining Optimal Cell Load for the Acellular Ventricular Extracellular Matrix

Three different concentrations of rat neonatal cardiac cells were passive-seeded onto each scaffold; $2x10^6$, $4x10^6$ and $6x10^6$ cells. Cells were isolated on two separate occasions within a 24hour period and loaded onto the superior and anterior surface of the acellular scaffolds; half the total population on each surface. The superior surface was cell loaded first and incubated for 24hours. The minutien pins were removed, the

scaffold was rotated 180º to expose the anterior surface for secondary cell loading and re-pinned (**Figure 4.2Ai and Bi**).

The cellularized constructs were cultured as shown in **Figure 4.2Aii and Bii**. A 35mm tissue culture plate was coated with 2ml of SYLGARD. The plate was air dried for two weeks and sterilized, with 80% ethanol and exposure to UV light for 20 minutes before use. The cellularized tissue construct was transferred from the conical tube to the tissue plate and pinned at four corners using minutien pins. A 3ml volume of culture medium was added and the construct was manually elevated to be suspended on the pins (**Figure 4.2Aii and Bii**), to increase the surface area during cell culture. Tissue cultures were maintained in an incubator at 37ºC supplied with 5%CO_2, with culture medium changes every 48hours.

Constructs were assessed to derive the optimal cell loading quantity of the final AVEM construct. Macroscopic contractile measurements were obtained for 15second intervals and extrapolated to estimate the number of contractions per minute for each cell loaded quantity. To determine porosity and differentiate cell deposition between cell loading quantities, after four days of culture, constructs were place in peel-a-way disposable embedding molds (VWR International), immersed in Tissue-Tek OCT compound (VWR International) and frozen at -80°C for 24hours. Planar sections of 10µm and 20µm thickness were cut using a Cryotome (ThermoScientific) and placed onto VWR Microslides for staining with Masson's Trichrome reagents, according to the manufacturer's protocol, to determine pore size and cell deposition, respectively. Masson's Trichrome images were obtained using a light microscope (Olympus, Center Valley, PA). ImageJ was used to analyse pore size.

4.2.5 Contractile Force Measurement

From days two to three, at macroscopic contraction observation, twitch force of the constructs was measured using a high sensitivity isometric force transducer (MLT0202, ADInstruments), connected to a quad bridge amplifier (FE224, ADInstruments). Data acquisition was through a 16 channel PowerLab system (PL3516/P, ADInstruments). The force transducer arm was attached to one free corner of the AVEM, while the other three ends were held fixed by minutien pins; spontaneous measurements were recorded for 20-60 seconds. The contractility of AVEM patches was collated over the 14 days culture period, at four to five day intervals, to map the contractile frequency behaviour of the construct. In order to obtain the Frank-Starling relationship, pretension was adjusted using a micro-manipulator (Radnoti LLC, Monrovia, CA) and measurements of spontaneous contraction were recorded. LabChart was used for data analysis with the peak analysis module, to calculate maximum twitch force and baseline force (pretension).

4.2.6 Structural, Contractile and Extracellular Matrix Histological Analysis

Fourteen days after plating, AVEM tissues were prepared as per the method outlined in Section 4.2.4, to produce planar tissue sections of 20μm thickness. Immunohistochemistry was used to compare native rat ventricular tissue, decellularized scaffolds and AVEM, with regards to desmin, troponin I, α-actinin and collagen type I.

Non-specific epitope antigens were blocked with 10% goat serum at room temperature for one hour. To show desmin, sections were incubated with mouse anti-desmin, 1:100 (Cardiomyocyte Characterization Kit, EMD Millipore, MA). To show contractile composition, sections were incubated with mouse anti-troponin I, 1:100(Cardiomyocyte Characterization Kit, EMD Millipore, MA). To show collagen-structure contrast, sections were incubated with mouse anti-α-actinin (Sigma, Catalog

No A7811) 1:200 and rabbit anti-collagen type I (Abcam, ab34710) 1:100. All sections were incubated with antibodies, for one hour at room temperature. All sections were counterstained for nuclei with 4,6-diamidino-2-phenylindole (DAPI) (2.5 µg/ml) for five minutes at room temperature. Fluorescent images were obtained with a Nikon C2+ confocal laser scanning microscope (Nikon Instruments Inc., Melville, NY). ImageJ was used to analyse cell count.

4.3 Results

4.3.1 Proof of Decellularization and Determining Optimal Acellular Ventricular Extracellular Matrix Cell Load

Figure 4.1B shows the decellularized heart; the tissue is translucent and structural features, such as the coronary vessel, remain visible. Detergent decellularization resulted in a comprehensively acellular cardiac matrix (**Figure 4.3**); no nuclei (blue) are evident in the decellularized tissue.

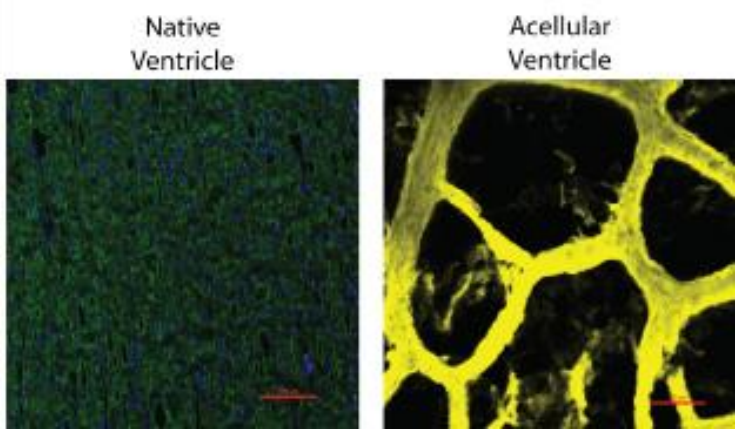

Figure 4.3: Representative tri-stained native and acellular ventricle tissues to define Collagen Type I (Yellow), α-actinin sarcomeres (Green) and nuclei (Blue) components at 40x objective.

Figure 4.3 shows the retention of tissue structural integrity (yellow collagen Type I) and ECM porosity post-decellularization. Using Masson's Trichrome stained tissue sections,

the average pore size of native and decellularized ventricular tissues (n=4 for both), for a 0.37mm^2 tissue section, were calculated to be 0.0019mm^2 ± 0.0018mm^2 (mean ± standard deviation) and 0.1355mm^2 ± 0.078mm^2, respectively. The diameter of cardiac cells ranges from 10-35µm [38] (~80-960µm^2 area). The calculated ECM pore size indicates that the scaffold would be amenable to cardiac cell migration.

Constructs loaded with different cardiac cell quantities, were assessed for macroscopic contraction and cell count, to derive the optimal cell load for AVEM. Macroscopic contractions were observed across all cell loading ranges (n=2 for each), following a four day culture period (**Figure 4.4A**; video data not provided).

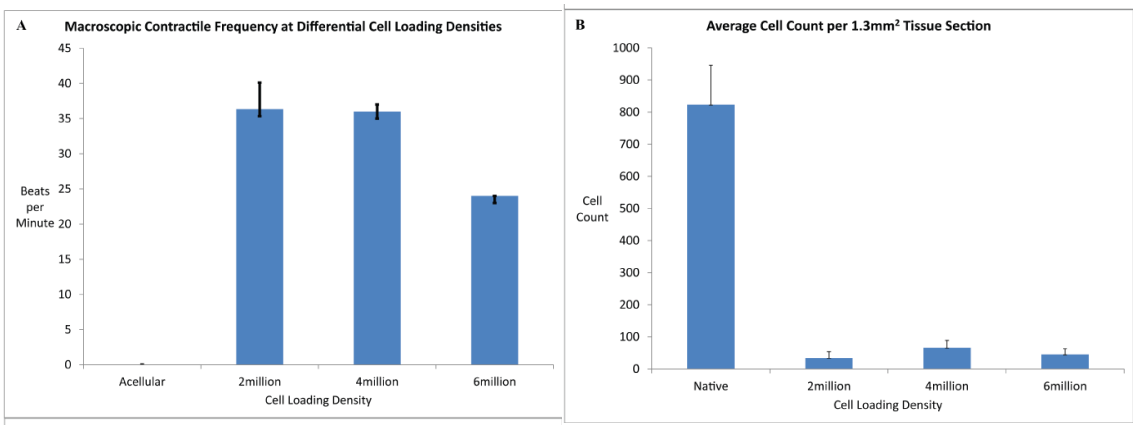

Figure 4.4: Determining optimal cell load of AVEM; **A:** Macroscopic contractile frequency at differential cell loads; **B:** Average cell count per 1.3mm^2 tissue section (p-values represented as native vs. cell load; $p<0.05$ for all).

The native rat heart has a contractile rate of 330-480bpm [38]. Scaffolds loaded with 2x10^6 and 4x10^6 cells, exhibited the highest average contractile rate of 36bpm (culture day three of four). The cell loading density of 4x10^6 macroscopically demonstrated more synchronous contraction throughout the entire construct and the stronger observable contraction, comparatively. ImageJ was used to calculate cell content per 1.3mm^2 of tissue, to determine which cell density was appropriate for the final AVEM (n=4 for each) (**Figure 4.4B**). The acellular average cell count was zero, proving the efficacy of the

decellularization process. Constructs loaded with $4x10^6$ had the highest average cell count per area, of 66cells ± 23cells. Compared to the native tissue, cell content was significantly lower in the recellularized constructs.

The AVEM is defined as an acellular ventricle scaffold loaded with $4x10^6$ cardiac cells, based on the results presented above. It is this defined AVEM which is referred to throughout the remainder of the study.

4.3.2 Fabrication of Acellular Ventricular Extracellular Matrix

Observable contractions occurred within 48-72hours of cell loading, primarily at the construct perimeter. Subsequently, contractions dissipated throughout the construct during the remaining culture period. Contraction began as localized arrhythmic events, developing to become more pervasive, synchronous and rhythmic.

4.3.3 Contractile Force Measurement

In total, 23 AVEM constructs were analyzed in this study; 10 (43%) demonstrated measurable contractions. **Figure 4.5** shows representative spontaneous twitch force results for the acellular ventricular ECM (negative control) and for recellularized AVEM, measured 72hours after cell loading at pretension ranges of ~800µN to ~2900µN, as five second excerpts to demonstrate relative base-to-peak amplitude and frequency. Previous studies [65] have extensively characterized fresh rat ventricular twitch force (42mN). **Figure 4.6** represents the Frank-Starling relationship, as pre-tension versus twitch force. The force generated by AVEMs (n=10) is sub-divided into pretension ranges (**Table 4.2)**.

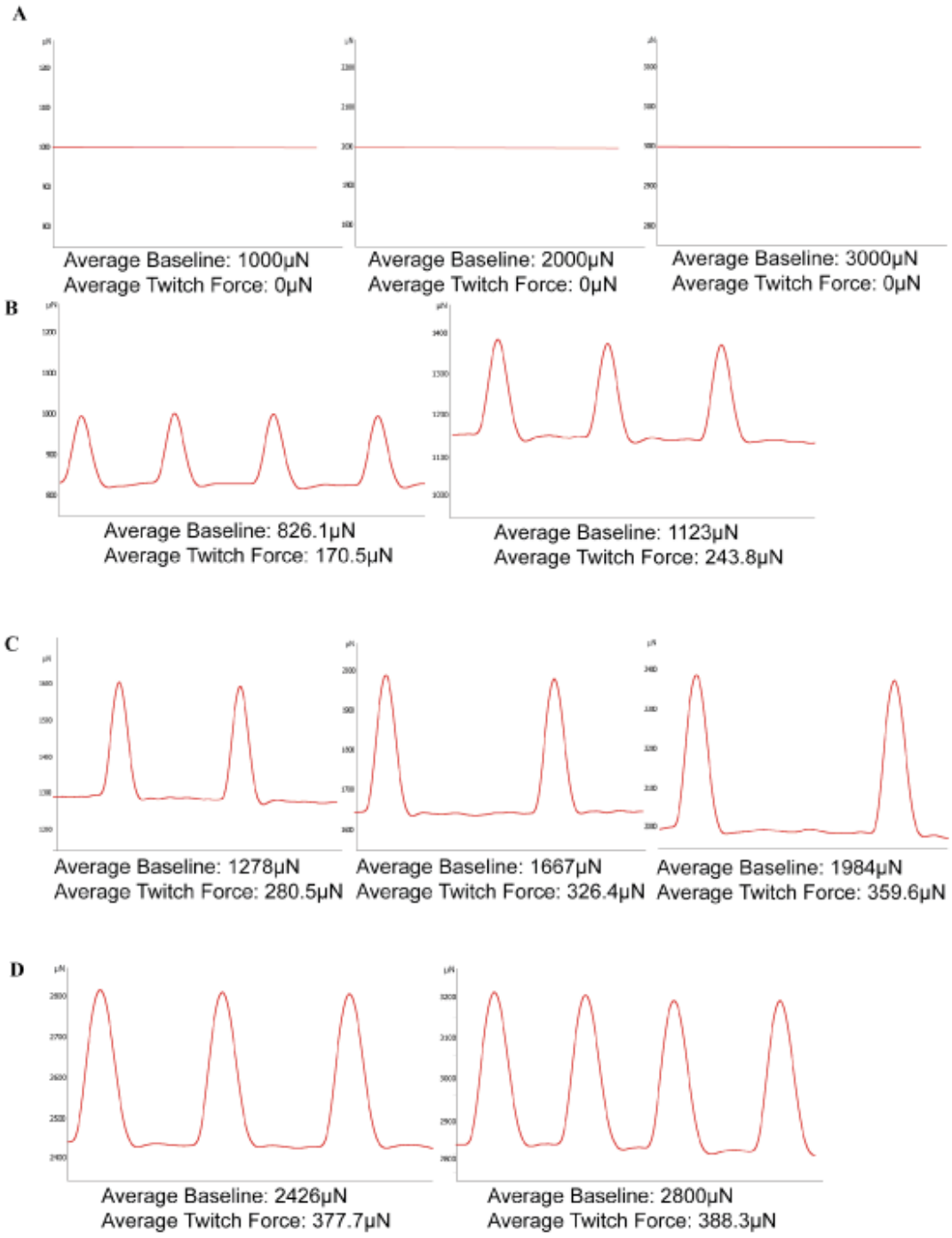

Figure 4.5: AVEM representative twitch force over 5 secs; **A:** Acellular ECM at pre-tension ~1000, 2000 and 3000μN. AVEM at approximate pretensions **B:** 800 and 1120μN; **C:** 1300, 1700 and 2000μN; **D:** 2400 and 2800μN.

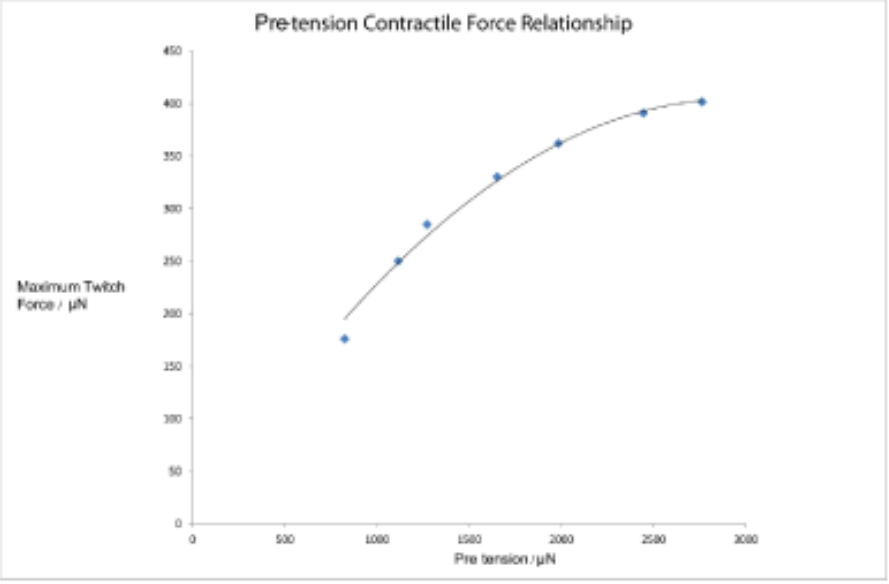

Figure 4.6: Defined AVEM representative Frank-Starling Length Tension relationship of pre-tension versus twitch force.

Table 4.2: Force generated by AVEM at pre-tensile ranges (total n=10).

N	Pre-tension (µN)	Twitch Force (Mean ± Standard Deviation) (µN)
3	<2500	320.851 ± 108.201
6	2500-5000	431.599 ± 225.756
4	5000-7500	224.892 ± 76.536
4	7500-10,000	92.728 ± 44.562
2	10,000-12,500	152.800 ± 12.869
4	12,5000-15,0000	79.583 ± 5.713
3	>15,000	77.683 ± 10.776

4.3.4 Characterization of Acellular Ventricular Extracellular Matrix Regenerated Myocardial Tissues

Figure 4.7 shows histological characterization of AVEM constructs, in comparison to healthy native heart and acellular ventricle scaffold tissues, for a range of cardiac specific factors.

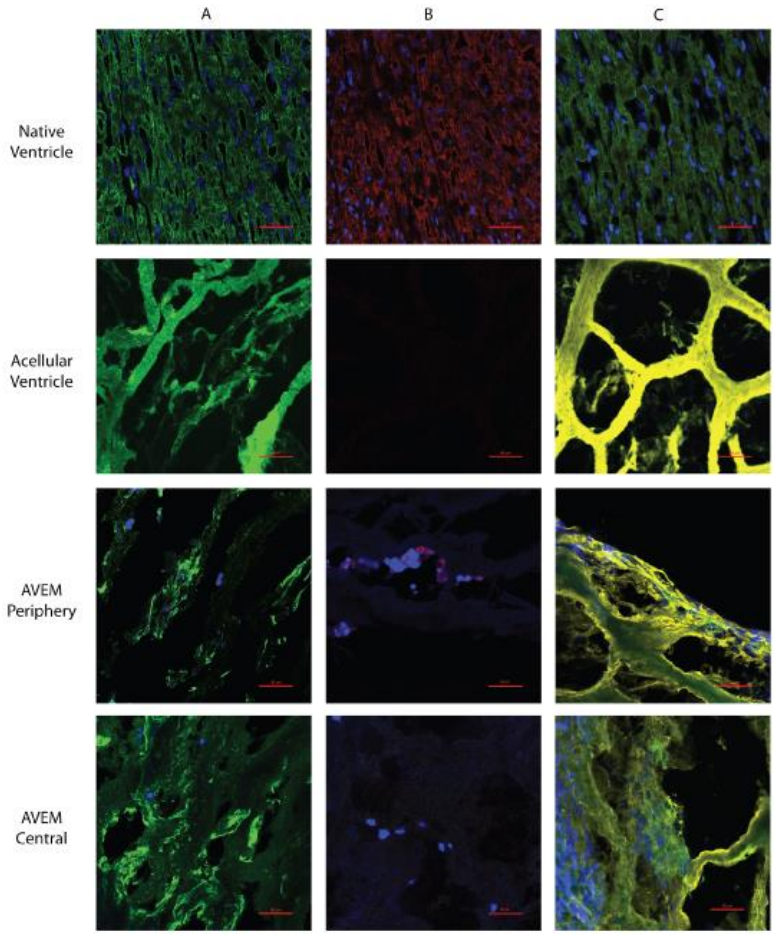

Figure 4.7: Immunoflourescent staining at 40x objective for native, acellular and AVEM tissues; **Column Stains** with DAPI (blue), **A:** desmin (green); **B**: troponin I (red); **C**: α-actinin (green), collagen type I (yellow).

The native ventricle demonstrates the presence of desmin, showing defined sarcomeric striations. Comparatively, the acellular ventricle lacks clear sarcomeric organization shown by desmin. The AVEM shows desmin presence around nuclei with a small degree of sarcomeric organization.

The native ventricle demonstrated high levels of troponin I whereas the acellular ventricle showed a complete absence. The AVEM demonstrated a greater degree of troponin I peripherally, where most contractile activity was observed. Comparatively, the

central part of the AVEM was more sparsely cellularized, observed to be less contractile and therefore showed little presence of troponin I.

α-actinin was abundant in the native tissue alongside underlying collagen. Only collagen remained in the acellular tissue. The AVEM images highlight the presence of α-actinin, both centrally and peripherally, in conjugation with cell clusters; coupled with desmin observations, the presence of sarcomeres, and therefore cardiomyocytes is reinforced.

Cells predominantly cluster at the AVEM periphery to form a mostly cohesive layer, with retention of the underlying ECM-Collagen structure. The presence of α-actinin and desmin indicate the preservation of myocyte expression to promote sarcomeric organization. Contractile macroscopic observations are validated by the presence and absence of troponin I at AVEM periphery and centre, respectively.

4.4 Discussion

The foundational stages of AVEM development have been described within this study. AVEM present a potentially biocompatible and biomimetic LVSD and ESHF treatment method to either replace damaged native tissue or facilitate regeneration. The AVEM presents a dual purpose; as a cell platform for cardiac myocyte delivery and as a 3D bio-artificial support structure for host integration.

Present research exploits a niche in using acellular ventricle ECM. Natural acellularized matrices have been characterized as cell delivery platforms for various organs and species. Ott et al., [38] utilized whole rat acellular hearts, loaded with cardiac cells, to promote functional differentiation, as a comparison of native and acellular ECM. Eitan et al., [55] characterized acellular porcine ventricle ECM mechanical properties and its propensity to functionally couple cardiac cells, measured by protein expression.

Figure 4.3 demonstrates the validity of acellular ECM viability as scaffolds, as porosity is retained following decellularization. The average pore size of tissue sections, native ($0.0019mm^2$) and acellular ($0.1355mm^2$), compared to the size of the cardiac myocyte (80-960μm^2 area) validates the suitability of acellular ventricular tissue to encourage myocyte infiltration. The differences in pore size between native and acellular tissue are explained by the relative density of cellular material and sarcomeric activity observable in each; native heart includes more structural components such as desmin and α-actinin to augment the underlying collagen structure. Viability of primary cardiac myocytes, and other cardiac cells, within the decellularized ventricle validates its retention of biocompatibility.

The AVEM was defined to be the acellular scaffold loaded with a total of $4x10^6$ cardiac cells. This cell quantity was chosen since it demonstrated the highest macroscopic contractile frequency (36bpm±2bpm, n=2, culture day three) during the optimal cell load studies (**Figure 4.4A**) and showed a greater qualitative force and coherence of contraction, comparatively. Additionally, this cell load had the highest cell count per area scaffold (66cells±23cells per $1.33mm^2$, n=4) compared to the other cell loads. The lower cell count in tissues loaded with $6x10^6$ cells may be explained by the short four day period allotted to passive-seeding, and the technique of passive-seeding inefficiently encouraging more cell infiltration into the scaffold, despite the use of a higher cell load. However, the cell content remained significantly lower than that of the native tissue (native vs cell load, t-test, $p<0.05$ for all) (**Figure 4.4B**).

Patch contraction was observed 48-72hours after cell loading. The twitch force and Frank-Starling relationship, shown in **Figures 4.5** and **4.6**, are experimentally validated by the acellular ventricle tissue negative control data (**Figure 4.5A**). Values for native tissue have been described extensively in previous studies (42nM) [65, 66]. The maximum

spontaneous twitch force observed within this study was 388.3μN. The twitch force of fresh rat ventricular tissue is 42mN [65]. The twitch force of mammalian tissue ranges over 25mN to 44mN, and is dependent on contractile frequency [66]. Contractile frequency plateaued between the pre-tension ranges of~1200 - ~2400μN. The magnitude of contraction, displayed as the Frank-Starling relationship in **Figure 4.6**, was initially exponential in response to an increased pre-tensile force, with a plateau at ~2400μN. AVEM tissues responded to pre-tensions as they do in native tissues. In order to simulate these biomechanical outputs, the AVEM would need to be optimised for cell loading and pre-tension.

Figure 4.7 characterizes the AVEM. Cell permeation and clustering were observed both at the AVEM periphery and centre. Presence of interior cell clusters and the measured porosity of the AVEM validate its conduciveness for cell migration and infiltration. Structurally, desmin and α-actinin staining, shows some observable myocyte sarcomeric organization in the AVEM both centrally and peripherally, clustered around nuclei. Contractions were predominantly observed at the scaffold periphery. This is explained by the presence of troponin I, in greater amounts at the scaffold periphery, in congruence with nuclei clusters. Although cells permeated further towards the centre of the AVEM, no troponin I was seen. Collagen staining shows retention of the underlying acellular scaffold architecture and the relative arrangement of nuclei.

This study provides a foundation to validate the applicability of AVEM, however numerous optimizations are required. Cell retention, cell-matrix infiltration and construct functionality represent the primary optimization variables. For any natural tissue engineered concept, biocompatibility and immune response remain significant variables. Autologous cardiac myocytes or stem cells must be made available to address these considerations. ECM sourcing must also consider these variables despite the acellular

nature of the structure. AVEM may overcome the limitations brought about by the complexities of storage and transport facing organ transplantation.

AVEM cell loading was a passive process; a cell solution was loaded onto both the superior and anterior surface of the scaffold, respectively. The cell loading process may be described as passive migration-seeding; diffusion represents the active process of cell migration with a 3D matrix, without bioreactor mediated control. This diffusion process relies on static culture conditions and matrix characteristics. Passive-seeding limits the degree to which myocytes can permeate the scaffolds, thus limiting AVEM twitch force and contractile frequency, due to the diminished number of functional interactions occurring towards the centre of the construct. A more effective cell seeding and dynamic culture protocol must be developed, to ensure cell-matrix infiltration. Cell loading techniques of direct scaffold injection coupled with diffusion loading or fibrin gel cell entrapment may be employed.

AVEM must be characterized to define mechanical and electrical properties, to ensure comprehensive function as regenerative scaffolds for cardiac myocyte delivery; chronological studies to define time to peak AVEM function in culture and time at which AVEM cells interact with the native heart. This information would serve to define variables to condition the tissue in future bioreactor studies. Following AVEM optimization, clinical implantation presents two options for application. The first is determination of *in vivo* model integration and vascularization capabilities; patch overlay on existing tissue to provide a regenerative cell delivery mechanism. Another application would be as 3D bioengineered heart muscle for complete replacement of non-functional tissue.

4.5 Conclusion

This foundation AVEM model has shown feasibility as a unique platform concept in bioengineering 3D artificial heart muscle. There are multiple validation considerations to further optimize the AVEM model. Primarily, optimization is required on a cellular level, through seeding methodology, with further mechanical and electrical validation by chronological and bioreactor development studies. AVEM has the potential to be a tissue-engineered cell delivery platform for the treatment of LVSD and ESHF.

4.6 Summary

The AVEM model allows us to answer the research question: Can we develop a better understanding of the ideal LV material platform, the LV itself? Passive cell seeding resulted in functional constructs, capable of generating contractile force, eliciting a Frank-Starling cardiac-type function with demonstration of cardiac myocyte infiltration both peripherally and centrally within the AVEM scaffold, based on scaffold pore size and cell-ECM coupling. We can now develop a BEOV model, with a view to emulating the characteristics evaluated in the AVEM model.

CHAPTER 5

THE DESIGN AND FABRICATION OF A THREE-DIMENSIONAL BIOENGINEERED OPEN VENTRICLE

Current treatments in HLHS include multiple surgeries to re-functionalize the right ventricle and/or transplant. The development of a tissue-engineered LV would provide a therapeutic option to overcome the inefficiencies and limitations associated with current treatment options. This study provides a foundation for the development and fabrication of the bioengineered open ventricle (BEOV) model. BEOV molds were developed to emulate the human LV geometry; molds were used to produce chitosan scaffolds. BEOV were fabricated by culturing 30million rat neonatal cardiac cells on the chitosan scaffold. The model demonstrated 57% cell retention following four days culture. The average biopotential output for the model was 1615μV. Histological assessment displayed the presence of localized cell clusters, with intercellular and cell-scaffold interactions.

5.1 Introduction

HLHS is a congenital condition developed *in utero*, which incapacitates the heart from supporting systemic circulation, primarily due to underdevelopment of the LV. HLHS is fatal if left untreated, with 95% of fatalities occurring within the first two weeks of birth [67], and it accounts for 25-40% of all neonatal cardiac deaths [68]. Current HLHS treatments are highly invasive, yielding an inefficient outcome; 55% survival rate within the first 5 years of treatment [69].

Three-dimensional cell-based tissue engineering strategies may provide alternative HLHS treatment options to potentially replace or augment current treatments. The ethics and source considerations associated with transplant may be superseded. The potential to overcome biocompatibility and biomimetic considerations, by use of autologous cell sources and optimized scaffolds, is also advantageous. Current surgical treatments do not directly address the underdeveloped LV and yield inefficient solutions in HLHS. Tissue engineering provides the potential to develop a 3D bioengineered LV to replace the underdeveloped component and conceivably restore heart function, with maintenance of the anatomical structure of the heart, to produce a more efficient HLHS treatment option.

Current tissue engineering strategies in HLHS are subdivided into four categories, as shown in **Table 5.1** [69].

Table 5.1: Current Tissue Engineering Strategies in HLHS

Tissue Engineering Strategy	Definition	Current Research
Bioengineering	Cell seeding on scaffolds	• Alginate-graft scaffold cell delivery method [33,34] ➢ Disintegrating platform to repair myocardial tissues
Biological Assembly	Cell entrapment in hydrogels for organization	• Planar collagen entrapment to replicate cardiac muscle [35,36] • 3D Matrigel entrapment simulating spherical left ventricle for high-throughput screening [40]
Cell Sheet	Serial stacking of monolayer cultures to form contractile tissues	• Temperature-sensitive cell-sheet system for model fabrication [37]
Re-seeding or decellularization/re-cellularization	Cell seeding on retained extracellular matrix substrates	• Cell-seeded extracellular matrix to replace mechanical pump systems [38,39]

Alginates [33, 34], collagen [35, 36, 40], cell-sheets [37] and ECM [38, 39] have been reported as appropriate scaffold materials for 3D tissue engineering. The majority are graft-type models applied as augments to the HLHS LV, by re-defining either the outer myocardial wall or single ventricle septation [33-35, 37-39]. At present, only one complete LV, based on a spherical model has been developed for high-throughput screening, by Lee et al., [40] using Matrigel cell entrapment. There are numerous considerations associated with scaffold biomaterials: the method to produce the 3D structure, biocompatibility, functional and mechanical biomimetic properties and longevity with regards to degradation kinetics. The use of chitosan mitigates these considerations; it has been extensively characterized to demonstrate structural integrity and favourable long-term degradation kinetics [70].

We propose the development of a 3D BEOV as the initial stage in developing an implantable treatment in HLHS. The study focuses on scaffold fabrication and determining fundamental biocompatibility. The presented concept is novel, with the potential to have a significant impact on the field of tissue engineering and furthermore, in the development of an alternative treatment option in HLHS.

The BEOV was based on the human neonate LV geometry [71]. BEOV molds were designed using CAD software. Models were fabricated using a 3D printer. Chitosan was used as the polymeric scaffold biomaterial, loaded into molds and lyophilized to produce the BEOV scaffold. Scaffolds were rehydrated and populated with rat neonatal primary cardiac cells. Scaffolds were characterized for material properties to assess composition, morphology and topology at lyophilized, rehydrated and cell-loaded stages. The cell-loaded BEOV model was further characterized for cell retention and cellularization efficiency, biopotential activity and histological assessment.

5.2 Materials and Methods

All protocols were approved by the Institutional Animal Care and Use Committee (IACUC) in accordance with the "Guide for the Care and Use of Laboratory Animals" (NIH publication 86-23, 1986).

5.2.1 Mold Fabrication: Computer-Aided Design and 3D Printing

CAD software was used to develop an open ventricle model. The two part mold, inner and outer, was designed to form a ventricle of the same geometry as the human neonate LV (**Figure 5.1A**) [71] and emulate the cone shape of the LV (**Figure 5.1B**). The combination of components provides a tapered cavity width (**Figure 5.1C**) to consistently produce scaffolds of defined wall thickness and geometry.

The CAD model was fabricated using a Makerbot Replicator2 3D printer with Makerware software (Makerbot LLC., Brooklyn, NY). Thermoplastic polylactic acid (PLA) filament (Makerbot LLC.) was the extruded material for the 3D printer. Molds were printed at high resolution (layer height 100µm) to retain tight tolerances on the curved geometry (**Figure 5.1D**).

To determine consistency between the CAD models and 3D printed molds, the values of cone height, diameter and wall thickness at three set points, were measured (**Figure 5.1E**). Significant variations between CAD models and 3D printed molds were measured using a t-test with $p \leq 0.05$.

5.2.2 Scaffold Fabrication, Preparation and Verification

Chitosan scaffolds were prepared using a previously described method [72]. Multiple chitosan concentrations of 0.5%, 1%, 2%, 2.5%, 5%, 10% and 15%w/v in acetic acid were fabricated. All outcomes were macroscopically examined for the variables of self-

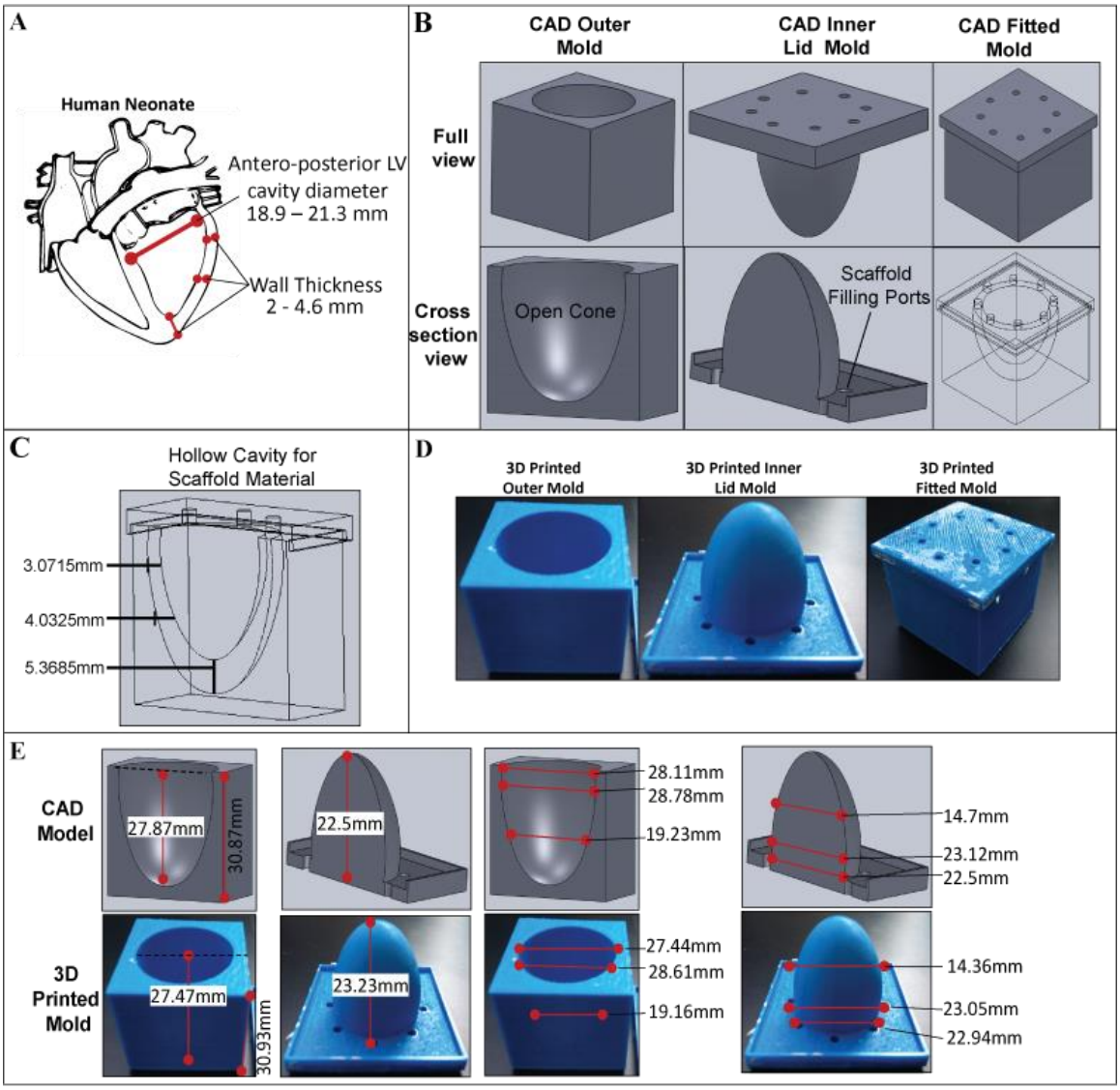

Figure 5.1: Geometry, design and fabrication of BEOV molds. **A:** Human Neonate LV. **B:** CAD LV model. **C:** BEOV design wall thickness. **D:** 3D Printed Mold Components. **E:** CAD and mold measurements.

supporting 3D structure, ability to withstand manipulation and manual handling and relative flexibility.

Chitosan (Carbomer Inc., San Diego, CA) was solubilized in 0.2M Acetic Acid (Glacial Acetic Acid, Macron Fine Chemicals, Centre Valley, PA) in de-ionised water, by continuous mixing at room temperature for 24hours. The solution was transferred to fill

the fabricated molds, which were then frozen at -80°C for 24hours. Samples were then lyophilized for 24hours (Labconco Freezone 4.5, Labconco Corporation, Kansas City, MO). **Figure 5.2A** describes the process.

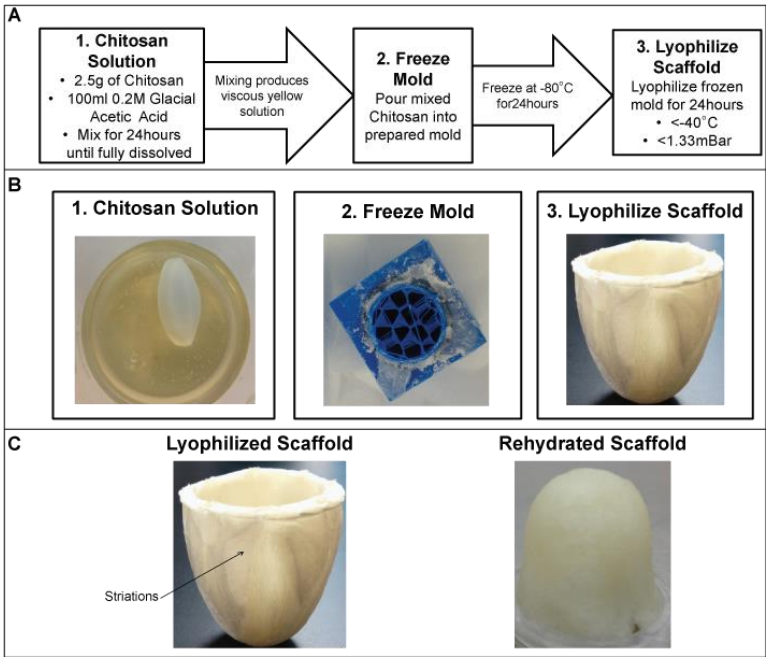

Figure 5.2: Fabrication of BEOV Scaffolds. **A:** Process to produce BEOV scaffolds. **B:** Individual stages of Scaffold Fabrication. **C:** Lyophilized and rehydrated BEOV scaffold.

Lyophilized scaffolds were rehydrated prior to cell loading using a previously described method [47]. Scaffolds were rehydrated by immersion in a 0.1M NaOH solution; NaOH pellets (Macron Fine Chemicals) in de-ionized water, for 30minutes. Scaffolds were then washed three times in PBS and sterilized in 80% ethanol for 1hour prior to storage. Sterilized scaffolds were stored in sterile PBS until use. Immediately preceding cellularization, scaffolds were sterilized using 80% ethanol, rinsed with sterile PBS, exposed to UV light for 20minutes and air-dried in a laminar flow hood.

The consistency between the CAD model, 3D printed mold, lyophilized and rehydrated scaffolds was evaluated by measuring the surface area (SA.mm^2) and

volume (V.mm^3) of the material cavity and scaffold material, respectively (**Figure 5.3A**), using the radius of the open face of the ventricle (*a*), separately, and the height of the scaffold (*h*).

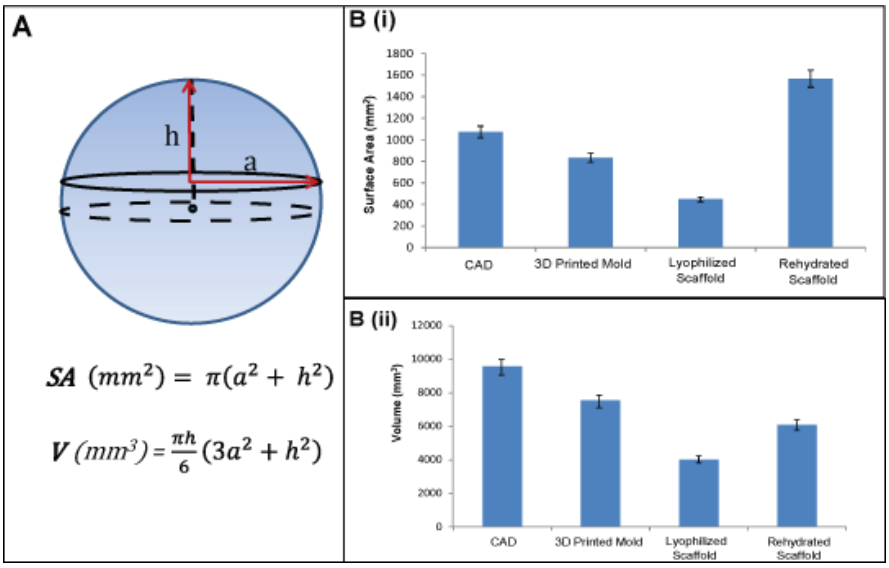

Figure 5.3: Scaffold Uniformity and Reproducibility. **A:** Surface area and volume formulae. **B: i)** Surface area and **ii)** Volume of the model, mold cavity, and scaffold material.

The outer face SA, inner face SA and SA of the planar open face ring were summed to find the total SA of the scaffold

$$\boldsymbol{SA} = \pi(a^2 + h^2). \qquad \textbf{(5.1)}$$

The V was calculated by subtracting the total V of the scaffold, based on the outer face radius, from the total V of the inner face radius, to account for the thickness of the scaffold

$$\boldsymbol{V} = \pi h/6(3a^2 + h^2). \qquad \textbf{(5.2)}$$

Using these values, the density (*D.mg/mm*^{3}) of the scaffold material in the lyophilized and rehydrated scaffolds was calculated, using mass (*M.mg*) and (*V.mm*^{3})

$$\boldsymbol{D} = M/V. \qquad \textbf{(5.3)}$$

The consistency of the design process, throughout the fabrication process, was evaluated using statistical analysis (t-test, p≤0.05).

5.2.3 Fabrication of a 3D Bioengineered Open Ventricle

Cardiac cells were isolated from the hearts of two to three day old neonatal Sprague-Dawley rats using an established method [50].

Prepared scaffolds were secured in clip rings and mounted onto a single platform, as shown in **Figure 5.4Ai**.

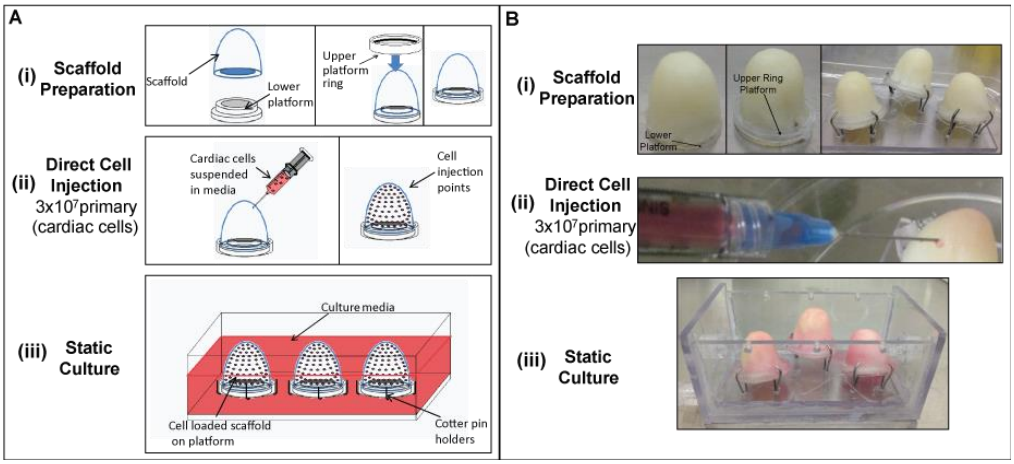

Figure 5.4: Fabrication of the 3D BEOV. **A: i)** Rehydrated scaffold prepared, **ii)** Direct cell injection, **iii)** Culture. **B: i)** Scaffolds secured on platform, **ii)** Direct cell injection with 3x10^7 cells, **iii)** BEOV Static culture.

A total of 3x10^7 rat neonatal cardiac cells were injected into the scaffold through the surface at multiple points. The total number of cells matches the loading density of our previous AVEM model using a decellularized extracellular matrix [39], based on relative scaffold volumes. Scaffolds were elevated from the base of the platform to increase the

surface area of the BEOV in contact with the culture medium and support cell viability during the culture period.

Cellularized BEOV were cultured as shown in **Figure 5.4Aiii**. The platform holding the BEOVs was secured into a custom housing for static culture. Culture medium composed of M199 (Life Technologies, Grand Island, NY), with 20% F12k (Life Technologies), 10% foetal bovine serum, 5% horse serum, 1% antibiotic-antimycotic, 40mg/ml hydrocortisone and 10ng/ml, was added to submerge the BEOV. BEOV were maintained in an incubated environment at 37°C supplied with 5%CO_2 for four days.

5.2.4 BEOV Materials Characterization

Lyophilized scaffolds, rehydrated scaffolds and BEOV were characterized for material properties.

FTIR was used to determine the scaffold composition, assessing quality and consistency. FTIR was performed by creating a pellet of sample and analyzing absorbance of the pellet on a Nicolet 6700 FTIR Spectrometer (ThermoFischer, Waltham, MA). The spectra were obtained using a total of 64scans accumulated at $4cm^{-1}$ resolution and reported after background subtraction, baseline correction and binomial smoothing, using OMNIC software (ThermoFischer Scientific).

SEM was used to determine construct surface morphology. Samples were washed with PBS and fixed in 2.5% glutaraldehyde (Electron Microscopy Sciences, Hatfield, PA) for 30minutes. After washing in PBS, scaffolds were dehydrated in ascending concentrations of ethanol (30%, 50%, 70%, 80%, 90%, 95% and 100%) for 10minutes each. Samples were then incubated in 50% ethanol-hexamethyldisilazone (HMDS) solution for 10minutes, followed by incubation in 100% HMDS for five minutes to prepare for overnight incubation in a desiccator. Specimens were mounted on SEM stubs using

a carbon conductive adhesive tape. Samples were sputter coated with a 7nm layer of Pt using a Cressington 208HR sputtering system (Cressington Scientific Instruments Inc., England, UK). SEM images were acquired under high vacuum, at 10kV, spot size 4.0nm, using an FEI NovaNanoSEM 230 (FEI, Hillsboro, Oregon). ImageJ (NIH, Bethesda, MD) was used to analyse pore size.

The scaffold topology was characterized by nano-indentation contact mode AFM using a Bruker Biocatalyst AFM (Bruker, Santa Barbara, CA), to assess the mechanical properties at a nanometric scale. For contact mode, the silicon nitride cantilevers (MLCT, Bruker) were set to a spring constant of 0.024N/m. Measurements were obtained in PBS under ambient conditions at room temperature. For Young's modulus determination, the cantilevers were first calibrated using a standard silicon sample to get the spring constant and sensitivity. Then elasticity moduli were calculated from force curves using Nanoscope Analysis 1.50r1 software (Bruker). Imaging was performed at a 0.1Hz scan rate with a contact force of 0.9nN. All offline image flattening and analyses were conducted with the same software.

5.2.5 BEOV Biopotential Measurement

BEOV cardiac biopotentials were measured to evaluate cardiomyocyte electrophysiological activity and cell-cell interactions. After the four day culture period, constructs were manipulated to increase the surface area in contact with a 32 electrode biopotential sensor and arranged in a 4x8 array. Raw output data was generated in PowerLab and processed in MATLAB using a custom script. Raw data channels were examined for periodic waveforms in multiple channels. In comparing the multiple channels, waveforms are expected to be out of phase to represent the latency in the depolarization wave at different points in the BEOV.

5.2.6 Cell Viability

The BEOV characteristics of cell retention and cellularization efficiency were evaluated using an MTT assay (Cell Viability MTT Assay Kit, Sigma-Aldrich, St Louis, MO). BEOV sections were excised at prescribed locations using a 6mm biopsy punch, immediately after cellularization and after four days of culture, and placed in a 48-well plate (Sigma-Aldrich). MTT stock solutions were prepared according to the manufacturer's protocol and added to a monolayer cardiac cell standard (300,000 to 50,000 cells) and BEOV sections were incubated for 12hours. Following incubation, scaffolds were moved to a new well and the formazan crystals within the BEOV sections and within the media were solubilized separately with isopropanol (0.04-0.1N HCl in absolute isopropanol). Absorbance of the converted dye was measured using an Epoch Microplate Spectrophotometer (Biotek, Winooski, VT), at a wavelength of 570nm with background subtraction at 690nm. Using the standard monolayer culture absorbance readings, a reference plot for absorbance versus cell quantity was produced.

MTT was used to determine the scaffold cell retention during culture. The average expected total cell content for the sections measured ($avge_s$) was calculated using the total rehydrated scaffold volume (V) calculated in **Eqn 5.2**, the initial cell load ($3x10^7$ cardiac cells),assumed to be uniformly distributed in the scaffold and the average volume of the 6 measured sections (V_{sec})

$$\boldsymbol{avge_s} = [(3x10^7)/V] * V_{sec}. \quad \textbf{(5.4)}$$

Utilizing the measured average cell counts present in the scaffold (cc_{scaf}) and in the culture solution (cc_{sol}), the average percentage cell retention of the sections was calculated for the amount of cells retained in the scaffold (*%scaf*) (**Eqn 5.5**), in the culture solution (*%sol*) (**Eqn 5.6**) and dead cells (*%dc*) (**Eqn 5.7**), as follows, overleaf:

$$\%\boldsymbol{scaf} = (cc_{scaf}/avge_s)x100\%, \quad \textbf{(5.5)}$$

$$\%\boldsymbol{sol} = (cc_{sol}/avge_s)x100\%, \text{ and} \quad \textbf{(5.6)}$$

$$\%\boldsymbol{dc} = 100\% - (\%scaf + \%sol). \quad \textbf{(5.7)}$$

Cellularization efficiency was used to determine the uniformity of cell distribution obtained by direct cell injection (DCI). The expected cell count per unit volume of scaffold ($avge_{uv}$) (cells/mm^3), for homologous cell injection was calculated using the initial cell load (3x10^7 cardiac cells) and the total scaffold volume (V), calculated in **Eqn 5.2**

$$\boldsymbol{avge_{uv}} = (3x10^7)/V. \quad \textbf{(5.8)}$$

The expected cell content for the average volume ($avge_{acc}$) of sections was calculated, using the value derived in **Eqn 5.8** and the average scaffold volume of sections (V_{sec})

$$\boldsymbol{avge_{acc}} = avge_{uv}\, x\, V_{sec}. \quad \textbf{(5.9)}$$

The expected average cell content value for sections was compared to the measured average cell content for sections.

5.2.7 BEOV Histology

Following culture, to determine contractile, sarcomeric and cell-cell interactions within the BEOV, constructs were placed in Peel-a-way disposable embedding molds (VWR International, Radnor, PA), immersed in Tissue-Tek OCT compound (VWR International) and frozen at -80°C for 24hours. Planar sections of 20µm thickness were cut using a Cryotome (ThermoFischer Scientific) and placed onto VWR microslides.

Non-specific epitope antigens were blocked with 10% goat serum in 0.05% Triton-X100 PBS, at room temperature for one hour. To show contractile factors, sections were incubated with rabbit anti-troponin I, 1:100 (ab47003, Abcam, Cambridge, MA). To show sarcomere presence, sections were incubated with mouse anti-α-actinin, 1:200

(Sigma-Aldrich, Catalog No. A7811). To show cell-cell interactions, sections were incubated with rabbit anti- Cx43, 1:100 (ab11370, Abcam). All sections were counterstained for nuclei with DAPI (2.5µg/ml) for five minutes at room temperature. Fluorescent images were obtained with a Nikon C2+ confocal laser scanning microscope (Nikon Instruments Inc., Melville, NY).

5.3 Results

5.3.1 Design, Fabrication and Geometry of BEOV Molds

Figure 5.1A shows the values associated with the structure of the human neonatal LV; the values are ranges, since the anterio-posterior (AP) LV cavity diameter varies between individuals and the outer myocardial LV wall thickness is tapered.

Figure 5.1B shows the cone-shaped BEOV design used to replicate the architecture of the LV. The outer and inner components fit together to produce a tapered wall cavity ranging from 3.02-5.37mm thickness (**Figure 5.1C**): a taper similar to that of the human neonate LV. The 3D printed mold (**Figure 5.1D**) shows retention of the shape and curved geometry of the design models.

Figure 5.1E shows the values associated with the AP LV cavity and variability in cone diameter contributing to the outcome model wall thickness. The CAD model wall thickness is 3.02-5.37mm and the 3D printed mold wall thickness is 2.94-5.37mm. The measured values for the 3D printed model are 2.6% less on the lower bound and exact on the upper bound compared to the CAD model and are deemed not statistically significant in difference ($p>0.05$, t-test).

5.3.2 Fabrication of BEOV Scaffolds

Multiple chitosan concentrations were used to produce scaffolds. The optimal chitosan concentration was determined by macroscopic observation and tangible

properties. Chitosan produced at a concentration of 2.5%w/v, yielded these preferred properties. The chitosan solution was a transparent yellow viscous solution (**Figure 5.2B**). Following lyophilization, **Figure 5.2B** shows the outcome BEOV scaffold. It is a 3D self-supporting structure, which has retained the 3D geometry and shape of the mold. Additionally, striations are observable in the material following lyophilization; chitosan polymer fibres are arranged around ice crystals formed during the pre-freezing process and these crystals are subsequently removed during sublimation, leaving a pore around which polymer fibres are arranged. **Figure 5.2C** shows the scaffold after rehydration; the scaffold striation is no longer observable due to material swelling, which reduces the pore size around which the polymer is arranged.

5.3.3 BEOV Scaffold Uniformity and Reproducibility

To establish the uniformity between CAD models, 3D printed models, lyophilized and rehydrated scaffolds, the SA, V and D were calculated, for the amount of material constituting the scaffold. As discussed in Results 5.3.1, the CAD model and 3D printed molds show no statistically significant difference with regards to geometry. The SA and V of the 3D printed mold is approximately 20% smaller than that of the CAD model (**Figure 5.3B**) (CAD model, n=1, SA = 1072.75mm^2, V = 9545.53mm^3).

Comparatively, the lyophilized scaffolds (n=10) had a SA 58% lower than that of the CAD model. The V of the lyophilized scaffolds was 64% lower than that of the CAD model. Rehydrated scaffolds (n=10) demonstrated a higher material SA than the CAD model. The rehydrated scaffold SA was 45% greater than that of the CAD model. The V of the rehydrated scaffolds was 36% lower than that of the CAD model.

The rehydrated scaffold had a density 62% greater than that of the lyophilized scaffolds (lyophilized scaffold, n=10, D=0.0617±0.0036mg/mm^3 and rehydrated

scaffolds, n=10, D=0.3906±0.038mg/mm^3).

5.3.4 Material Characterization of BEOV

BEOV were characterized in terms of chemical structure using FTIR, morphology and physical structure using SEM and surface topography and mechanical properties using AFM.

By observing the chemical bonds present in chitosan, the absorbance peaks occurring at specific wavelengths in the FTIR spectra can be interpreted to correspond with specific bonds. When the chitosan scaffolds are lyophilized and then rehydrated with NaOH, conformational changes may occur, due to cross-linking, which results in structural rearrangement of chitosan molecules to form covalent bonds and/or cross links [73]. The main characteristic absorbance bands of chitosan, were at 1650-1550cm^{-1}, 1430-1360cm^{-1} and 1190-990cm^{-1}, to show amide I (C=O), amide II (NH_2) and glycosidic linkage, respectively (**Figure 5.5A**, Chitosan Powder). Lyophilized scaffolds, wherein chitosan solution was prepared with aqueous acetic acid, showed the presence of three defined peaks at 1450cm^{-1}, 1295cm^{-1} and 1190cm^{-1}, representing amide III (C-N stretching and N-H deformation) and glycosidic linkage, respectively (**Figure 5.5A**, Lyophilized Scaffold). Rehydrated scaffolds, washed with NaOH solution, showed the presence of three bands at 1680-1575cm^{-1}, 1310cm^{-1} and 1120-1020cm^{-1}, representing amide I (C=O, stretching), amide II (shifted spectra NH_2 deformation) and amide III (C-N stretching and N-H deformation), respectively (**Figure 5.5A**, Rehydrated Scaffold). Cellularized scaffolds, the BEOV, showed the presence of 2 peaks at 1700-1600cm^{-1} and 1100-900cm^{-1} to show C=O stretching and glycosidic linkage, respectively (**Figure5.5A**, BEOV). The wave number associated with specific bands may shift due to samples being obtained at different times.

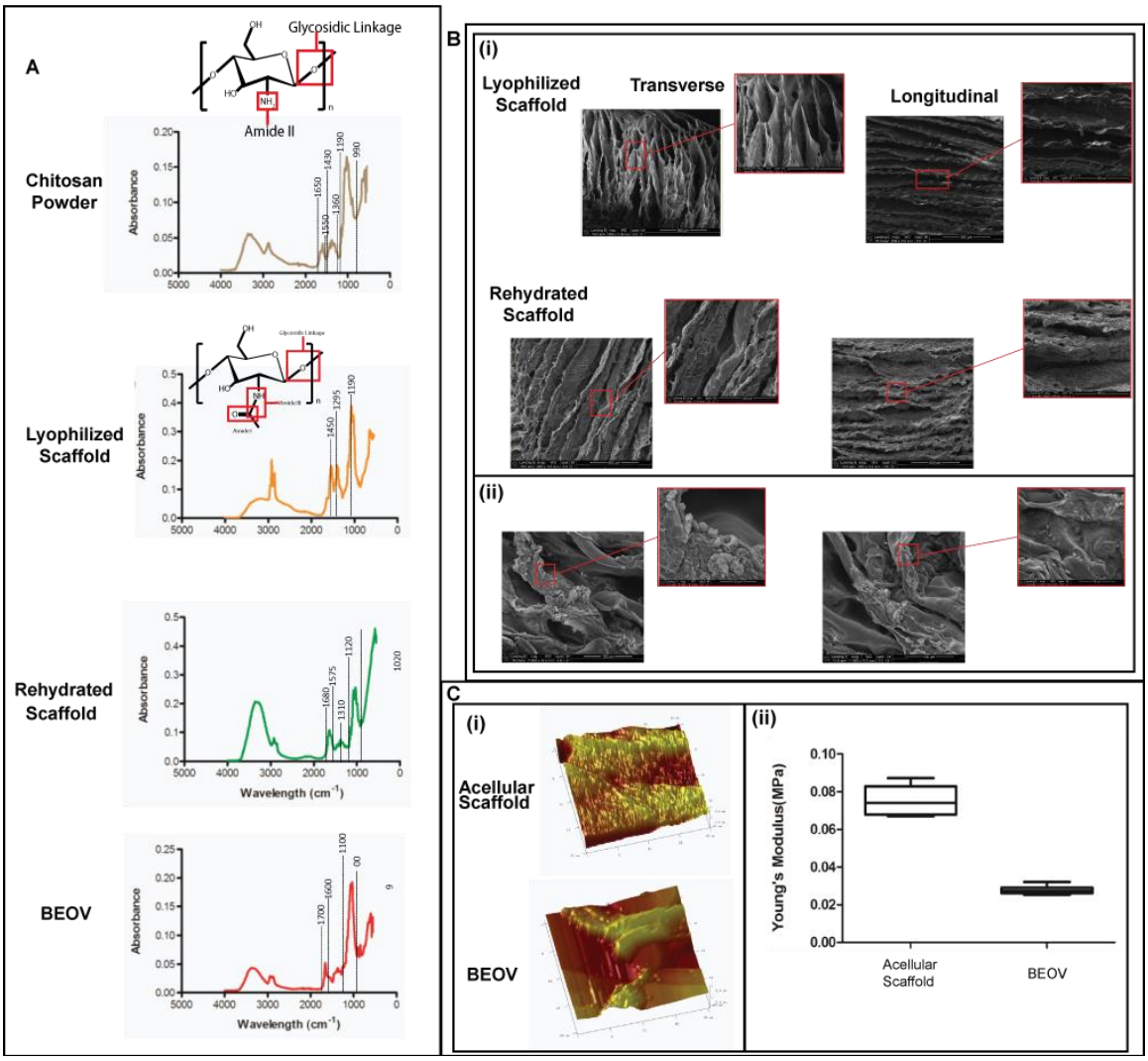

Figure 5.5: Material Characterization. **A:** FTIR spectra. **B.** SEM for **i)** Lyophilized and rehydrated scaffolds and **ii)** BEOV. **C. i)** AFM topological maps and, **ii)** Young's modulus for rehydrated acellular and BEOV.

Figure 5.5Bi shows SEM for transverse and longitudinal scaffold sections, both for lyophilized and rehydrated samples. Using ImageJ, the average pore size, cell sheet thickness and inter-sheet distance were calculated for both lyophilized and rehydrated samples. The average pore size of the native rat ventricular tissues is $0.0019\pm0.0018mm^2$ (mean ± standard deviation) [39]. Pore size decreased by 13% on rehydration. The average pore size for lyophilized scaffolds (n=1) was $0.0265\pm0.1655mm^2$ and for rehydrated scaffolds (n=1), $0.0035\pm0.0203mm^2$. Cell sheet

thickness increased by 39% on rehydration. The average cell sheet thickness for lyophilized scaffolds (n=1) was 50.49±12.43µm and for rehydrated scaffolds (n=1), 70.17±8.93µm. Inter-sheet distance decreased by 54% on rehydration. The inter-sheet distance for lyophilized scaffolds (n=1) was 70.19±15.88µm and for rehydrated scaffolds (n=1), 38.13±9.54µm.

Figure 5.5Ci shows the 20x20µm image of both lyophilized chitosan and the cellularized BEOV surface. Cell clusters are observable on the surface of the cellularized BEOV. Additionally, following rehydration and cellularization, the scaffold surface appears smoother. **Figure 5.5Cii** shows the comparative Young's modulus for lyophilized and cellularized BEOV scaffolds. The elastic modulus, or the relative material rigidity, decreases by 60%, from 0.075mPa to 0.03mPa following cellularization.

5.3.5 BEOV Cardiac Biopotentials

In total, six BEOV were analysed in this study; all samples demonstrated measureable biopotential activity, with localized contractions observable under a 2D light microscope, within 48-72hrs of direct cell injection. **Figure 5.6A** represents the measurement setup and **Figure 5.6B** represents eight channels demonstrating biopotential activity. For BEOV (n=6), the number of electrodes detecting biopotential signals ranged from 8-32 of a potential 32 electrodes. Individual channels were examined, and peak values were tabulated to calculate the average biopotential for the constructs. A threshold value was set between 250-3500µV for the averaged values. The average biopotential amplitude of BEOVs was 1615.267±1129.787µV (mean ± standard deviation).

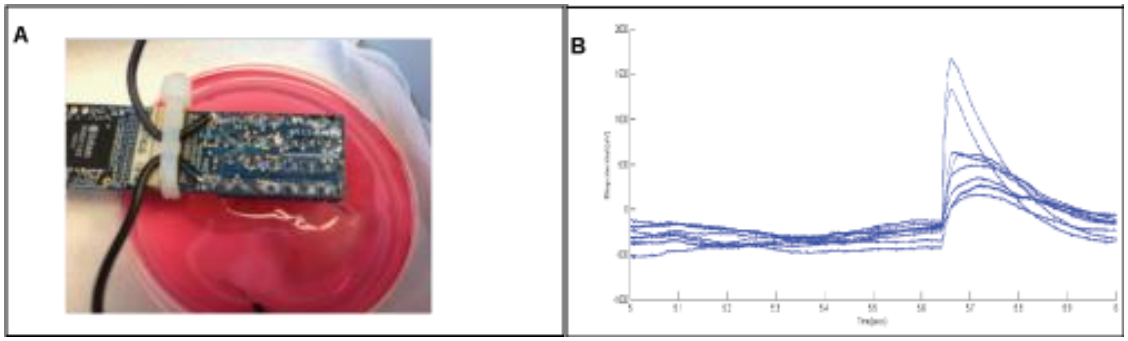

Figure 5.6: BEOV Biopotentials. **A:** Biopotential measurement setup. **B:** Overlayed biopotential readings from 8 of 32 channels, representing BEOV biopotential activity.

5.3.6 Material Cell Retention and Cellularization Efficiency

Figure 5.7A illustrates the BEOV section excision process.

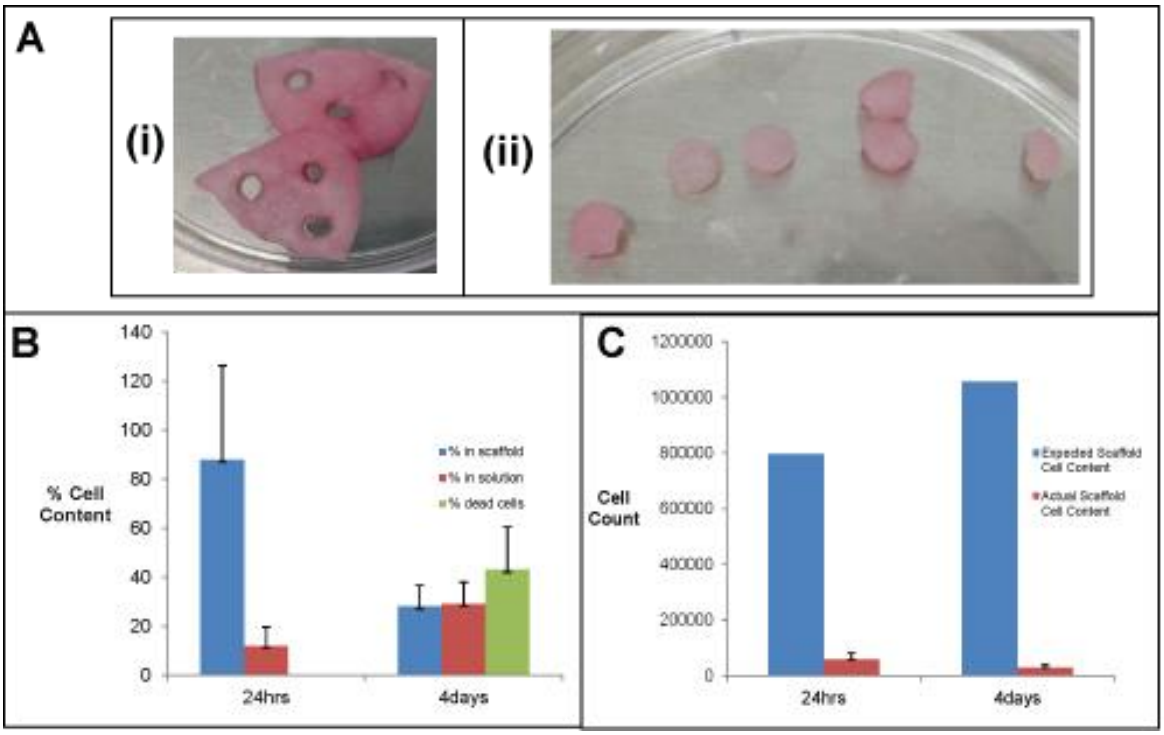

Figure 5.7: MTT Analysis. **A. i)** Scaffold setup, **ii)** Six biopsy punched 6mm diameter cellularized scaffold sections. **B.** Cell retention and **C.** Direct cell injection efficiency at 24hours after cell injection and after four days culture.

Figure 5.7B shows cell retention efficiency; the given percentage values describes the average cell retention in the six excised sections. The variable of cell loading uniformity was assumed to be a completely homologous process. Twenty four hours after cell injection, the average total number of cells expected to be retained in sections compared to those retained 24hours after cell loading, was 100%, with 88±38.39% (mean ± standard deviation) of cells retained in the scaffold and 12±7.63% retained in the culture solution. After the four day culture period, the proportion of the total number of cells retained was 57% of the expected amount to be retained, with 28±8.65% in the scaffold and 29±8.95% in the culture solution. The remaining 43±17.44% was assumed to be dead cells.

Figure 5.7C shows the efficiency of the direct injection cellularization process. The expected number of cells per unit volume of the scaffold only, was approximately 5000cells/mm^3. The average number of cells per scaffold section, 24hours after cell injection was 59744±20902cells (370cells/mm^3) and four days after cell injection, 29292±9835cells (138cells/mm^3).

5.3.7 Characterization of the BEOV Regenerated Tissue

Figure 5.8 shows histological BEOV characterization in comparison to healthy native heart tissues and acellular BEOV scaffolds, for a range of cardiac specific factors. As expected, the native rat ventricle demonstrates a high level of cardiac-specific troponin I. α-actinin is abundantly present and Cx43 is also present. The chitosan scaffold, without cardiac-cells shows a complete absence of cardiac-specific troponin I (CTnI), α-actinin and Cx43. BEOV show the presence of CTnI with localized cell clusters. α-actinin is present with some observable sarcomeric organization to indicate the underlying presence of cardiomyocytes. Cx43 occurred in cell clusters to verify cell-cell interactions in BEOV.

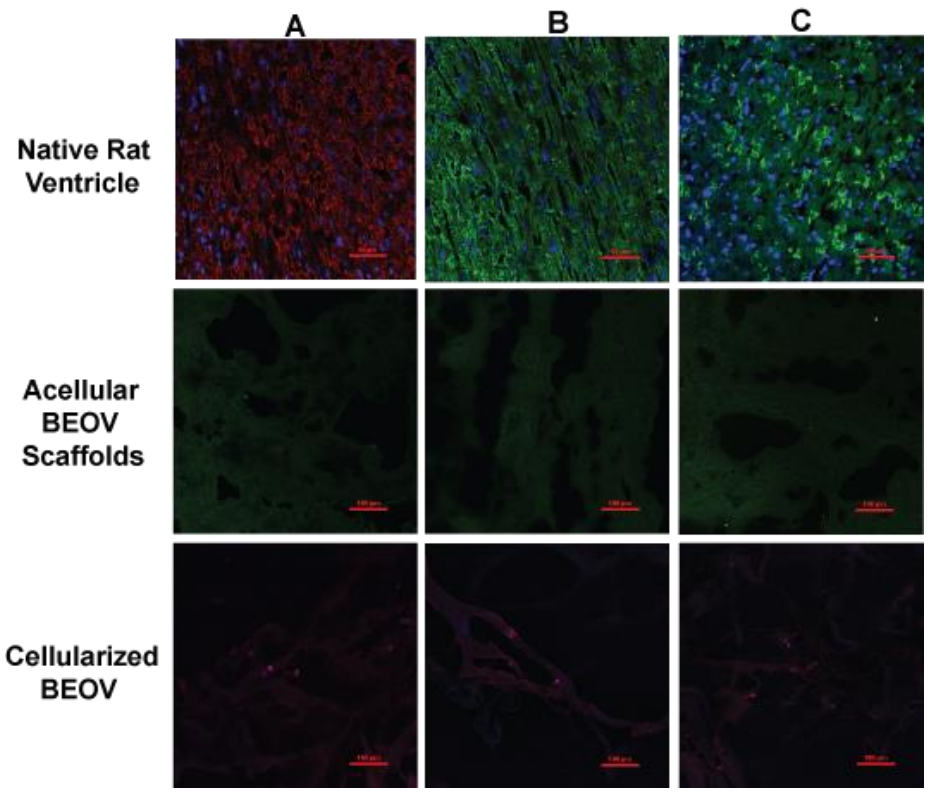

Figure 5.8: Immunostaining at 40x for the native tissue and 20x for the acellular and cellularized BEOV, with DAPI in blue, for **A.** CTnI (red/green), **B.** α-actinin (red/green) and **C.** Cx43 (red/green).

Cells predominantly form localized clusters within the scaffold structure. The presence of the three factors existed only in areas with cell clusters.

5.4 Discussion

This study describes the fundamental stages in designing a physiologically replicative and direct treatment method for HLHS, to replace the underdeveloped LV component. The BEOV provides a self-supporting 3D structure which replicates the architecture and geometry of the LV, with the potential to emulate physiological LV function.

Present research solutions in HLHS demonstrate a niche, with respect to the development of a self-supporting 3D LV. The singular 3D LV model described at present is the cardiac organoid model for drug screening, developed by Lee et al [40].

The cardiac organoid model employs a balloon catheter to provide a spherical LV-type architecture, with encapsulation using a Matrigel cell entrapment system. Following culture and balloon catheter removal, the organoid spherical shape is maintained using a Langendorff system. The model has a spherical architecture, as opposed to the cone-shaped architecture of the LV and is not self-supporting as it requires a continuous flow-pressure loop to maintain shape. The remainder of tissue engineering research to address HLHS is focussed on graft-type applications to either provide an augmentative support structure, single ventricle wall septation or as a cell delivery platform [33-39].

Chitosan was chosen as the biomaterial for BEOV, as it has been extensively characterized in terms of planar material properties, as a naturally sourced biosynthetic material, and in terms of its numerous clinical applications, such as wound dressings [70]. This study characterizes the material properties of chitosan with respect to production in a complex 3D geometry, both in scaffold development and on cellularization with cardiac cells, to determine endurance to the physiological stresses of ventricular tissue. The nature of the scaffold fibre orientation, following lyophilization, emulates the orientation of a layer of heart muscle fibres in the native LV myocardium. Scaffold fibres follow a patterned orientation with regions of uniformity based on pore size and orientation. These observations can be attributed to chitosan concentration, time to pre-freezing temperature, mold orientation at pre-freezing and lyophilization sublimation conditions. The production of the chitosan solution in highly aqueous acetic acid, coupled with a 24hour period of pre-freezing, wherein the temperature gradient fluctuates, results in the formation of non-uniform water ice crystals. The mold was frozen in one orientation, with the apex at the base for the 24hours period, so pore sizes decrease towards the apex of the scaffold; this explains the observation of striations becoming denser towards the apex of the scaffold. The temperature at which lyophilization was carried out was

lower that than of the pre-freezing temperature, therefore, some ice crystals may have reverted to liquid state prior to sublimation, further contributing to the non-uniformity of striations. Rehydration serves to stabilize the porous structure of the scaffold and neutralize it in preparation for cellularization. Sodium hydroxide rehydration results in material swelling, cross-linking and therefore, reduced pore sizes thus striations are no longer macroscopically observable.

The measured differences between CAD model design and 3D mold geometries are not significant (model versus mold, t-test, $p>0.05$ for all values) (**Figure 5.1E**), thus showing that the 3D mold met the BEOV scaffold modelling standards, with a high degree of tolerance. The determination of material SA and volume in **Figure 5.3** shows that the lyophilized scaffolds demonstrate shrinkage relative to the model and mold. Rehydrated scaffolds have a higher SA, volume and density compared to lyophilized scaffolds. The increased SA can be attributed to the scaffold stretching on rehydration. The increased volume can be attributed to the potential occurrence of cross-linking between chitosan polymers due to partial NaOH acetylation. Cross-linking results in a greater number of small pore divisions and therefore a greater capacity to retain liquid volume. Furthermore, the increased scaffold density at rehydration can also be attributed to the presence of cross-linking.

Figure 5.5 defines the material characteristics of chitosan and the adjunct effects of rehydration and cellularization on a molecular level, morphologically and with regards to physical properties using FTIR, SEM and AFM, respectively. These tests further validate the observations made in **Figure 5.2**.

Figure 5.5A demonstrates the chemical composition of BEOV scaffolds at each stage of preparation. The chitosan powder is de-acetylated. The spectra for lyophilized

scaffolds, demonstrates acetylation, on interaction of the acetic acid and chitosan powder, to enable chitosan dissolution. The acetic acid (CH_3COOH) carboxylic acid group (COOH) interacts with the amide II region of the chitosan molecule. This interaction is demonstrated by the presence amide I and amide III moieties with C-N stretching and N-H deformation (1295cm^{-1}).

The spectra for NaOH rehydrated scaffolds demonstrate the neutralization and structural stabilization of the scaffolds, potentially through cross-linking. Rehydration converts the acetylated amide I and III groups, back to amide II. The spectra shows that a combination of acetylated and de-acetylated molecules remain following rehydration, with the presence of amide I and III C-N stretching and N-H deformation (1200cm^{-1}) and C=O stretching (1680-1575cm^{-1}), and NH_2 deformation (1310cm^{-1}). The peak profile observed with the presence of mixed amide groups on rehydration, may further explain the cross-linking component of rehydration, as it demonstrates the presence of a conformational change in the molecule attributable to hydrogen bonding interactions.

Cellularization appears to stabilize the cross-linking interactions further and therefore the structural conformation of rehydrated scaffolds, with C=O stretching (1700-1600cm^{-1}) and glycosidic linkage (1100-900cm^{-1}) as the remaining spectra observed.

Figure 5.5B demonstrates the morphological changes occurring throughout the BEOV developmental process. The average pore size of a native rat heart ventricular tissue is 0.0019mm^2 [39] and the average cross-sectional area of a cardiac-myocyte is 80-960μm^2 [38]. The average pore size of the BEOV is 0.0265mm^2 and 0.0035mm^2 for lyophilized and rehydrated scaffolds, respectively. Overall, the average BEOV scaffold pore size is amenable to myocyte delivery and retention, thus demonstrating the suitability of the scaffold as the BEOV platform. The calculated BEOV scaffold pore

sizes are larger than that of the native tissue due to chitosan concentration, time to pre-freezing temperature, mold orientation at pre-freezing and lyophilization sublimation conditions, as discussed. Controlling these parameters enables modulation of the BEOV scaffold pore size. Due to the presence of a large amount of water in the scaffold, through aqueous acid dissolution of chitosan, large ice crystals are formed therefore sublimation results in larger pores.

Surface topology showed that the scaffold surface becomes smoother following rehydration and cellularization, with the localization of cell clusters (**Figure 5.5Ci**). The smoother surface properties may be attributed to the presence of cross-linking and chitosan sheet swelling with NaOH, as discussed previously. Cell clusters can be attributed primarily to the direct injection method of cellularization, which results in non-homogeneous cell distribution.

The Young's modulus refers to the rigidity of the scaffold material. In BEOV, material rigidity reduces following cellularization and culture (75kPa-30kPa) (**Figure 5.5Cii**). Comparatively, the Young's modulus of the rat left ventricle is 3-6kPa [74] and in humans, 160-280kPa (diastolic) [75, 76] and 380-25000kPa (systolic) [77, 78], in the LV, during the cardiac cycle. Reduction in the Young's modulus in BEOV shows that cellularization improves the elasticity of the chitosan scaffold, to show its propensity to deform in response to systolic and diastolic loads.

Biopotentials represent the depolarization and repolarization action of cardiomyocytes. **Figure 5.6** represents the BEOV biopotential activity to show the presence of myocyte activity. The biopotential range for human cardiac cells is 0.1-0.5mV [74] and for rats, 0.495-0.775mV [75]. The average BEOV biopotential was 1.615±1.130mV. The ability to detect biopotentials on the BEOV relies of the efficiency

of uniform cell distribution on the scaffold and sensor electrode contact efficiencies. To develop BEOV with biopotentials in an order of magnitude comparable to that of the human cardiac cell range, the parameters of uniform cell distribution, cell culture conditions and sensor electrode contact efficiency need to be optimized.

Figure 5.7B demonstrates a reduction of cell retention during the cell culture period. This decline may be associated with the relative pore sizes measured in scaffolds and their propensity to allow cell infiltration with a reduced ability to retain cells, compared to those of the native tissues (Lyophilized: 0.0265mm^2, Rehydrated: 0.0035mm^2, Native: 0.0019mm^2 [39]). The scaffolds have a larger pore size, and as such, cells may not be able to interact and colonize, as a result of this increased bridging distance. The assumption of non-uniform of pore size throughout the scaffold is also deducible, based on the degree of variability in the average cell retention. **Figure 5.7C** shows the variability associated with the cellularization process. The variability observed between individual scaffold sections indicates there is extensive variability between individual areas of the scaffold, with regards to cellularization. Some samples contained 20% more than the expected amount, while some contained less than 60% of the expected amount. At cellularization, if a greater amount of initial cells were injected at a specific point on the scaffold, the likelihood of cell expansion is augmented at that point. Conversely, over time, and following interaction and attachment of cells to the scaffold, further cardiac cells may migrate to different points in the scaffold.

BEOV cell distribution is expected to change during culture as the localized cardiac cell clusters migrate throughout the scaffold. The derived pore sizes and cell retention validate the ability of BEOV to retain cells and allow migration. However, only localized contractions were observed under a 2D light microscope. The cardiac-specific factors of CTnI, α-actinin and Cx43 were observed within cell cluster regions. This correlation in

observation explains the localized nature of contractions observed under the 2D light microscope (CTnI; **Figure 5.8A**), as a function of cardiac myocyte specific cell type presence (α-actinin; **Figure 5.8B**). The presence of connexin formation by myocyte intercellular interactions (Cx43; **Figure 5.8C**) further replicates the specific cell-gap junction interactions of ventricular myocardial tissues. Cell clusters may have been observed due to the short culture period; a longer culture allows the myocyte population to expand and dissipate throughout the scaffold.

Numerous optimizations to the BEOV model are required. Cell injection uniformity, cell retention efficiency and BEOV functionality represent the primary optimization variables for this model. For any tissue engineered model, considerations must be made regarding biocompatibility, immune response and autologous cardiac myocyte or stem cell sourcing. These variables are pertinent when using a natural biosynthetic material such as chitosan. The use of a pre-formed natural biosynthetic scaffold platform provides an amenable solution to the complexities otherwise associated with organ storage and transport, for transplant.

The cellularization approach to produce BEOV was direct injection of cardiac cells into the chitosan scaffold. This process is associated with a high degree of cell distribution variability. As a result of non-uniform cell distribution, cell clusters may occur in localized regions with a reduced potential for inter-cluster and functional coupling reactions so as to produce consistent function throughout the BEOV. The application of a novel cell seeding technique and dynamic culture provides a foundation to improve the uniformity of cell distribution, cell retention and function. Cell loading with direct injection of cardiac cells with the addition of fibrin gel entrapment may be used, in conjunction with dynamic culture.

This proof-of-concept model to develop a functional BEOV determines the feasibility of bioengineering a 3D LV as a therapeutic solution in HLHS. Multiple optimization and developmental considerations are to be implemented, in order to enhance the BEOV model. Primary optimizations are focussed on cellular considerations of cell delivery and retention with dynamic culture. BEOVs have the potential to be a functional 3D tissue-engineered LV replacement system in HLHS.

5.5 Conclusion

The goal of the present study was to develop a proof-of concept BEOV, with regards to design, scaffold fabrication and determining fundamental biocompatibility. As such, the concept feasibility was validated and further model optimizations were identified, including cell delivery and retention techniques and dynamic culture. The presented concept is novel and provides a foundation for the future development of a 3D bioengineered LV for application in the treatment of HLHS.

5.6 Summary

The BEOV allows us to answer the research question: Is it possible to design and fabricate a 3D LV? Does it function when cellularized? BEOV scaffolds were produced to the same geometry as the human neonate LV, and were 3D self-supporting structures. On direct injection cellularization, BEOV resulted in functional constructs, observed to generate microscopic local points of contraction with the presence of measurable biopotential activity. Cardiac myocytes were distributed in clusters throughout the BEOV, at injection sites. We can now develop an optimized cell seeding strategy, the TPCV model, with a view to improving cell retention and function in our fabricated left ventricle.

CHAPTER 6

OPTIMIZING CELL SEEDING OF A THREE-DIMENSIONAL BIOENGINEERED CARDIAC VENTRICLE: THE TWO-STAGE CELLULARIZATION MODEL

Current hybrid cell seeding strategies include the combination dynamic cell seeding techniques, with cell delivery to the surface, followed by culture to induce cell permeation throughout the construct; cell retention efficiencies remain low. The development of a novel two-stage cellularization process, coupled with perfusion culture, provides a cell seeding technique to improve cellularization efficiency. This study utilizes the BEOV scaffold as the cellularization platform, to produce the two-stage perfusion TPCV model. TPCV were fabricated by initial direct injection of 10million rat neonatal cardiac cells into the chitosan scaffold, followed by wrapping of the outer scaffold surface, with a 3D fibrin gel AHM patch. The average cell retention per 0.77mm^2 tissue section was 94cells, following three days perfusion culture. The average biopotential output was 1731µV. Cardiac cells were deposited on the scaffold surface and formed intercellular connections. Histological assessment displayed localized cell clusters, with some cell dissemination and validated the observed presence of intercellular and gap-junction interactions.

6.1 Introduction

Cell seeding is a pivotal component in the development of 3D tissue-engineered constructs. Currently, multiple cell seeding strategies exist, however Villanova et al., [79]

identify the need for further investigation to develop improved seeding techniques and optimize the process of cellularization in tissue engineering.

In our previous work (Chapter 5) we characterized the process of developing a BEOV, as the initial stage of creating an implantable treatment in HLHS; HLHS is a congenital condition primarily characterized by the underdevelopment of the LV. The study was focussed on scaffold fabrication and determining functional biocompatibility. The primary optimization identified for the BEOV model in this study, was cell delivery and cell retention. The development of an effective cell seeding strategy provides the potential to improve the biomimetic function and longevity of the BEOV model, with further promise for application to multiple models in the field of tissue engineering.

Current tissue engineering cell seeding strategies can be subdivided into several categories; static, dynamic, cell-sheet, hydrogel, nanoparticles, electrostatic and hybrid [79]. Static [34, 45] and dynamic seeding [43, 80] are widely used. The seeding efficiency of both techniques is dependent on cell concentration, seeding time and scaffold material properties and porosity; non-uniform cell distribution is often observed [81]. To facilitate uniform cell distribution, bioglue scaffold coating has been coupled with the aforementioned seeding techniques; uniformity is dependent on complete and even dissipation of the bioglue on the scaffold [82]. Scaffold-free cell-sheet based [83, 84] methods account for uniformity of cell distribution; the process to develop 3D structures remains complex and lengthy. Hydrogel scaffolds mimic the ECM and promote uniform cell distribution on the gel surface [33, 85, 86] or utilize hydrogels as cell-entrapment mediums [40]; mechanically, hydrogels require optimization to withstand the stresses associated with the cardiac environment. Cells and scaffold materials may be adjusted to facilitate seeding efficiency using magnetic nanoparticles [87] and the induction of electrostatic cell-attractant surface charges [88], respectively. Current hybrid systems

incorporate multiple dynamic seeding techniques, including rotational vacuums [33] and perfusion bioreactors [89 -91] which improve seeding efficacy, but systems are complex and require lengthy culture periods. The majority of current seeding techniques are applied individually. At present, hybrid systems apply multiple seeding techniques from only one category of seeding methods; rotational vacuums apply multiple dynamic culture methods only.

We propose the development of a novel two-stage hybrid cell seeding technique, wherein the techniques of direct cell injection (DCI) , hydrogels and perfusion culture are combined to improve the seeding efficiency of the BEOV model; the resulting model will be referred to as the Two-Stage Perfusion Cultured-BEOV (TPCV). The study focusses on the effect of this two-stage hybrid cellularization method on cell retention and fundamental outcome TPCV function. The presented concept is novel, with the potential to have a significant impact on the progressive development of the BEOV model as a treatment alternative in HLHS and on the field of tissue engineering.

BEOV scaffolds were produced and prepared according to a previously described method (Chapter 5). Primarily, scaffolds were populated with rat neonatal primary cardiac cells through DCI. Subsequently, a 3D fibrin AHM patch [86] was wrapped around the cellularized structure. The TPCV was characterized for cell retention, biopotential activity and histological assessment comparatively to singular DCI and AHM patch wrapping, respectively.

6.2 Materials and Method

All protocols were approved by the Institutional Animal Care and Use Committee (IACUC) in accordance with the “Guide for the Care and Use of Laboratory Animals” (NIH publication 86-23, 1986).

6.2.1 Scaffold Fabrication and Preparation

BEOV molds were fabricated according to a previously described method (Chapter 5). Chitosan scaffolds, of 2.5%w/v in acetic acid, were prepared according to a previously described method (Chapter 5) (**Figure 6.1Ai, ii and iii**) [72].

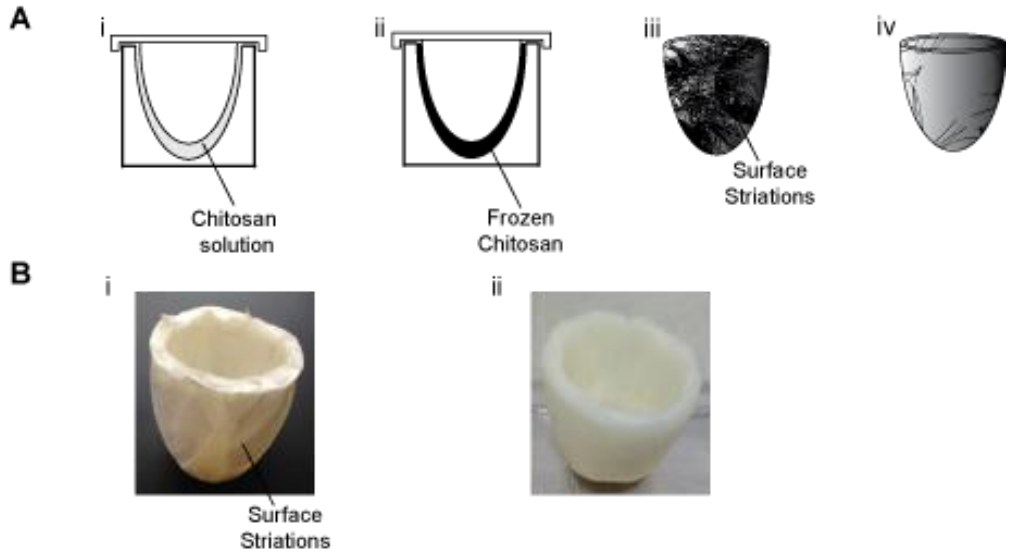

Figure 6.1: BEOV Scaffold Fabrication and Preparation. **A:** Schematic, **i)** Mold with chitosan solution, **ii)** Pre-freezing, **iii)** Lyophilized and **iv)** Rehydrated BEOV scaffold. **B:** BEOV Scaffold, **i)** Lyophilized and **ii)** Rehydrated.

Lyophilized scaffolds were rehydrated and sterilized prior to cellularization according to a previously described method (Chapter 5) (**Figure 6.1Aiv**) [47].

6.2.2 Isolation of Primary Cardiac Myocytes and Fabrication of Artificial Heart Muscle

Cardiac cells were isolated from the hearts of two to three day old neonatal Sprague-Dawley rats using an established method [50].

AHM was fabricated using an established protocol [92]. Briefly, primary cardiac cells were diluted in culture medium composed of M199 (Life Technologies, Grand Island, NY), with 20% F12k (Life Technologies), 10% foetal bovine serum, 5% horse serum, 1%

antibiotic-antimycotic, 40mg/ml hydrocortisone and 10ng/ml insulin, at a density of $2x10^6$ cells/ml. Two millilitres of the cell suspension was transferred to the fibrin gel surface, for a density of $4x10^6$ cells per plate. The AHM were cultured in an incubator at 37°C, supplied with 5% CO_2. AHM fabrication was complete within three to four days.

6.2.3 Two-Stage Cellularization and Perfusion Culture

Stage one of cellularization is DCI of isolated primary cardiac cells, as shown in Figure **6.2Ai, ii and iii**.

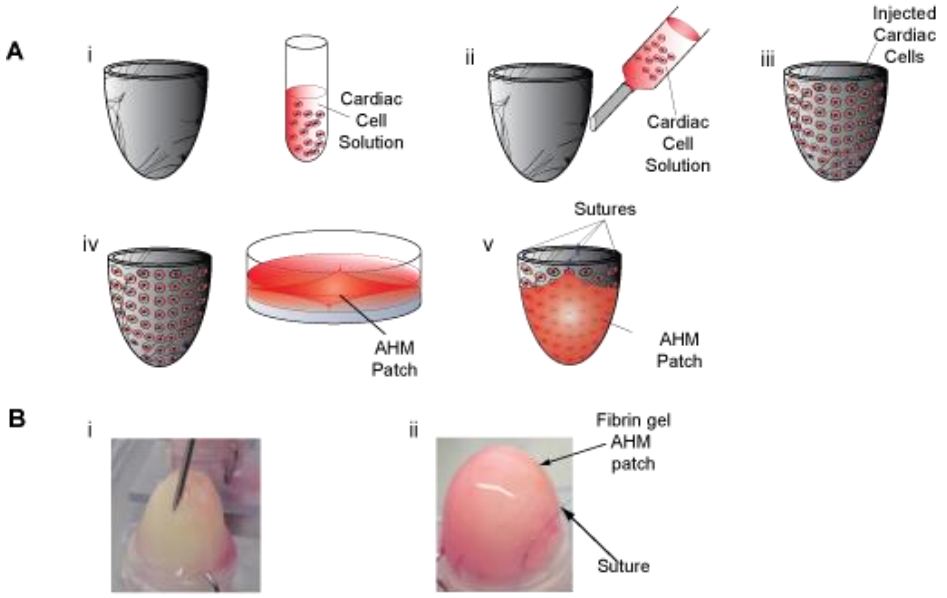

Figure 6.2: Two-Stage Cellularization. **A:** Schematic of, **i)** rehydrated scaffold and cell solution, **ii)** DCI, **iii)** Cell-injected BEOV scaffold, **iv)** AHM patch and **v)** Two-stage cellularized BEOV. **B: i)** DCI and **ii)** AHM Patch wrapping.

DCI was performed using a 16 gauge hypodermic needle (BD, Franklin Lakes, NJ). A total of $1x10^7$ rat neonatal cardiac cells were injected into the scaffold through the surface, at multiple points. The total number of injected cells was adjusted based on the relative cell retention observed in the initial BEOV model, proportional to the loading density (Chapter 5, Section 5.3.6).

Immediately following stage one DCI, stage two, AHM patch wrapping, was implemented (**Figure 6.2Aiv and v**); the AHM was wrapped around the stage one cellularized BEOV and secured with polypropylene sutures (AD Surgical, Sunnyvale, CA). The AHM was wrapped proximally, with the cardiac cell-side between the scaffold and fibrin gel.

The two-stage cellularized constructs were secured on ring clips and mounted onto individual platforms, as described in a previous method (Chapter 5, Section 5.2.3) (**Figure 6.3A**). Constructs were elevated from the platform base to increase the surface area in contact with the culture medium and facilitate cell viability during the culture period.

Constructs were perfusion cultured as shown in **Figure 6.3B**. The individual platforms holding the cellularized constructs were secured into individual cubicles in a custom housing for perfusion culture. Culture medium, at a total volume of 350ml, was added to submerge the constructs and a continuous flow of media was applied at a total volume flow rate of 50ml/min; the flow rate per cubicle was approximately 16ml/min, for a volume of 100ml per cubicle. Constructs were maintained in an incubated environment at 37°C supplied with 5% CO_2 for three days. The perfusion flow rate was adjusted based on the BEOV scaffold volume, proportional to the cardiac myocyte perfusion flow rate described in a previous study [90].

The outcome model constructs are referred to as TPCV for the remainder of the study.

6.2.4 TPCV Biopotential Measurement

Cardiac biopotentials were measured to assess the effect of two-stage cellularization on cardiomyocyte electrophysiological activity and cell-cell interactions. After the three

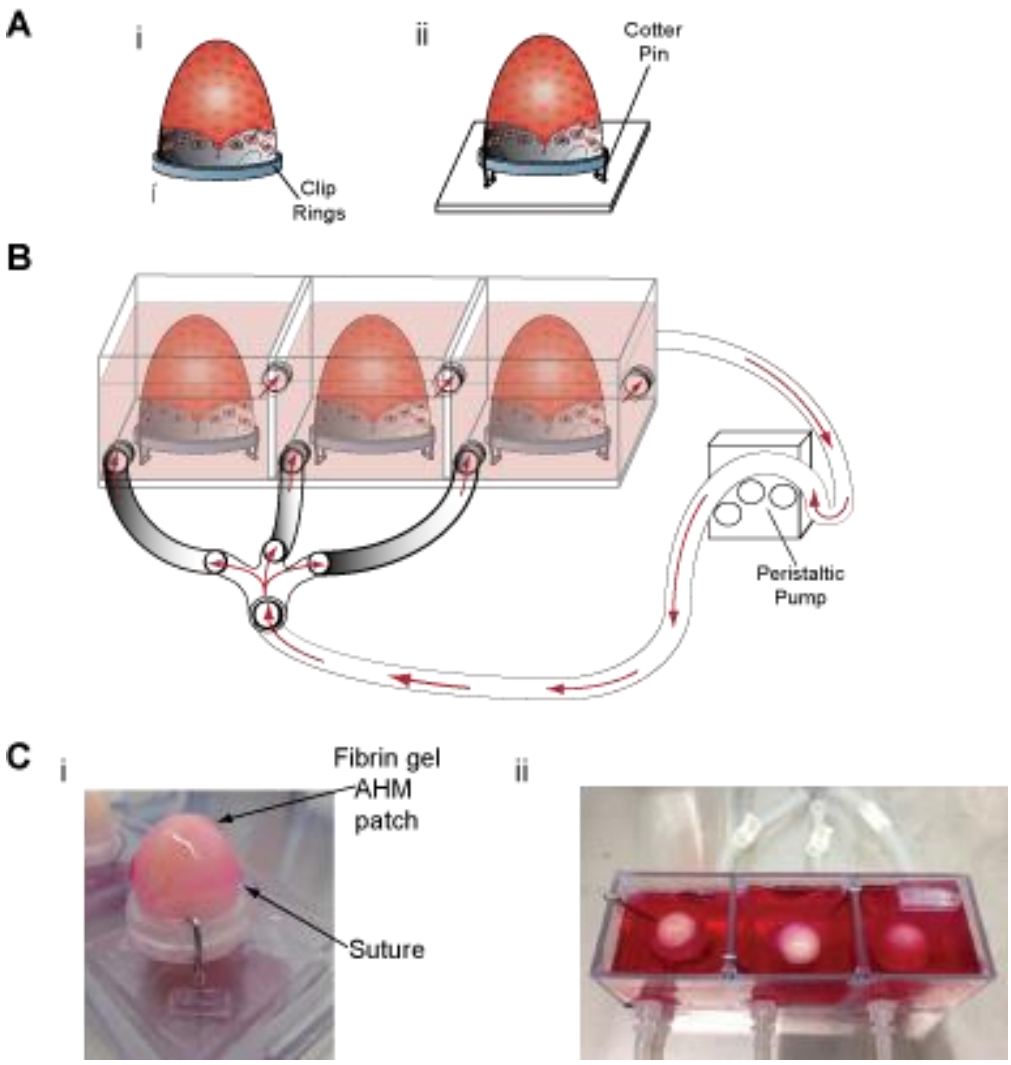

Figure 6.3: TPCV Perfusion Culture. **A:** Two-stage cellularized scaffold, **i)** Secured, **ii)** On platform. **B:** Perfusion culture with continuous flow. **C:** Perfusion Culture, **i)** Two-stage cellularized scaffold on platform **ii)** Perfusion Bioreactor.

day culture period, biopotential activity was measured using a 32 electrode biopotential sensor, arranged in a 4x8 array. Raw output data was generated in Powerlab and processed in MATLAB using a custom script. Raw data channels were examined for periodic waveforms in multiple channels. In the comparison of multiple channels, waveforms are expected to be out of phase to represent the latency in the depolarization wave at different points in the construct.

6.2.5 TPCV Morphology

SEM was used to determine TPCV morphology. Samples were washed with PBS and fixed in 2.5% glutaraldehyde (Electron Microscopy Sciences, Hatfield, PA) for 30minutes. After washing in PBS, scaffolds were dehydrated in ascending concentrations of ethanol (30%, 50%, 70%, 80%, 90%, 95% and 100%) for 10minutes each. Samples were then incubated in 50% ethanol-HMDS solution for 10minutes, followed by incubation in 100% HMDS for 5minutes to prepare for overnight incubation in a desiccator. Specimens were mounted on SEM stubs using a carbon conductive adhesive tape. Samples were sputter coated with a 7nm layer of Pt using a Cressington 208HR sputtering system (Cressington Scientific Instruments Inc., England, UK). SEM images were acquired under high vacuum, at 10kV, spot size 4.0nm, using an FEI NovaNanoSEM 230 (FEI, Hillsboro, Oregon).

6.2.6 Determining cell deposition for the TPCV

To determine cell deposition for the two-stage perfusion cellularization method comparatively to that of application of each stage individually, constructs were placed in a peel-a-way disposable embedding molds (VWR International, Radnor, PA) immediately after the three day culture period. Constructs were immersed in Tissue-Tek optimum cutting temperature compound (VWR International) and frozen at -80°C for 24hours. Planar sections of 20μm thickness were cut using a Cryotome (ThermoScientific, Waltham, MA) and placed onto VWR microslides for staining with Masson's Trichrome reagents, according to the manufacturer's protocol, to determine cell deposition. Masson's Trichrome images were obtained using a light microscope (Olympus, Centre Valley, PA).

6.2.7 Histological Assessment

After the three day perfusion culture period, TPCV were prepared as per the method outline in Section 6.2.6, to produce planar tissue sections of 20µm thickness. Immunohistochemistry was used to compare DCI only, AHM wrapped only and TPCV, for the factors, CTnI , α-actinin and Cx43.

Non-specific epitope antigens were blocked with 10% goat serum in 0.05% Triton-X100 PBS, at room temperature for one hour. To show contractile factors, sections were incubated with rabbit anti-troponin I, 1:100 (ab47003, Abcam, Cambridge, MA). To show sarcomere presence, sections were incubated with mouse anti-α-actinin, 1:200 (Sigma-Aldrich, Catalog No. A7811). To show cell-cell interactions, sections were incubated with rabbit anti-Cx43, 1:100 (ab11370, Abcam). All sections were counterstained for nuclei with DAPI (2.5µg/ml) for five minutes at room temperature. Fluorescent images were obtained with a Nikon C2+ confocal laser scanning microscope (Nikon Instruments Inc., Melville, NY).

6.3 Results

6.3.1 Fabrication of TPCV

Figure 6.1B shows the outcome BEOV scaffold, following lyophilization and rehydration, respectively. The scaffold is a self-supporting 3D cone-shaped structure which retains its frame during processing in preparation for cellularization. The lyophilized scaffold shows surface striations; these are formed through the sublimation of the ice-crystals, which are formed on pre-freezing, around which chitosan fibres are arranged. On rehydration, these striations are no longer visible; this is attributed to the swelling of the material and a subsequent reduction in pore size.

The sequential stages of cellularization are shown in **Figure 6.2B**, and the final two-stage cellularized construct was mounted on the platform, and placed into the custom fabricated perfusion bioreactor for culture (**Figure 6.3C**). Contractions were observed using a 2D light microscope, within 72hours of cellularization at localized points on the TPCV.

6.3.2 TPCV Cardiac Biopotentials

In total, three TPCV were analysed in this study; all samples demonstrated measureable biopotential activity. **Figure 6.4A** shows representative channel excerpts, for 6 channels of 32, demonstrating biopotential activity, for both the positive control models of DCI scaffolds only and AHM patch wrapped scaffolds only, with perfusion culture (n=3 for each model), and the TPCV model. For TPCV (n=3), biopotentials were detected by a range of 11 to 29 of 32 electrodes. Individual channels were examined and peak values were calculated for both positive control models and the TPCV model; a minimum biopotential peak threshold was set at 250μV to account for noise.

The distribution of biopotential readings for each model is show in **Figure 6.4B**; DCI readings range from 400-5000μV, AHM patch readings from 285-2200μV and TPCV from 253.47-6390μV. The average biopotential amplitude was calculated for each model; the DCI only and AHM patch only model average biopotential amplitudes were 1250±1075.563μV (mean ± standard deviation) and 1326.461±399.016μV, respectively. The TPCV average biopotential amplitude was 1731.109±1827.487μV. The average biopotential amplitude of the TPCV was significantly greater than that of both positive control models ($p<0.05$ for positive controls, t-test).

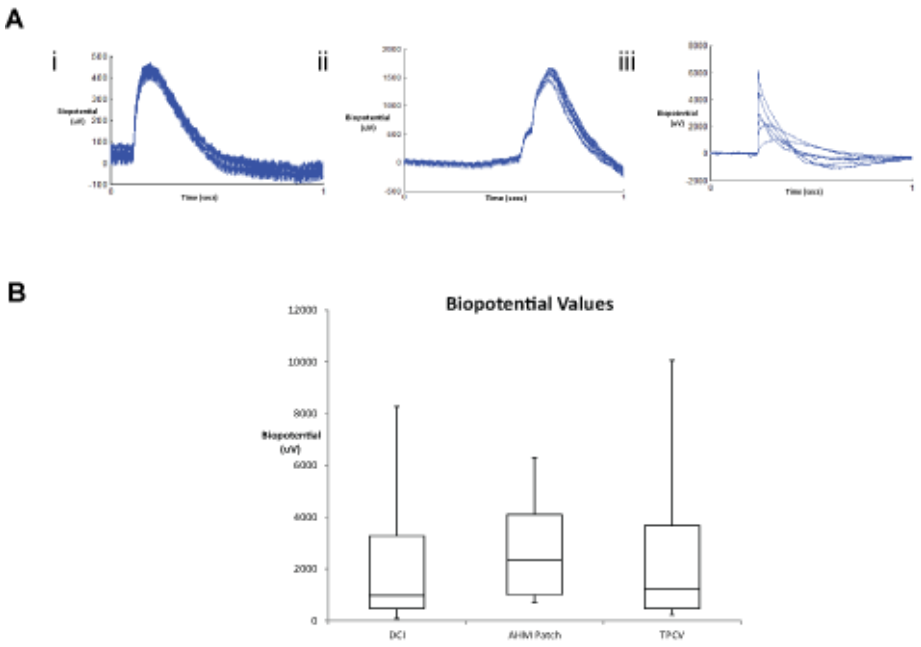

Figure 6.4: TPCV Biopotentials. **A:** Overlayed from 6 of 32 channels **i)** DCI only, **ii)** AHM Patch only and **iii)** TPCV. **B:** Biopotential ranges for DCI only, AHM Patch only and TPCV.

6.3.3 TPCV Morphology

Figure 6.5 shows the SEM for the DCI only, AHM Patch only and TPCV surface, respectively (n=1 for each). The effects of scaffold rehydration for cellularization, in terms of pore size, cell sheet thickness and inter-sheet distance have been quantitatively assessed in our previous work (Chapter 5, Section 5.3.4).

Figure 6.5A shows the DCI only control. Scaffold-cell attachment is observable, with cells variably distributed on the scaffold surface. Cells appear in localized clusters; this may be attributed to the DCI method, wherein cells aggregate at the injection site. Intercellular connections were not observed.

Figure 6.5B shows the AHM patch only control. The AHM fibrin gel has a smooth surface, with few cells distributed on the gel surface (**Figure 6.5Bi**). An increased presence of cells is observed on the chitosan scaffold surface cultured in contact with

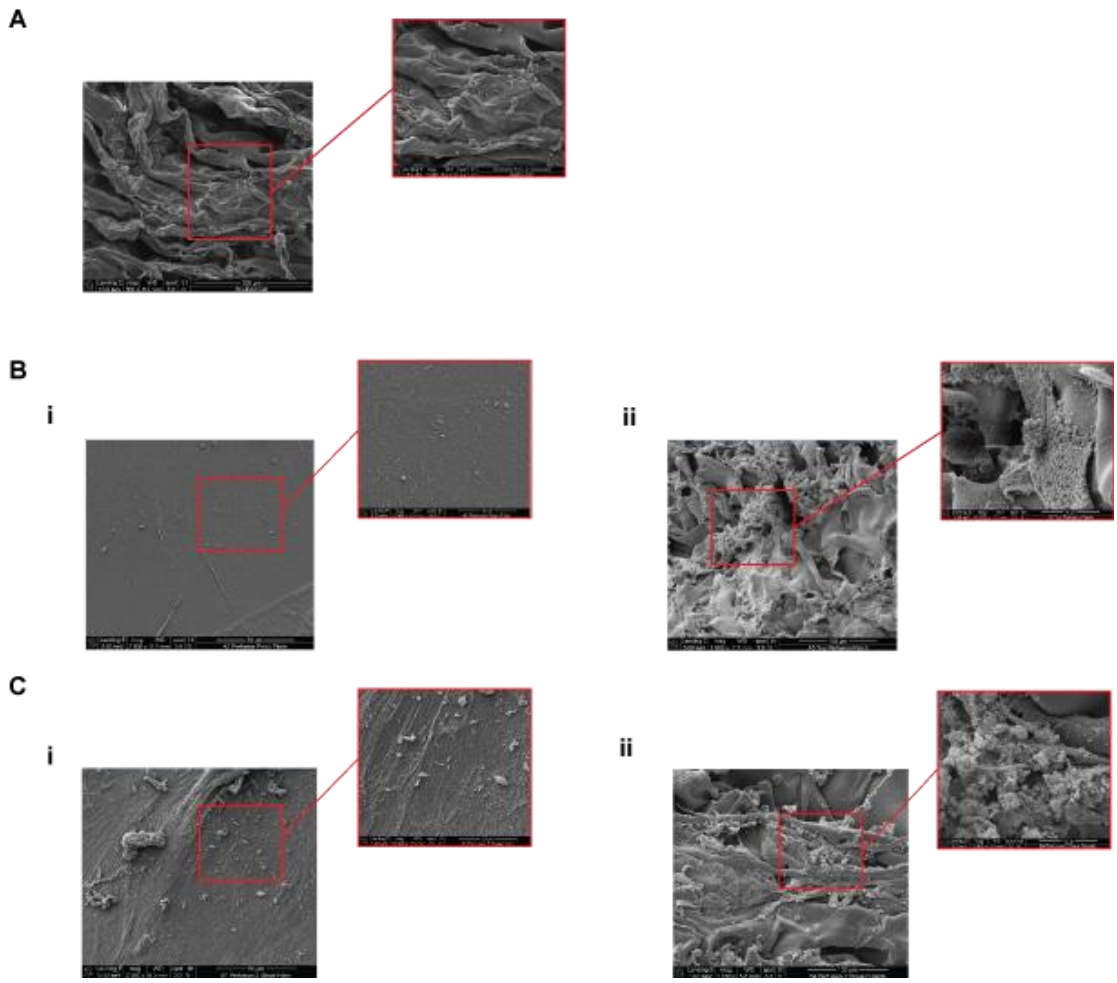

Figure 6.5: TPCV SEM. **A:** DCI only. **B:** AHM Patch only **i)** Fibrin gel only and **ii)** Chitosan Scaffold Surface and **C:** TPCV **i)** Fibrin gel only and **ii)** Chitosan Scaffold Surface.

the cell-loaded side of the AHM patch (**Figure 6.5Bii**). Cells are more extensively distributed on the scaffold surface, compared the DCI only control. Furthermore, the cells can be observed to be organized on the scaffold surface, with evidence of cell-scaffold attachment and fibrin gel integration onto the scaffold.

Figure 6.5C shows the TPCV model. The AHM fibrin gel shows increased cell presence (**Figure6.5Ci**), with a more textured surface than that of the AHM patch only control. Additionally, the TPCV show a very high presence of cells on the chitosan scaffold surface (**Figure6.5Cii**) compared to that of the control models. Cells are

attached to the chitosan surface with a relatively homogenous distribution and intercellular connections are observable.

6.3.4 TPCV Cell Content

The cell content per 0.77mm^2 tissue section was counted for both the TPCV and positive control models (n=2 for each model), to determine the resulting cell density following culture (**Figure 6.6**).

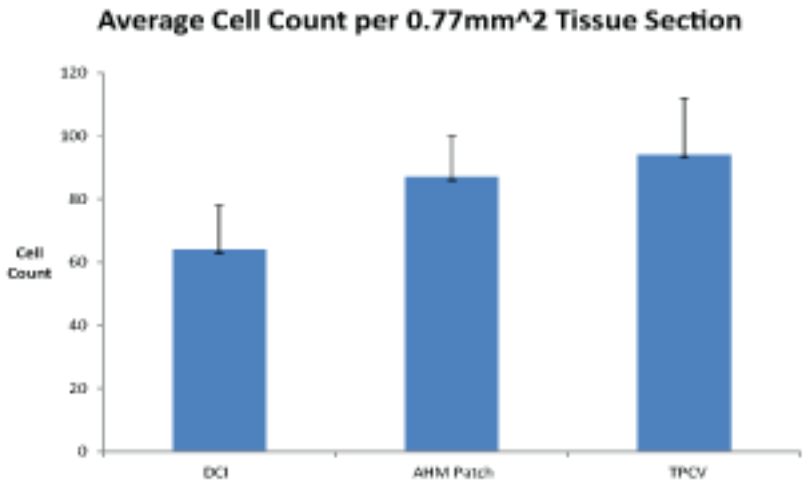

Figure 6.6: TPCV Cell Content: Average cell count per 0.77mm^2.

The average cell count for TPCV was 94±18 cells (mean ± standard deviation) in a 0.77mm^2 tissue section. The DCI only positive control model had a significantly lower cell content than the TPCV following culture (64±14cells, $p<0.05$, t-test). Alternatively, the AHM patch wrapped control model did not have a significantly different cell count to that of the TPCV (87±13 cells, $p>0.05$, t-test). The cell content of all three models was significantly lower than that of the native tissue (487±73cells per 0.77mm^2 tissue section, $p<0.05$ for all, t-test) [39].

6.3.5 Characterization of TPCV

Figure 6.7 shows histological TPCV characterization in comparison to DCI only and AHM patch only cellularization, for a range of cardiac specific factors.

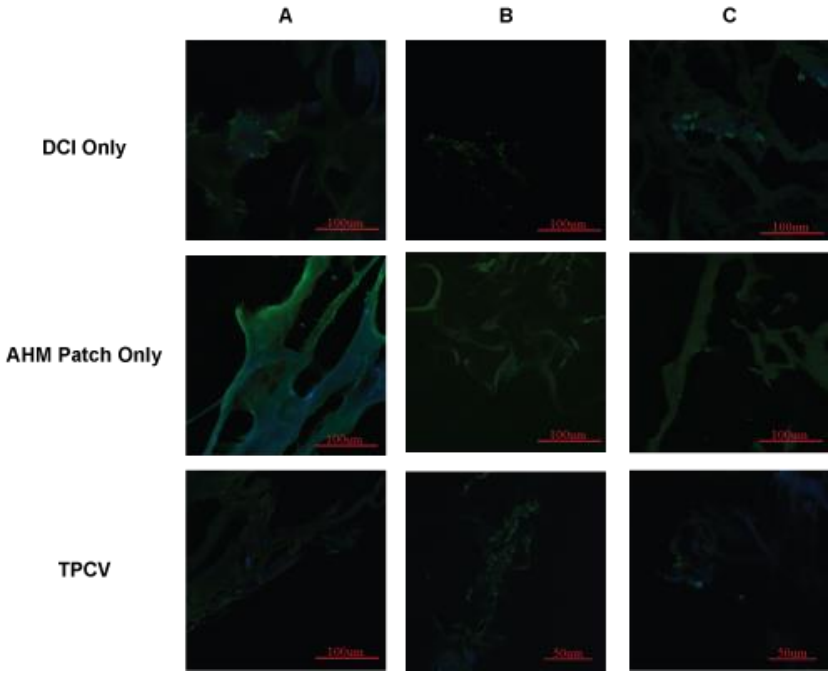

Figure 6.7: Immunostaining at 40x and 60x objectives for DCI only, AHM Patch only and TPCV, with DAPI in blue, for **A:** α-actinin (Green) and **B:** Cx43 (Green), **C:** Cardiac Troponin I (Green).

The TPCV shows the highest presence of α-actinin, Cx43 and CTnI. The DCI only control shows some presence of α-actinin and CTnI within cell clusters; very little Cx43 was observed. The AHM patch only control shows a diminished presence of α-actinin, Cx43 and CTnI within the chitosan scaffold. In TPCV, some α-actinin presence was observed to potentially indicate sarcomeric organization and the underlying presence of cardiac myocytes. Cx43 occurred in cell clusters, oriented along a chitosan fibre, to verify TPCV cell-cell interactions. CTnI was present within localized cell clusters.

Cells formed localized clusters with evidence of distribution throughout the scaffold

structure. The presence of the three factors was observed predominantly in areas of cell clusters.

6.4 Discussion

This study describes a novel two-stage cellularization strategy to optimize the cell seeding efficiency of a BEOV. The BEOV is a self-supporting 3D structure, which replicates the geometry of the human neonate LV. The two-stage cellularization process utilizes DCI and AHM patch wrapping, with perfusion culture conditions, to produce the TPCV and improve both cell retention and function of the engineered LV.

Present cell seeding strategies demonstrate a niche, with respect to hybrid cellularization techniques in the concurrent application of DCI, hydrogels and perfusion culture. Current hybrid cellularization techniques apply multiple strategies from one category of cell seeding; multiple dynamic cell seeding techniques are utilized with rotational vacuums [33] and perfusion bioreactors [89-91]. The majority of cell seeding techniques focus on cell delivery to the surface of the scaffold, followed by conditioning to permeate throughout the scaffold [33, 34, 45, 83, 85-88]. Cell-sheet [83, 84] and hydrogel entrapment [40] are the exception, as the cellularization process is incorporated in the scaffold formation process.

Our previous work describes the process to bioengineer a BEOV (Chapter 5). The work characterizes the biomaterial chitosan, with respect to the scaffold formation process and manipulation for cellularization. BEOV were shown to have a high degree of tolerance to manual handling and preparation for cellularization, quantitatively meeting modelling standards throughout the cellularization process. The BEOV were characterized to validate observed properties in terms of molecular, morphological and physical properties, using FTIR, SEM and AFM, respectively. Following DCI, BEOV

showed the presence of biopotentials indicating cardiac myocyte activity. Cell retention was reduced during the culture period and variability was identified in the DCI process. Histological assessment validated the variability associated with the cellularization process, with the presence of localized cell clusters at injection sites. Based on these outcomes, cellularization was identified as one of the primary optimization variables in the BEOV model.

Chitosan has been extensively characterized as a naturally sourced biomaterial with regards to potential clinical applications [70]. BEOV scaffolds are porous lyophilized structures, with polymer fibres oriented around pores produced by the sublimation process (**Figure6.1Bi**). Rehydration with NaOH, in preparation for cellularization, stabilizes the porous structure resulting in material swelling, cross-linking and reduced pore sizes, thus surface striations are no longer observable (**Figure 6.1Bii**).

The depolarization and repolarization activity of cardiac myocytes is represented by biopotentials. **Figure 6.4** represents the biopotential activity of the TPCV and perfusion cultured positive controls of DCI only and AHM patch only, to show the presence of cardiac myocyte activity. The biopotential range for cardiac cells, in humans, is 0.1-0.5mV [74] and in rats, 0.495-0.775mV [75]. The average TPCV biopotential reading was 1.731±1.827mV, and was significantly greater than both control models ($p<0.05$ for both vs TPCV, t-test). The increased TPCV biopotential activity may be attributed to potential increased cell retention as a result of the two-stage cellularization strategy. The measured biopotential values are higher than those of the human and rat range, as measurements are taken directly at the cell surface. The biopotentials may also be more readily detectable with stronger output, as there is minimal extracellular material interference insulating the signal output intensity. The TPCV biopotential values measured showed a high degree of variability which can be explained by detection

ability; efficient detection relies on uniform cell distribution on the scaffold and sensor electrode contact efficiencies. The parameters of cell distribution and sensor electrode contact efficiencies need to be optimized to reduce the variability of measured biopotentials, to an order comparable to that of the human and rat cardiac cell range.

The morphology of the BEOV scaffold during the development process has been quantitatively characterized in our previous work (Chapter 5, Section 5.3.4). The average pore size of the BEOV was shown to be 0.0265mm^2 and 0.0035mm^2 in lyophilized and rehydrated scaffolds, respectively (Chapter 5, Section 5.3.4); this pore size is amenable to cardiac cell infiltration (average cross-sectional are of 80-960μm^2) [39]. The TPCV showed the greatest distribution of cell-scaffold coverage with the observable presence of intercellular connections, compared to the control morphologies (**Figure 6.5**). The increased cell presence and distribution may be attributed to entrapment of directly injected cells, by the AHM fibrin gel and its concurrent action as a bioglue for directly injected cells, on the outer surface of the scaffold. The rougher fibrin gel surface may occur as a result of gel integration with the chitosan scaffold and an increased cell-fibrin gel interaction, as a function of the bioglue effect.

TPCV had a relatively high cell retention (94±18cells) compared to the control models; cell retention in the DCI only model was significantly lower (64±14cells, $p<0.05$, t-test), whereas the AHM patch only model was not significantly lower (87±13cells, $p>0.05$, t-test) (**Figure 6.6**). The DCI only control model had a high degree of variability in observed cell retention, as cells clustered at injection sites. Conversely, cells are more evenly distributed on the fibrin gel surface and thus attach to the chitosan scaffold with a more uniform coverage, to increase the observed cell retention per tissue section. As expected, the TPCV had the highest cell retention; this increased cell retention and the relative variability observed can be explained as a function of both the DCI and AHM

patch evaluations. The cell retention of all three models was significantly lower than that of the native tissue (487±73cells per 0.77mm^2; $p<0.05$ for all three models, t-test) [39]. This reduced cell retention can be attributed to the large pore sizes of the BEOV scaffold (0.0035mm^2 for rehydrated scaffolds) (Chapter 5, Section 5.3.4), compared to the native rat heart ventricular tissue (0.0019mm^2) [39]. Scaffold pore sizes are amenable to cardiac cell infiltration (cross-sectional area 80-960μm^2) [39], however, they are larger than those of native tissues due to material properties including chitosan concentration, pre-freezing time to temperature and mold orientation, and lyophilization sublimation conditions.

TPCV cell distribution is expected to change during culture, as directly injected cells migrate and the fibrin gel integrates with the chitosan scaffold. The derived morphology and cell retention validate the augmented ability of the TPCV to retain cells and allow migration. The cardiac specific factors of α-actinin, Cx43 and CTnI, were predominantly observed in cell cluster regions. The presence of specific cardiac myocyte cell types (α-actinin; **Figure 6.7A**) is validated by extensive formation of myocyte connexin intercellular interactions (Cx43; **Figure 6.7B**); this substantiates the morphological intercellular connections observed for TPCV (**Figure 6.5Cii**). Contractions were observed under a 2D light microscope (data not provided); contractions emanated from small localized areas and disseminated over a wider region of the TPCV, however the contractions were not synchronous or congruent throughout the construct (CTnI; **Figure 6.7C**). A longer culture period, coupled with differential perfusion conditioning may promote both the expansion of the cardiac myocyte population and dissemination throughout the construct.

Numerous optimizations may be applied to the TPCV model. Cell retention, cell distribution uniformity, TPCV function and additional bioreactor conditioning have been identified as the primary optimization variables for this model. The use of characterized

BEOV scaffolds provides a readily available biocompatible pre-formed natural biosynthetic platform for cellularization to engineer an LV.

The cellularization approach to TPCV was DCI of cardiac cells and AHM patch wrapping of the chitosan scaffold. The DCI process results in cell distribution variability, wherein cell clusters occurred at injection sites. The concurrent use of the AHM patch mitigated cluster formation, to a point, to provide a greater area of cell-scaffold coverage and was shown to ameliorate inter-cluster and functional coupling interactions to improve TPCV function. Cell retention and distribution uniformity and TPCV function may be improved by the addition of multiple AHM patches, on the internal cavity surface and the outer scaffold surface to fully encapsulate the construct after DCI. Conversely, the scaffold may be pre-treated with fibrin gel prior to DCI or cells may be suspended in thrombin solution, directly injected and the scaffold is then immersed in fibrinogen to form a gel to entrap the cells within the scaffold, prior to AHM patch wrapping.

TPCV were cultured for a total of three days, in perfusion conditions at a flow rate of 16ml/min. An extended culture period may allow cells to disseminate further throughout the construct, for a more uniform cell distribution, and to form intercellular linkages and undergo functional coupling interactions, to ultimately improve TPCV function. Additionally, mechanically conditioning the TPCV may improve tissue function; pulsatile flow mechanical stretch provides an LV-type physiological stimulus.

6.5 Conclusion

This novel two-stage cell seeding strategy to develop a TPCV model shows improved cell retention and function. Multiple cell delivery and culture considerations may be implemented to further enhance the model. Cell delivery, culture period and bioreactor conditioning are the primary optimizations, with a focus on improving cell retention and

function. TPCVs have the potential to have a significant impact to progress the development of a functional 3D bioengineered LV replacement system, applicable to HLHS.

6.6 Summary

The TPCV allows us to answer the research question: How can we improve cell retention in our fabricated left ventricle? TPCV showed improved cell retention compared to singular cellularization techniques and were observed to have a greater and more uniform cell distribution on the chitosan scaffold, with the formation of intercellular connections. TPCV demonstrated enhanced biopotential activity. We can now develop a mechanical stretch pulsatile flow bioreactor, the PFCV model, with a view to replicating the LV-type physiological flow and improving the function of our engineered LV.

CHAPTER 7

BIOREACTOR CONDITIONING OF A THREE-DIMENSIONAL BIOENGINEERED CARDIAC VENTRICLE: THE PULSATILE FLOW MODEL

Current physical stimuli bioreactor conditioning models in cardiac tissue engineering are focussed on planar and/or tubular engineering heart muscle. The development of a pulsatile flow mechanical stretch bioreactor for our engineered LV provides a platform to improve function. This study utilizes the chitosan BEOV scaffold as the cellularization framework to produce the pulsatile flow conditioned ventricle (PFCV) model. PFCV were fabricated by wrapping a fibrin gel AHM patch on the outer surface of the scaffold, loading into a custom fabricated pulsatile flow bioreactor, to complete the system, and conditioning at a flow rate of 16ml/min for 20hours. The average pressure generated was 3.6mmHg. The average biopotential output was 1649µV.

7.1 Introduction

Bioreactor conditioning of 3D tissue engineered constructs is pivotal to improve tissue structure, construct properties and cell integration. Currently, multiple bioreactor types have been developed in cardiac tissue engineering to simulate numerous physiological stimuli, however, Freed et al., [93] identify that these systems focus on planar tissue constructs.

In our previous work (Chapters 5 and 6) we characterized the process of developing BEOV and optimizing cell seeding with perfusion culture. These developmental models

present the initial stages in fabricating an implantable treatment alternative in HLHS; the congenital condition, HLHS, primarily describes the underdevelopment of the LV. These studies have validated the potential of the BEOV scaffold to retain its structure, its biocompatibility and the propensity to develop a novel, efficient cell seeding technique. Bioreactor conditioning provides the potential to improve mechanical function and biopotential activity, to enhance the biomimetic properties of our engineered LV, with further promise for application in the field of tissue engineering.

Current physical stimuli bioreactor conditioning models in cardiac tissue engineering include dynamic compression [94-96], cyclic stretch [36, 97- 99] and pulsatile flow preconditioning with mechanical loading [100]. Dynamic compression conditioning is utilized in engineered cartilage tissues, in either planar and/or cylindrical configurations [94-96]; ECM synthesis in constructs increases and biomechanical properties are augmented. Cyclical mechanical stretch conditioning is utilized in engineered cardiac tissues in planar configurations [36, 97-99]; contractility was improved and myotubule alignment was increased. Pulsatile flow preconditioning with mechanical loading was utilized in an arterial model, with tubular polyglycolic acid scaffolds secured in a bioreactor [100]; the construct was subjected to high pulsatile pressures to produce a patent vascular graft. Ott et al., [38] perfusion cultured the anterior LV chamber of a decellularized-recellularized whole rat heart at differential pressures to simulate diastolic and systolic load, resulting in a partial restoration of contractile function after re-seeding. Lee et al., [40] produced a cardiac organoid, with pump function induced by adjusting fluid inflow-mediated chamber pressure, through a modified Langendorff system. The majority of current physical stimuli bioreactor conditioning techniques are applied to planar and/or tubular engineered cardiac muscle. The two 3D models use either an ECM whole heart scaffold [38] or a cardiac organoid [40] with induced pump function.

We propose the development of a complete pulsatile flow loop to mechanically condition an AHM wrapped BEOV scaffold, as an initial step to improve the function of our fabricated LV; the resulting model will be referred to as the pulsatile flow conditioned ventricle (PFCV). The study focusses on the development of a pulsatile flow bioreactor and its effects on the outcome function of the AHM wrapped BEOV. The presented concept is novel, with the potential to have a significant impact on improving the functional capacity of our engineered LV, in producing a biomimetic treatment alternative in HLHS, and in the field of tissue engineering.

BEOV scaffolds were fabricated and prepared as described in Chapter 5. Scaffolds were wrapped with AHM fibrin gel patches, loaded into a custom fabricated pulsatile flow bioreactor and conditioned for 20hours. PFCV were characterized for pump function and biopotential activity.

7.2 Materials and Methods

All protocols were approved by the Institutional Animal Care and Use Committee (IACUC) in accordance with the “Guide for the Care and Use of Laboratory Animals” (NIH publication 86-23, 1986).

7.2.1 Scaffold Fabrication, Preparation and Cellularization

BEOV molds and chitosan scaffolds were fabricated as described in Chapter 5 (**Figure 7.1A**). Lyophilized scaffolds were mounted onto custom fabricated inflow-outflow fittings and secured in place with a ring clip (**Figure 7.1Bi**). Secured scaffolds were rehydrated and sterilized in preparation for AHM patch wrapping, as described in Chapter 5 (**Figure 7.1Ci**). The AHM patch was wrapped around the rehydrated scaffold and secured with polypropylene sutures (AD Surgical, Sunnyvale, CA) (**Figure 7.1Di**).

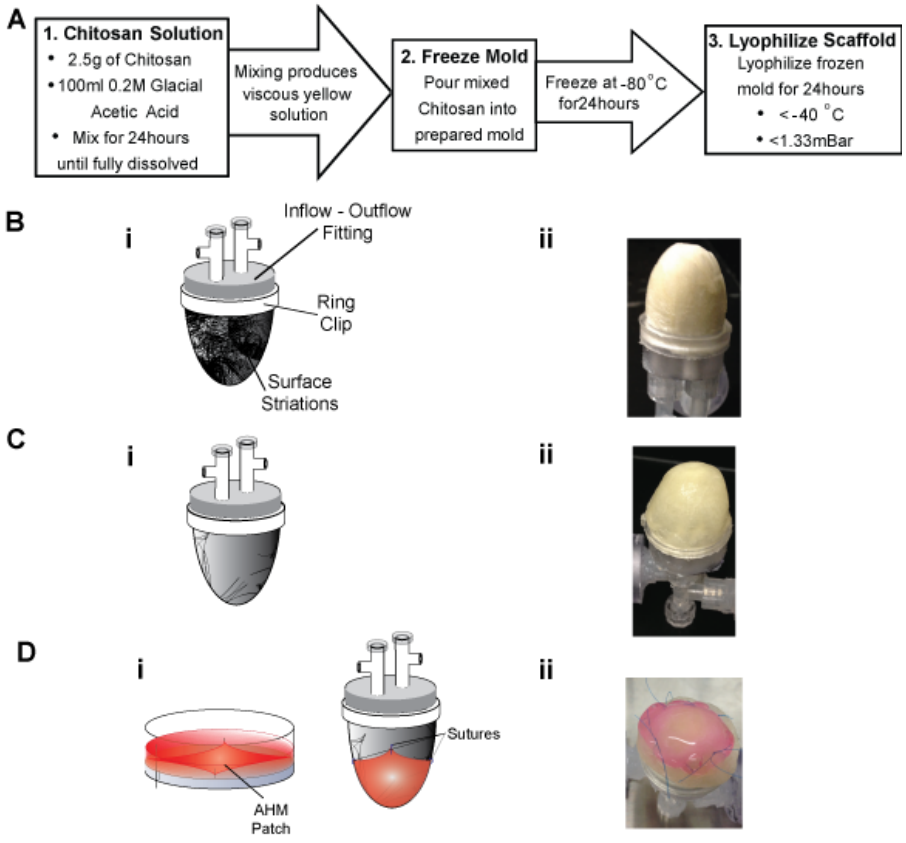

Figure 7.1: PFCV Fabrication. **A:** Chitosan scaffold fabrication. **B:** Assembly, **i)** schematic and **ii)** Lyophilized scaffold on fitting. **C:** Rehydration, **i)** schematic and **ii)** on fitting. **D:** AHM Patch attachment, **i)** schematic and **ii)** on scaffold.

The AHM was wrapped proximally, with the cardiac cells in contact with the chitosan scaffold surface.

7.2.2 Pulsatile Flow Conditioning Bioreactor

AHM wrapped constructs were secured into a custom fabricated bioreactor housing and cultured under pulsatile flow conditions (**Figure 7.2A**). The individual scaffolds were secured into the individual cubicles of the custom housing for conditioning and culture. Each scaffold was submerged in 120ml of culture medium, with an additional 150ml to complete the flow loop. A total pulsatile flow rate of 50ml/min was applied to the closed

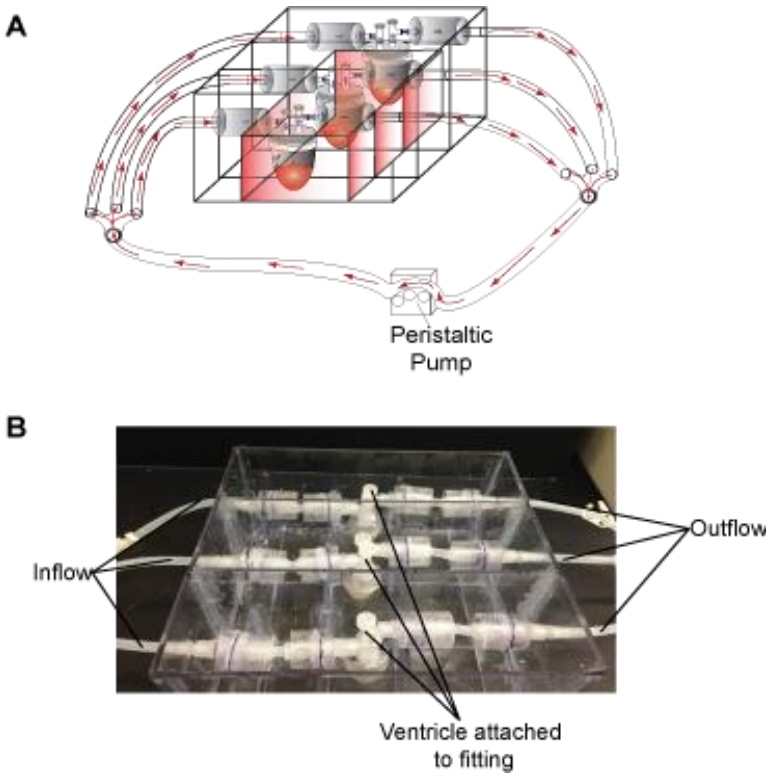

Figure 7.2: PFCV Conditioning and Culture. **A:** Schematic describing complete flow loop setup with pulsatile flow. **B:** Pulsatile flow bioreactor with flow rate of 16ml/min per individual cubicle.

loop; the individual cubicle flow rate was 16ml/min, as per the TPCV perfusion culture flow rate (Chapter 6). Constructs were maintained in an incubated environment at 37°C and 5% CO_2, for 20hours. The outcome model constructs are referred to as the PFCV.

7.2.3 PFCV Pressure Measurement

PFCV pressure was measured to assess the effect of AHM patch wrapping and stretch conditioning on pressure generation. After the 20hours culture period, PFCV pressure was measured whilst maintaining the pulsatile flow loop, using a Mikro-Tip Catheter transducer (SPR-524; Millar Instruments, Houston, TX), as shown in **Figure 7.3A**.

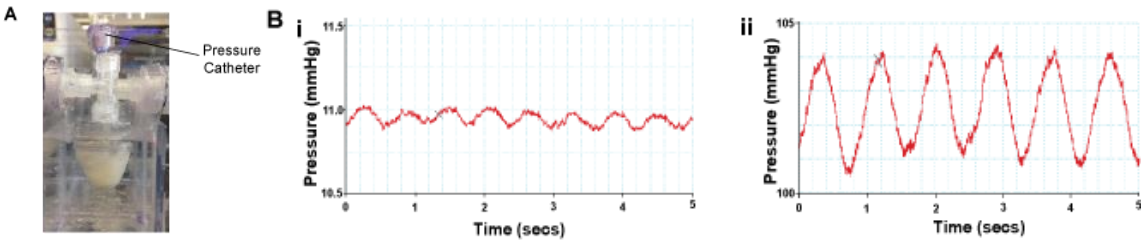

Figure 7.3: PFCV Pressure. **A:** Catheter setup. **B:** Representative Pressure readings over five secs for **i)** Acellular BEOV, 1hour and **ii)** PFCV, 20hours after flow loop induction, at flow rate 16ml/min.

The catheter was connected to a quad bridge amplifier (FE224; AD Instruments, Dunedin, NZ) and data was acquired through a 16 channel PowerLab system (PL3516/P; AD Instruments, Dunedin, NZ). LabChart was used for data analysis with the peak analysis module to calculate average pressure generated.

7.2.4 PFCV Biopotential Measurement

Cardiac biopotential measurements were obtained to assess the effect of pulsatile flow conditioning on cardiac myocyte electrophysiology and activity. After the 20hour culture and conditioning period, biopotential activity was measured using a 32 electrode biopotential sensor, as per the method outlined in Chapter 5.

7.3 Results

7.3.1 Fabrication of PFCV

Figure 7.1Bii shows the lyophilized scaffold mounted onto the custom inflow-outflow fitting and secured with a ring clip. The rehydrated scaffold (**Figure 7.1Cii**) retains its frame on the fitting when prepared for AHM patch wrapping. As described in Chapters 5 and 6, Sections 5.3.2 and 6.3.1, lyophilized scaffold striations, formed through sublimation, extend through to the surface of the scaffold. On rehydration, these surface striations are no longer visible, due to material swelling and a subsequent reduction in pore size. The process of AHM patch wrapping is shown in **Figure 7.1Dii**.

The AHM patch wrapped construct was mounted into the custom bioreactor housing to complete the pulsatile flow loop for culture and tissue conditioning (**Figure 7.2B**). Spontaneous AHM patch-scaffold contraction was observable immediately following patch attachment, prior to initiating the pulsatile flow loop. On induction of pulsatile flow conditions, augmented contractions were observed.

7.3.2 PFCV Pump Function

In total, three PFCV were analysed in this study; all three demonstrated measurable pressure output. The acellular control output pressure, at a flow rate of 16ml/min, was 0.08168±0.0249mmHg (mean ± standard deviation), one hour after flow loop initiation (**Figure 7.3Bi**). PFCV were assessed after patch wrapping and 20hours culture and conditioning; the average pressure was 3.627± 0.494mmHg (**Figure7.3Bii**). The pressure generated by the PFCV is significantly lower than that of the human neonate LV (11±3mmHg at end diastole and 127± 19mmHg at systole) [101] and the rat LV (102±3mmHg at end diastole and 142± 4mmHg at systole) [102] (t-test, $p<0.05$ for both).

7.3.3 PFCV Cardiac Biopotentials

All PFCV (n=3) demonstrated measurable biopotential activity. **Figure 7.4** shows channel excerpts for seven channels over a five second time period, demonstrating PFCV biopotential activity. For the three constructs, biopotentials were detected by a range of four to 32 electrodes over 60seconds. Individual channels were examined and peak values were calculated; a minimum biopotential peak threshold of 250µV was set to account for noise. The distribution of acquired readings ranged from approximately 270-5500µV. The average biopotential amplitude was 1649.722 ± 668.957µV (mean ± standard deviation).

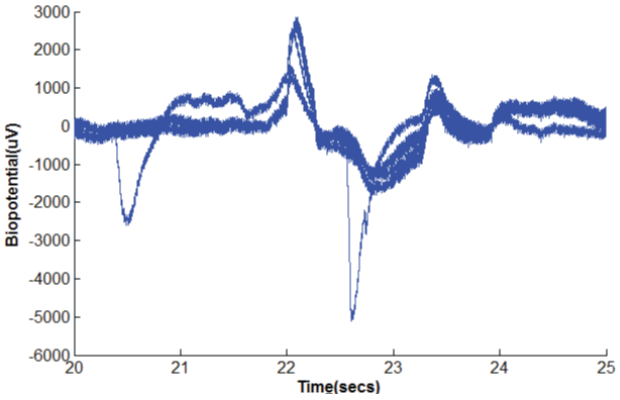

Figure 7.4: PFCV Biopotentials: Overlayed biopotential readings from seven of 32 channels over five secs.

7.4 Discussion

This study describes pulsatile flow conditioning to optimize our bioengineered LV. The self-supporting 3D BEOV structure replicates the geometry of the human neonate LV. An AHM fibrin gel patch was wrapped around the scaffold, and the cellularized scaffold was fitted into a custom pulsatile flow bioreactor, closing the flow loop, to produce the PFCV and improve the function of the engineered LV.

Presently, cardiac tissue engineering 3D flow conditioning studies have only been carried out on preformed structures, the decellularized-recellularized whole rat heart [38] and the cardiac organoid, wherein architecture is maintained using flow [40]. The remainder of pulsatile flow conditioning studies are applied to planar and/or tubular constructs, using cyclic mechanical stretch [36, 97-99] or vessel structures, using pulsatile preconditioning with mechanical load [100]. The benefits associated with mechanical stretch conditioning in cardiac tissues include improved contractile function and myotubule alignment.

Our previous work describes the process to bioengineer a BEOV with extensive material property characterization and validation of material biocompatibility (Chapter 5). The novel two-stage cellularization strategy was used to develop the TPCV; TPCV elicited improved cell retention, with some improvement of function. Based on these outcomes, improving function was identified as a further optimization variable in our bioengineered ventricle.

Chitosan scaffolds were prepared and the porous lyophilized BEOV was mounted onto a custom fabricated inflow-outflow fitting and secured with a ring clip (**Figure 7.1Bii**). The scaffolds were rehydrated using NaOH, *in situ*, on the fitting, stabilizing the porous structure, thus resulting in the absence of surface striations, as described previously (**Figure 7.1Cii**). The scaffolds retained their structure on rehydration and AHM patch attachment (**Figure 7.1Dii**) and were fitted into the custom bioreactor housing to complete the flow loop (**Figure 7.2B**).

The pressure generated by the PFCV represents the functionality of the cardiac myocytes in the scaffold. The representative pressure generated by the acellular BEOV scaffold and PFCV, in the closed pulsatile flow loop, is shown in **Figure 7.3Bi and ii**, respectively. The LV pressure generated by human neonates is 11±3mmHg at end diastole and 127± 19mmHg at systole [101] and in rats, 102±3mmHg at end diastole and 142± 4mmHg at systole [102]. The average acellular scaffold pressure was 0.08168 ± 0.0249mmHg (mean ± standard deviation), after a one hour conditioning period, when maintained under pulsatile flow conditions. The average PFCV pressure was 3.627 ± 0.49mmHg, after a 20hour conditioning period, when maintained under pulsatile flow conditions and without flow maintenance, 0.1284 ± 0.061mmHg. The PFCV model generates significantly less pressure than the human and rat LV (t-test, $p<0.05$ for both). The PFCV generated significantly more pressure than the acellular scaffold (t-test,

$p<0.05$). This indicates potential patch-cell-scaffold integration and functional coupling as a result of conditioning; this assumption must be histologically validated. The low PFCV pressure generated, compared to that of the respective native LVs, may be attributed to the degree of complete closure of the system and the porous nature of the scaffold material, resulting in leaks. Additionally, the low cell load, of $4x10^6$ cells per AHM and short conditioning period of 20hours, limits the maximum potential function of the system, due to a reduced potential for cell expansion to further populate the scaffold. The pulsatile flow applied in the system is not in an order of magnitude comparable to that of the *in vivo* system. The parameters of sealing the system, adjusting cell load, conditioning time and pulsatile flow intensity need to be optimized to improve the pressure generated by the PFCV.

Biopotentials represent cardiac myocyte depolarization and repolarization activity. **Figure 7.4** represents the activity of the PFCV, to show the presence of cardiac myocyte activity. The biopotential range for cardiac cells, in humans, is 0.1-0.5mV [74] and in rats, 0.495-0.775mV [75]. The average biopotential for PFCV was 1649.722 ± 668.957µV. The output was greater than that of the AHM patch only perfusion control model in Chapter 6 (1326.461 ± 399.016µV); this difference is not significant (t-test, $p>0.05$). The AHM patch utilized in the PFCV model was attached seven days after AHM fabrication, whereas in the Chapter 6 model, patches were attached three days after fabrication. The non-significant difference may also be attributed to the short conditioning duration of 20hours; a longer culture and conditioning duration would enable functional coupling and cell-scaffold integration and expansion. The PFCV biopotential values showed a high degree of variability which can be explained by sensor electrode contact efficiencies. The measured biopotential PFCV values were greater than those of the human and rat, as measurements were obtained directly from the cell surface, and without extracellular

material to insulate output signal intensity. The parameters of conditioning, culture time and sensor electrode contact efficiencies need to be optimized to improve output PFCV biopotential activity and reduce measured biopotential variability, respectively.

Numerous optimizations may be applied to the PFCV model, including adjusting initial cell load, sealing the system, increasing conditioning and culture time, and adjusting the pulsatile flow load.

The use of a larger sized fibrin gel with a greater cell load mitigates several optimization considerations. The gel provides a seal over the porous chitosan scaffold to potentially improve pressure generation. The addition of a greater cell load increases the number of cells per surface area section of the scaffold so as to improve both pressure generation and biopotential activity. Increasing the culture and conditioning time may allow for cell expansion, intercellular interactions, cell-scaffold interactions, functional coupling and ECM production; the increased mechanical stretch period may improve cell alignment and result in synchronous function throughout the scaffold. Adjusting the pulsatile load provides a control mechanism by which cell ECM production and the contractile function of cardiac myocytes can be balanced, to optimize the PFCV.

7.5 Conclusion

The pulsatile flow conditioning of the AHM wrapped BEOV, to develop the PFCV, shows pressure generation and functional improvement. Multiple system and conditioning considerations may be implemented to further optimize the model. Cell load, sealing the scaffold, extending the conditioning time and adjusting the pulsatile flow load are the primary optimizations to improve function. PFCVs have the potential to contribute to the development of a functional 3D bioengineered LV replacement system, applicable to HLHS.

7.6 Summary

The PFCV model allows us to answer the research question: Can we develop a custom pulsatile flow stretch bioreactor to condition our fabricated LV? PFCV showed improved function compared to the AHM patch only wrapped perfusion cultured model in Chapter 6, generating enhanced biopotential activity. PFCV generated increased pressure output comparatively to the acellular scaffold. We can now develop a trileaflet valve to produce an engineered complete ventricle, the BECV model, with a view to replicating the entire LV, as a closed system.

CHAPTER 8

THE BIOENGINEERED COMPLETE CARDIAC LEFT VENTRICLE

At present, only two 3D LV models exist; the decellularized rat heart [38] and the cardiac organoid [40]. These models do not incorporate an engineered valve to close the system; either the existing ECM scaffold structure or a modified pressure control apparatus are used to complete the system. Current strategies in valve tissue engineering, are focussed on the right side of the heart, and utilize synthetic or decellularized ECM scaffolds. The development of a bioengineered trileaflet valve (BETV), composed of chitosan, to fit our existing BEOV model would overcome limitations associated with current models. This study proposes the development of a bioengineered complete ventricle (BECV), composed of the BETV and BEOV. BETV molds were developed to emulate infant aortic valve geometric proportions; molds were used to produce chitosan trileaflet valves. BEOV chitosan structures were produced as described in our previous work (Chapter 5). The two components were assembled and secured, with BETV in both a closed and open configuration.

8.1 Introduction

Left ventricular outflow tract (LVOT) obstruction accounts for 6% of all congenital heart defects (CHDs) in children [18]. Valvular aortic stenosis is the most common form of LVOT obstruction in children, constituting 71-86% of cases [103]. Aortic valvular stenosis (AVS) occurs due to improper formation of the aortic valve; stenotic valves may be unicuspid or bicuspid, with only one or two leaflets, respectively, as opposed to the normal trileaflet structure [18]. Additionally, valves may be thick and stiff, as opposed to

thin and flexible. The pathophysiology of AVS consists of stenosed or narrowed valves and/or insufficiency; blood leaking back through the valve and increasing the pressure on the LV to pump both the normal and regurgitated blood volume into the systemic circulation, causing long term hypertrophy and heart muscle damage [104]. It is estimated that 10-15% of AVS presentations are in patients under 1year old, and presentation occurs with other CHDs, such as HLHS [105]. The prognosis in AVS depends on valve anatomy, severity, detection and intervention response. If left untreated in infants, AVS has a fatality rate of 10%; current AVS treatments are inefficient with a 25% mortality rate and 25-50% rate of complications occurring within 25years post-treatment [106].

Three-dimensional tissue engineering strategies may provide alternative AVS treatment options to potentially augment and/or replace current treatments. The ethics and source considerations associated with donor valve based transplant may be superseded. The potential to overcome the biocompatibility and biomimetic considerations associated with donor and mechanical valve replacement is also advantageous. Current treatments do not restore the normal valve function, but aim to improve obstruction and leakage; they provide inefficient long term solutions in AVS. Tissue engineering provides the opportunity to develop a BECV, composed of a BEOV scaffold with a fitted BETV, to address both the underdeveloped LV and AVS pathophysiology associated with HLHS.

Current heart valve tissue engineering strategies are divided to focus on scaffold biomaterials, cell sources and bioreactors. Synthetic polymer scaffolds include polyglycolic acid and polylactic acid [107], chitosan [108], smart scaffolds [109, 110] and bioactive biomaterials with ECM function [111, 112]; the challenges associated with synthetic scaffolds include regulation of cell adhesion, 3D tissue organization, local tissue inflammation and degradation kinetics. Natural scaffolds, such as collagen [113, 114]

and fibrin gels [115, 116] have improved cell distribution uniformity and decellularized scaffolds [117, 118] provide the ideal natural ECM properties; the challenges associated with natural scaffolds include the effect of the chosen decellularization strategy on scaffold integrity and potential immune response.

Current *in vitro* tissue engineered valve models include the P4HB model by Hoestrup et al., [119] and the PLLA model by Sutherland et al., [120] applied to replace all three leaflets of the pulmonary valve in a sheep model. Dohmen et al., [121] utilized decellularized allografts to reconstruct the right ventricular outflow tract. These models focus on the development of a singular valve, to replace and/or augment valvular stenosis on the right side of the heart [119-121]. There are numerous considerations associated with tissue engineering cardiac valves; rapid and complete leaflet closure, stable mechanical properties, reducing thrombosis and viability to repair injury, remodelling and potential growth in the patient [122]. Based on these considerations, Albanna et al., [108] proposed the use of chitosan as a valve scaffold material, as its biocompatibility and degradation kinetics have been established; our previous work (Chapter 5), in developing a bioengineered open ventricle further supports the use of chitosan as a valve biomaterial.

We propose the development of a BETV assembled with a BEOV scaffold, to produce the BECV model. This study focusses on the BETV scaffold fabrication and assembly of the BECV. The presented concept is novel, with the potential to have a significant impact on the development of alternative treatment options independently in AVS, as a complete model in HLHS and in the field of tissue engineering.

The BETV were based on infant aortic valve geometry [123], with adjustment to fit the BEOV. Trileaflet valve molds were designed using CAD software. Models were

fabricated using CNC machining. Chitosan was used as the polymeric scaffold biomaterial, loaded into the molds and lyophilized to produce the BETV scaffolds. BETV were characterized for individual leaflet geometry and reproducibility in fabrication, both on lyophilization and rehydration. The BETV were assembled with the BEOV scaffold to produce the BECV.

8.2 Materials and Methods

8.2.1 Mold Fabrication: CAD and Computer – Numerical Code Machining

Solidworks CAD software was used to develop a trileaflet valve model. The two part mold, inner and outer, was designed to form a valve with geometric proportions comparable to that of the infant aortic valve (**Figure 8.1A**) [123], adjusted to fit the BEOV geometry defined in Chapter 5, **Figure 5.1A** and emulate the posterior (L1), right (L2) and left (L3) cusp trileaflet structure of the aortic valve (**Figure 8.1B**).

The combination of components provided a valve of set inlet diameter and height (**Figure 8.1C**) and consistent, defined leaflet thickness (**Figure 8.1D**). The CAD model was fabricated using CNC machining. A polycarbonate block was machined, using a Sherline mill (Sherline Inc., Vista, CA) to produce molds of tight tolerance in the curved leaflet architecture (**Figure 8.1E**).

To determine consistency between CAD models and CNC machined molds, valve height, inner and outer inlet diameter and individual leaflet thickness at four points were assessed, for both the model and mold, as shown in **Figure 8.1C and Di**.

8.2.2 Scaffold Fabrication, Preparation and Verification

Chitosan was used as the valve fabrication biomaterial. The outcome structures were macroscopically examined for the variables of self-supporting 3D structure, ability to withstand manipulation and manual handling, and relative flexibility.

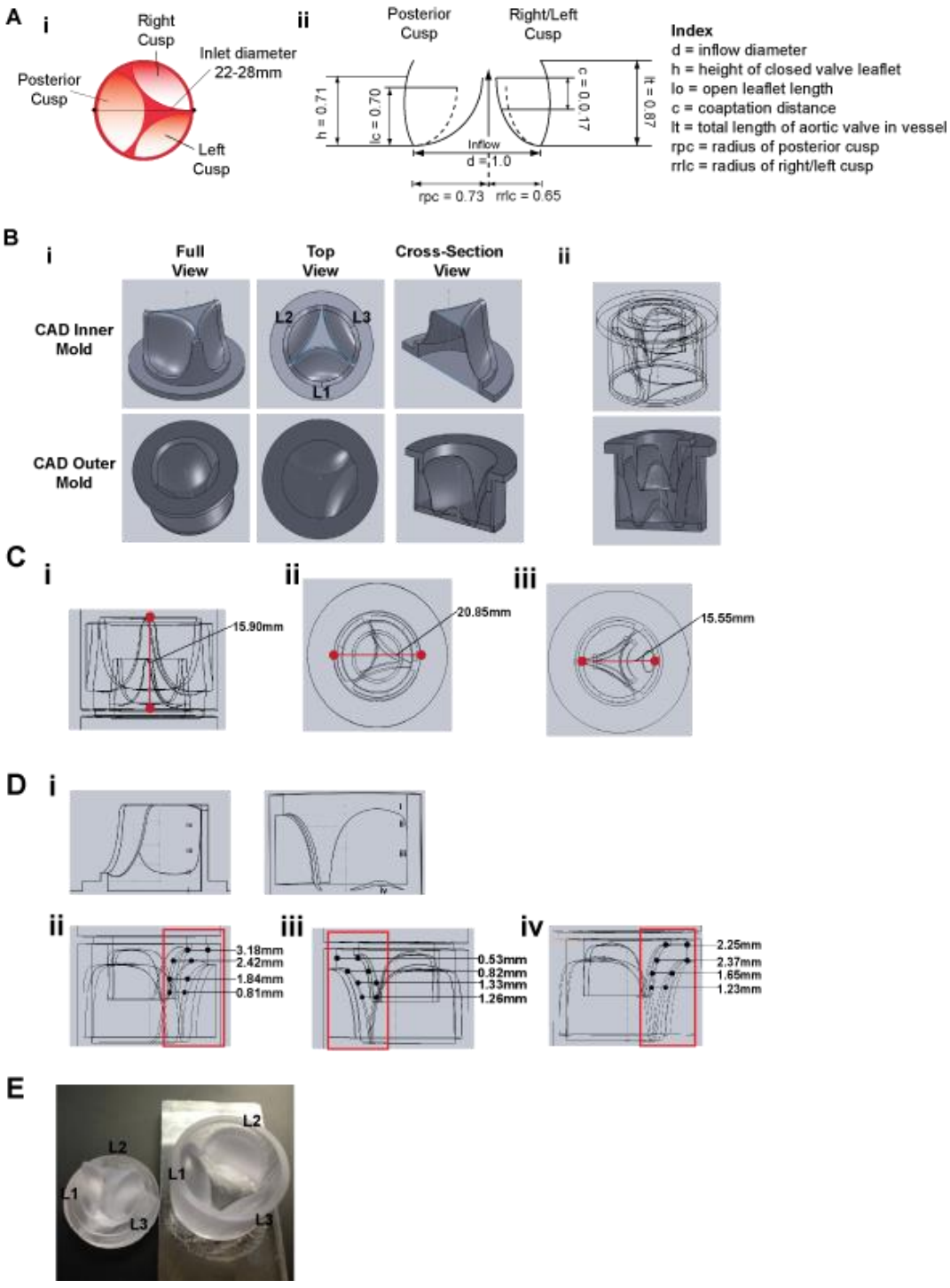

Figure 8.1: BETV design. **A:** Infant aortic valve **i)** Diameter, **ii)** Proportions. **B:** CAD **i)** Inner, Outer, **ii)** Assembled. **C: i)** Height, **ii)** Outer, **iii)** Inner Diameter. **D:** Leaflet **i)** Measurements points, **ii)** L1, **iii)** L2**, iv)** L3 and **E:** CNC mold.

Chitosan scaffolds, of 2.5%w/v in acetic acid, were prepared according to a previously described method (Chapter 5) (**Figure 8.2Ai and ii**) [72], to produce the BETV (**Figure 8.2Aiii**). Lyophilized scaffolds were rehydrated using a previously described method (**Figure 8.2Aiv**) [47].

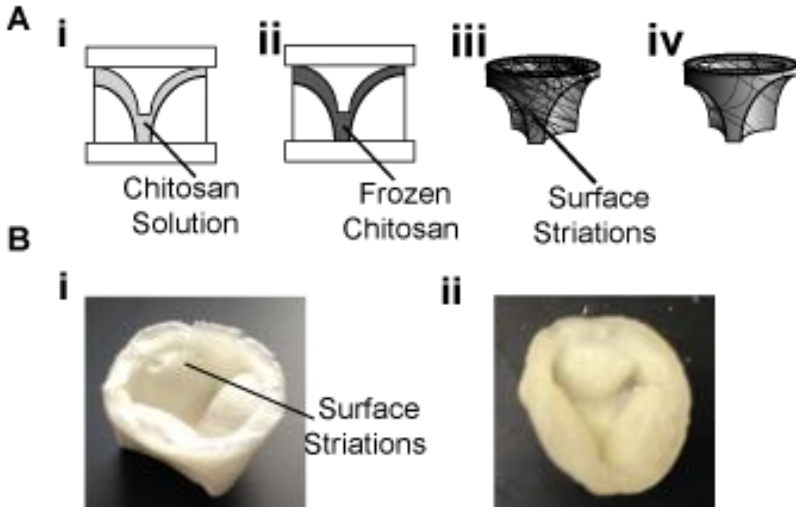

Figure 8.2: BETV Fabrication. **A:** Schematic, **i)** Mold with chitosan solution, **ii)** Pre-freezing, **iii)** Lyophilized and **iv)** Rehydrated BETV. **B:** BETV, **i)** Lyophilized and **ii)** Rehydrated.

The consistency between the CAD model, 3D printed mold, lyophilized and rehydrated scaffolds was evaluated by measuring the height of the scaffolds, inner and outer inflow diameter and individual leaflet thickness, as per the method described in Section 8.2.1.

8.2.3 BECV Fabrication

BEOV scaffolds were prepared as described in Chapters 5. Lyophilized BETV were secured into the lyophilized BEOV using cyanoacrylate adhesive and polypropylene sutures (AD Surgical, Sunnyvale, CA) (**Figure 8.3A**); BETV were attached both in a closed and open state, to produce the BECV model.

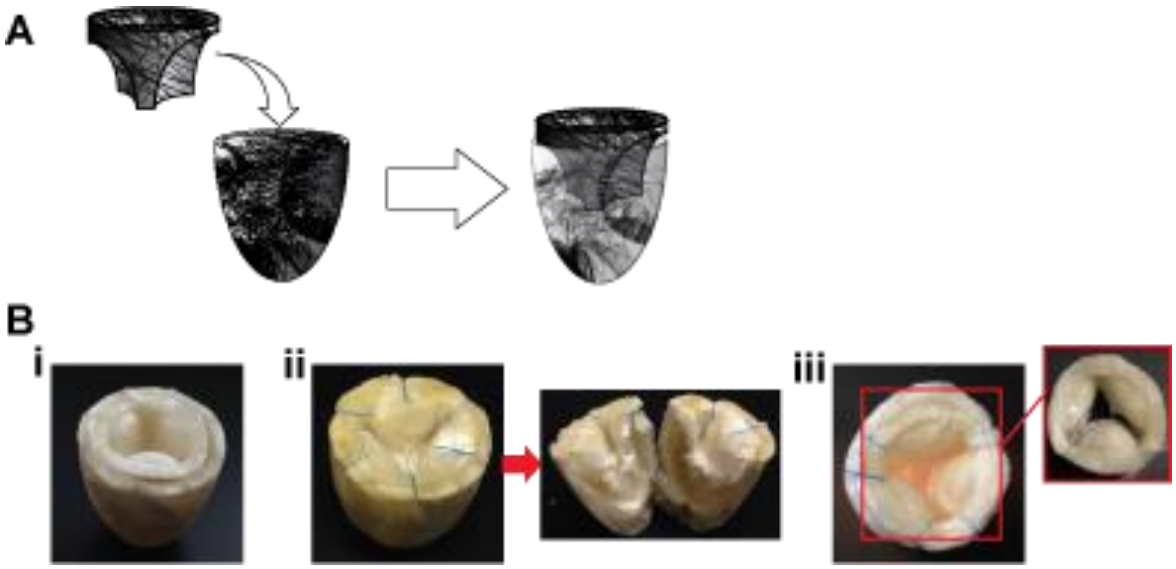

Figure 8.3: Fabrication of the BECV model. **A:** Schematic of BEOV and BETV assembly. **B:** BECV with, **i)** with free valve fitting, **ii)** closed BETV sutured and secured, and cross-section and **iii)** open BETV sutured and secured.

8.3 Results

8.3.1 Design, Fabrication and Geometry of BETV Molds

Figure 8.1A shows the values associated with the structure of the infant aortic valve. The diameter is a range value, due to individual variability and differential inflow pressure (**Figure 8.1Ai**). The particulars of leaflet geometry are presented as proportions to inflow diameter, to account for individual variability (**Figure8.1Aii**); the proportions demonstrate the distinction between the geometry of individual valve leaflets.

Figure 8.1B shows the trileaflet design used to replicate the architecture of the aortic valve. The outer and inner components fit together to produce differential tapered leaflets, as observed in the human aortic valve (**Figure 8.1Bii**). The height of the assembled valve model cavity is 15.90mm, the outer diameter is 20.85mm and the inner diameter is 15.55mm (**Figure 8.1C**). These values follow the proportional range of valve

components, to inflow diameter, of the normal aortic valve, outlined in **Figure 8.1Aii**. The taper range was measured at four points along the leaflet (**Figure 8.1Di**). The measured range for L1 was 0.81-3.18mm, for L2, 0.53-1.33mm and for L3, 1.23-2.37mm (**Figure 8.1D**).

The CNC machined mold (**Figure 8.1E**) shows retention of the shape and curved geometry of the design models. In comparison to the CAD model, the height of the machined mold was 4.3% smaller (15.22mm), the outer diameter was 3.5% greater (21.79mm) and the inner diameter was 3.0% smaller (15.08mm). The taper range for the CNC mold of L1 was 0.07-3.13mm, for L2, 0.36-3.52mm and for L3, 0.55-2.74mm. The taper ranges for CNC mold leaflets show greater variability and appear significantly different to those of the CAD model.

8.3.2 Fabrication of BETV

Chitosan scaffolds were produced as per the BEOV method (Chapter 5) at a concentration of 2.5%w/v in 0.2M acetic acid. **Figure 8.2Bi** shows the outcome BETV. It is a 3D self-supporting structure, which has retained the 3D geometry and shape of the trileaflet mold. Striations are observable in the material following lyophilization, as a result of polymer fibre orientation around ice crystals in pre-freezing and sublimation during lyophilization. **Figure 8.2Bii** shows the scaffold after rehydration wherein striation is no longer observable at the structure surface, due to material swelling, which subsequently reduces the pore size around which the polymer is arranged.

In comparison to the CAD model, the average height of the lyophilized BETV (n=10) was 14.7% smaller (13.56± 0.42mm, mean± standard deviation), the outer diameter was 3.7% smaller (20.07± 0.85mm) and the inner diameter was 4.1% smaller (14.92± 0.59mm). The taper range of the lyophilized BETV (n=10), for L1, was 0.76-3.85mm, for

L2, 1.01-3.37mm and for L3, 1.15-2.64mm. The taper ranges for CNC mold leaflets show greater variability and appear significantly different to those of the CAD model. The taper ranges for lyophilized BETV leaflets show greater correlation to those of the CAD model.

In comparison to the CAD model, the average height of the rehydrated BETV (n=10) was 32% smaller (10.82± 0.52mm, mean± standard deviation), the outer diameter was 28% smaller (15.01± 1.03mm) and the inner diameter was 23.8% smaller (11.86± 0.77mm). The taper range of the lyophilized BETV (n=10), for L1, was 0.69-1.69mm, for L2, 0.86-1.87mm and for L3, 0.98-2.29mm. The taper ranges for rehydrated models are approximately 30% smaller than those of the CAD model; the effect of NaOH rehydration and scaffold shrinking is validated from the BEOV model (Chapter 5).

8.3.3 Fabrication of BECV

Figure 8.3B shows the complete bioengineered ventricles, composed of the lyophilized BETV and BEOV. The valve fits into the open ventricle structure, as the average outer diameter of the BETV is 20.07 ± 0.85mm (mean± standard deviation), and the open face diameter of the BEOV is 24.44± 0.87mm. The lyophilized BETV held position when placed into the lyophilized BEOV scaffold (**Figure 8.3Bi**). The completed structure was then secured, to effectively enclose the construct, using cyanoacrylate adhesive and sutures, to produce the BECV model, with the valve both closed and open (**Figure 8.3Bii and iii**). A cross-section of the BECV showed the distance between the base of the valve and the inner face of the BEOV chamber to be 6.36mm (**Figure 8.3Bii**); this distance is not significantly different to that of the fitted CAD model (6.6mm).

8.4 Discussion

This study describes the development of a physiologically replicative BECV, with combination of a BETV and a BEOV, as a direct LV replacement in HLHS. The BECV is a self-supporting closed 3D structure which replicates the architecture of the LV chamber, and the trileaflet aortic valve, with the potential to emulate physiological function.

Present research solutions in HLHS demonstrate a niche, with respect to the development of a complete self-supporting 3D LV. Current heart valve tissue engineering studies focus on singular valve constructs, produced using synthetic and decellularized ECM scaffolds, to replace and/or augment valvular stenosis on the right side of the heart [119-121]. Two complete 3D LV models exist to date; the first is the work by Ott et al., [38] using a decellularized-recellularized whole rat heart. The model includes a comprehensive LV structure, complete with valves. The second is the cardiac organoid model developed by Lee et al [40]. The engineered organoid is completed through attachment to a modified Langendorff apparatus. These models either utilize a pre-existing structure to produce a complete LV, or an alternative apparatus to complete the system, in place of a valve.

Chitosan was chosen as the biomaterial for BETV, as it has been extensively characterized both in terms of planar material properties as a naturally sourced biosynthetic material, and in terms of its numerous clinical applications, such as wound dressings [70]. Furthermore, Albanna et al., [108] proposed the use of chitosan as a valve scaffold material, based on its established biocompatibility and degradation kinetics; our previous work (Chapter 5), in developing the BEOV, further supports the use of chitosan as a valve biomaterial.

The measured differences between the CAD model design (**Figure 8.1C and D**) and 3D mold geometries are not significant overall however there is significant variability

between individual leaflets. Overall, the CNC machined mold met the BETV scaffold modelling standards however the tolerance with respect to leaflet tapering was variable. This outcome may be attributed to subjective optical methods to measure the taper of the mold geometry and CNC machining capabilities.

Both the lyophilized and rehydrated BETV chitosan scaffolds demonstrated shrinkage relative to the CNC mold; lyophilization sublimation and pressure results in material compression, and rehydration, with NaOH, results in cross-linking to reduce internal pore size and the overall size of the scaffold. These observations are validated in **Figure 8.2B**, wherein the porous striated surface of the lyophilized construct is no longer observable following rehydration.

Prior to being secured, the BETV and BEOV are shown to fit together (**Figure 8.3Bi**). Suturing and cyanoacrylate adhesion are shown to secure and seal the construct at the edges where the BETV and BEOV are joined; the cross-section shows spacing between the BEOV inner wall and valve leaflets, and the distance from valve base to ventricle base is ample to allow for valve movement and a sizeable flow volume within the chamber, respectively (**Figure 8.3Bii**). The fitted model replicates the CAD fitted model, with regards to distance from valve base to ventricle inner face, with high tolerance (6.36mm in BECV and 6.6mm in CAD model). **Figure 8.3Biii** demonstrates that BETV can be adjusted to allow for flow, through leaflet separation.

The BECV can be studied in numerous ways. Potential future works include the cellularization of the BECV, with two-stage cellularization of the body of the ventricle, and fibroblast seeding of the valves, both in open and closed configurations, with perfusion culture. The cellularized BECV may be bioreactor conditioned and cultured to simulate physical stimuli.

This innovative model presents the first complete bioengineered LV model, incorporating an engineered open LV and trileaflet valve. The BECV component geometry was shown to produce a fitted model, secured with sutures and cyanoacrylate adhesive. Cellularization, function and bioreactor studies may be developed using the BECV. The BECV has the potential to provide a complete structural LV replacement system in HLHS, addressing both the underdeveloped LV and aortic valve.

8.5 Conclusion

The goal of the present study was to produce a BECV, with the design and fabrication of a trileaflet valve, to fit the BEOV. The primary future studies applicable to this model were discussed to be differential cellularization and bioreactor conditioning, to generate and optimize function. This is the first complete bioengineered LV, with trileaflet valves. The BECV provides a complete structural 3D bioengineered platform to develop a functional LV replacement for application in the treatment of HLHS.

8.6 Summary

The BECV allows us to answer the research question: Is it possible to design and fabricate trileaflet valves to produce a complete bioengineered 3D left ventricle? BEOV scaffolds were produced as described in Chapters 5, based on human neonate LV geometry. BETV were fabricated based on infant aortic valve proportional geometry, with adjustment to fit the BEOV. Chitosan was utilized as the valve biomaterial, as we have extensively characterized its material properties and biocompatibility in our previous studies (Chapter 5). The BETV was shown to fit the BEOV, and was secured in place to produce the BECV. We can now review the series of models that culminated in the development of a BECV.

CHAPTER 9

SUMMARY AND CONCLUSION

9.1 Summary

The overall aim of our research was to bioengineer a 3D cardiac LV, as a replacement construct in HLHS. From this general aim, a series of specific research questions emerged:

1. Can we develop a better understanding of the ideal LV material platform, the LV itself?
2. Is it possible to design and fabricate a 3D cardiac LV? Does it function when cellularized?
3. How can we improve cell retention in our fabricated LV?
4. Can we develop a custom pulsatile flow stretch bioreactor to condition our fabricated LV?
5. Is it possible to design and fabricate trileaflet valves to produce a complete bioengineered 3D cardiac LV?

A series of five models were developed and assessed to address each of these research questions. The fabricated models are shown in **Figure 9.1**.

The AVEM allowed us to develop a better understanding of the ideal LV material platform. Passive cell seeding on the ECM scaffold produced functional constructs, which generated contractile force and elicited a Frank-Starling relationship. Cardiac

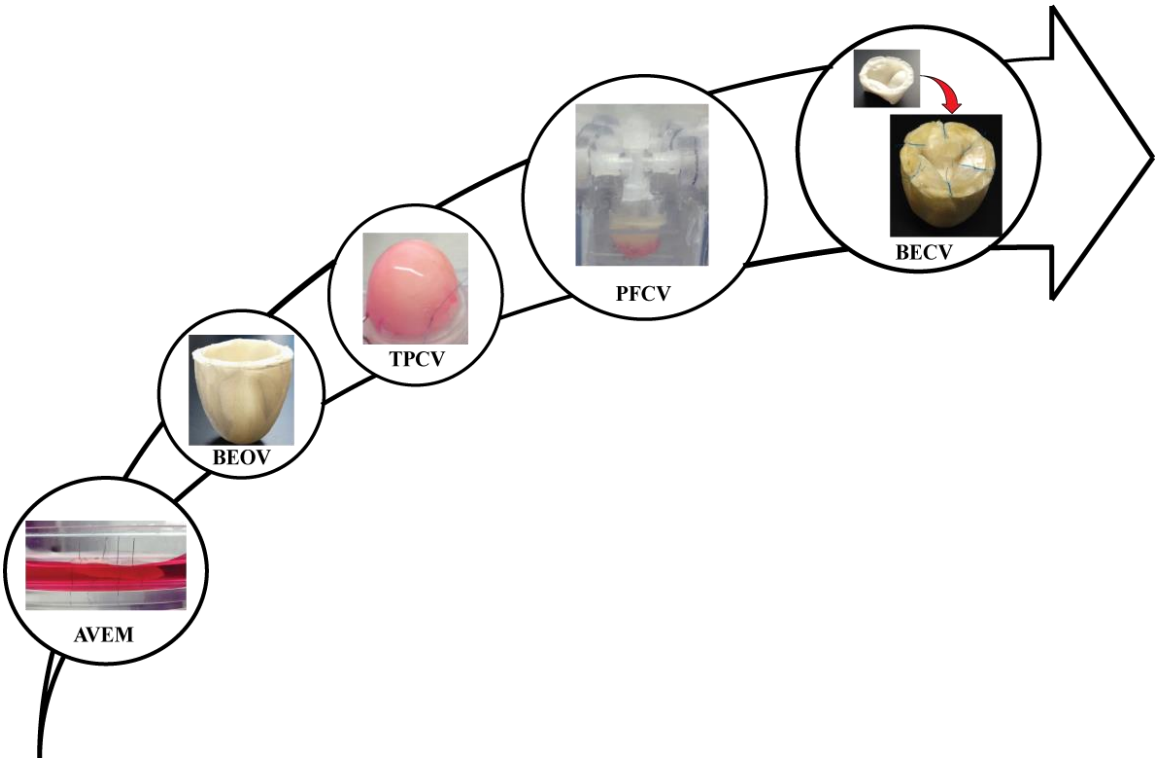

Figure 9.1: Models to Bioengineer a 3D Cardiac LV

myocyte infiltration was observed as a function of scaffold pore size and cell-ECM coupling, both peripherally and centrally within the AVEM.

The BEOV model validated the design and fabrication of a 3D LV chamber and proved the biocompatibility of chitosan as a biomaterial scaffold, by producing function on cellularization. The BEOV was a self-supporting structure of the same geometry as the human neonate LV. DCI, coupled with static culture, produced functional constructs which showed microscopic localized contraction points, biopotential activity and cell clusters throughout the scaffold.

The TPCV model improved cell retention in our fabricated LV, compared to singular cellularization techniques. Cardiac myocyte biopotential activity was enhanced. Cell distribution was more uniform with a greater proportion of coverage over the scaffold surface and the formation of intercellular connections.

The PFCV model evidenced the design and fabrication of a custom pulsatile flow bioreactor to condition our bioengineered LV. In comparison to perfusion culture, pulsatile flow conditioning improved cardiac myocyte biopotential activity in our LV. Additionally, PFCV generated measureable pressure.

The BECV model validated the design and fabrication of trileaflet valves to complete the bioengineered 3D cardiac LV. The BETV was a trileaflet structure of geometry comparable to that of the infant aortic valve. Chitosan was utilized as the scaffold biomaterial, based on its previously characterized biocompatibility and material properties, in the BEOV model. The BECV was produced by assembly of the BEOV and BETV.

9.2 Conclusion

We have developed a complete 3D bioengineered cardiac LV, composed of a BEOV chamber and a BETV. Each study and model built on the previous, to achieve this overall aim. The design and development of the BECV is an innovation that addresses a current niche in HLHS and cardiac tissue engineering; creating a complete tissue engineered LV to potentially be utilized as an implantable replacement system in HLHS. We have addressed the specific gaps in knowledge, by bioengineering a 3D cardiac LV of physiological size and shape, with a 3D self-supporting structure, using a biocompatible biomaterial scaffold and the addition of valves to complete the system.

9.3 Future Work

The fabrication of a bioengineered 3D cardiac LV requires continual optimization and augmentation of models, to produce a completely physiologically simulate LV construct. Our future work is focussed on optimizing the BECV platform, with incorporation of techniques developed in our current models. BECV cellularization, using the two-stage strategy on the BEOV chamber and passive fibroblast seeding on the valve, presents

initial future work. Further to cellularization, bioreactors may be designed to reproduce physiological stimuli, such as mechanical stretch and electrical stimulation, to condition the construct and improve function. On optimization of the BECV, an additional bicuspid valve may be designed and incorporated into the system to produce a dual valve, inflow-outflow LV architecture and further LV components, which are affected in HLHS, may be engineered and incorporated into the bioengineered 3D cardiac LV.

REFERENCES

1. Langer R., Vacanti J.P.: Tissue Engineering. *Science* 260(5110):920-926, 1993.
2. Birla R.K. (1st Edition): *Introduction to Tissue Engineering: Applications and Challenges*. Houston, TX, Wiley-IEEE Press, 2014.
3. Vacanti J.P., More M.A., Saltzman W.M., Damb A.J., Perez-Atayole A., Langer R.: Selective Cell Transplantation using Bioresorbable Artificial Polymers as Matrices. *J Pediatr Surg* 23(1:Pt2):t-9, 1988.
4. Goh A.S., Mozaffaria D., Roger V.L., Benjamin E.J., Berry J.D., Blaha M.J., Dai S., Ford E.S., Fox C.S., Franco S., Fullerton H.J., Gillespie C., Hailpern S.M., Heit J.A., Howard V.J., Huffman M.D., Judd S.E., Kissela B.M., Kittner S.J., Lackland D.T., Lichtman J.H., Lisabeth L.D., Mackey R.H., Magif D.J., Marcus G.M., Marelli A., Matchar D.B., McGuire D.K., Mohler E.R., Moy C.S., Mussolino M.S., Neumar R.W., Nicol G., Pandey D.K., Paynter N.P., Reeves M.J., Sorlie P.D., Stein J., Towfighi A., Turan T.N., Virani S.S., Wong N.D., Woo D., Turner M.B.: Heart Disease and Stroke Statistics—2014 Update A Report From the American Heart Association. *Circulation* 129:e28-e292, 2013.
5. Centre for Disease Control and Prevention: National Centre for Health Statistics. (2014, May 14). Inpatient Surgery. Retrieved 2015, January 29 from http://www.cdc.gov/nchs/fastats/inpatient-surgery.htm
6. 2004 Annual Report of the U.S. Organ Procurement and Transplantation Network and the Scientific Registry of Transplant Recipients: Transplant Data 1994-2003. Department of Health and Human Services, Health Resources and Services Administration, Healthcare Systems Bureau, Division of Transplantation, Rockville, MD; United Network for Organ Sharing, Richmond, VA; University Renal Research and Education Association, Ann Arbor, MI.
7. Moore K.L., Dalley A.F., Agur A.M.R. (7th Edition): *Clinically Oriented Anatomy*. Toronto, Canada, Wolters Kluwel Health/Lippincott Williams & Wilkins, 2013.
8. Goldberg D.J.: *About Hypoplastic Left Heart Syndrome (HLHS)*. Retrieved from http://www.chop.edu. (2013, September 1).

9. Hall J. (12th Edition): *Guyton and Hall Textbook of Medical Physiology*. Philadelphia, PA, Saunders/Elsevier, 2011.
10. Anderson R.M. (2nd Edition): *The Gross Physiology of the Cardiovascular System*. Tuscon, AZ, Racquet Press, 2012.
11. Betts J.G., DeSaiz P., Johnson E., Johnson J.E., Korol O., Kruse D.H., Poe B., Wise J.A., Womble M., Young K.A.: *Anatomy and Physiology*. Houston, TX, OpenStax, 2013.
12. Pocock G., Richards C.D., Richards D.A. (4th Edition): *Human Physiology (Oxford Core Texts).* Oxford, Oxford University Press, 2013.
13. Levine J., Miller K.R.: *Biology*. Upper Saddle River, NJ, Pearson Prentice Hall, 2002.
14. Carreño J.E., Apablaza F., Ocaranza M.P., Jalil J.E.: Cardiac Hypertrophy: Molecular and Cellular Events. *Rev Esp Cardiol* 59(5):473-86, 2006.
15. Saladin K.(4th Edition): *Anatomy and Physiology: The Unity of Form and Function.* McGraw-Hill, 2006.
16. Hall A.C., Guyton J.E. (11th Edition). *Textbook of Medical Physiology.* Philadelphia, W.B. Saunders, 2005.
17. Robertson I., Sun Y.B., Li M.X., Sykes B.D.: A structural and functional perspective into the mechanism of Ca^{2+}-sensitizers that target the cardiac troponin complex. *Journal of Molecular and Cellular Cardiology* 49(6):1031–1041, 2010.
18. Hoffman J.L., Kaplan S.: The incidence of congenital heart disease. *J Am Coll Cardiol* 39(12):1890-1900, 2002.
19. Oster M., Lee K., Honein M., Colarusso T., Shin M., Correa A.: Temporal trends in survival for infants with critical congenital heart defects. *Pediatrics* 131(5):e1502-8, 2013.
20. Botto L.D., Correa A., Erickson D.: Racial and temporal variations in the prevalence of heart defects. *Pediatrics, 107*(3):e32, 2001.
21. Oyen N., Poulsen G., Boyd H.A., Wohlfahrt J., Jensen P.K.A., Melbye M.: Recurrence of congenital heart defects in families. *Circulation* 120:295-301, 2009.

22. Miller A., Riehle-Colarusso T., Alverson C.J., Frias J.L., Correa A.: Congenital heart defects and major structural noncardiac anomalies, Atlanta, Georgia, 1968-2005.*J Pediatr* 159:70-8, 2011.
23. Boulet S.L., Grosse S.D., Riehle-Colarusso T., Correa-Villasenor A.: Health Care Costs of Congenital Heart Defects, in Wyszynski DF, Correa-Villasenor A., Graham T.P., *Congenital Heart Defects: From Origin to Treatment,* New York, Oxford University Press Inc., 2010, pp.493-501.
24. Gordon B.M., Rodriguez S., Lee M., Chang R.K.: Decreasing number of deaths of infants with hypoplastic left heart syndrome. *J Pediatr* 153:354-8, 2008.
25. Norwood W.I. Jr.: Hypoplastic left heart syndrome. *Ann Thorac Surg* 52(3):688-95, 1991.
26. Freedom R.M., Williams W.G., Dische M.R., Rowe R.D.: Anatomical variants in aortic atresia. Potential candidates for ventriculoaortic reconstitution. *Br Heart J* 38(8):821-6, 1976.
27. Fyler D.C.: Report of the New England Regional Infant Cardiac Program. *Pediatrics* 65(2 Pt 2):375-461, 1980.
28. Rao P.S., Striepe V., Merrill W.H.: *Hypoplastic left heart syndrome. Cardiac Anesthesia for Infants and Children*. St. Louis, MO, CV Mosby, 1994.
29. Rudolph A.M.: *Congenital Diseases of the Heart*. Chicago, Year Book Medical, 1974.
30. Ohye R.G., Sleeper L.A., Mahony L., Newburger J.W., Pearson G.D., Lu M.: Comparison of shunt types in the Norwood procedure for single-ventricle lesions. *N Engl J Med* 362(21):1980-92, 2010.
31. Hornik C.P., He X., Jacobs J.P., Jaquiss R.D.B., Jacobs M.L., O'Brien S.M., Peterson E.D., Pasquali S.K.: Complications after the Norwood operation: an analysis of The Society of Thoracic Surgeons Congenital Heart Surgery Database. *Ann Thorac Surg* 92(5):1734-40, 2011.
32. Rao P.S., Turner D.R., Forbes T.J.: Pediatric Hypoplastic Left Heart Syndrome. *Medscape*. Retrieved 3/22/2013 from http://emedicine.medscape.com/article/890196-overview#a0199.
33. Dar A., Shachar M., Leor J., Cohen S.: Optimization of Cardiac Cell Seeding and Distribution in 3D Porous Alginate Scaffolds. *Biotechnol Bioeng* 80(3): 305-312, 2002.

34. Li R.K., Yau T.M., Weisel R.D., Mickle D.A.G., Sakai T., Choi A., Jia Z.Q.: Construction of a bioengineered cardiac graft. *J Thorac Cardiovasc Surg* 19:368-375, 2000.
35. Eschenhagen T., Fink C., Remmers U., Scholz H., Wattchow J., Weil J., Zimmerman W.H., Dohmen H.H., Schäfer H., Bishopric N., Wakatsuki T., Elson E.L.: Three-dimensional reconstitution of embryonic cardiomyocytes in a collagen matrix: A new heart muscle model system. *FASEB J* 11:683, 1997.
36. Zimmerman W.H., Schneiderbanger K., Schubert P., Didié M., Münzel F., Heubach J.F., Kostin S., Neuhuber W.L., Eschenhagen T.: Tissue engineering of a differentiated cardiac muscle construct. *Circ Res* 90:223-230, 2002.
37. Shimizu T., Yamato M., Isoi Y., Akutsu T., Setomaru T., Abe K., Kikuchi A., Umezu M., Okano T.: Fabrication of pulsatile cardiac tissue grafts using a novel 3-dimensional cell sheet manipulation technique and temperature-responsive cell culture surfaces. *Circ Res* 90(3):e40, 2002.
38. Ott H.C., Matthiesen T.S., Goh S-K., Black L.D., Kren S.M., Netoff T.I., Taylor D.A.: Perfusion-decellularized matrix: using nature's platform to engineer a bioartificial heart. *Nature Medicine* 14:213-221, 2008.
39. Patel N.M., Tao Z-W., Mohamed M.A., Hogan M.K., Gutierrez L., Birla R.K.: Engineering 3D Bio-artificial heart muscle: The Acellular Ventricular Extracellular Matrix Model. *ASAIO Journal* 61:61-70, 2015.
40. Lee E.J., Kim D.E., Azeloglu E.U., Costa K.: Engineered Cardiac Organoid Chambers: Toward a Functional Biological Model Ventricle. *Tissue Engineering Part A* 14(2):215-225, 2008.
41. Zimmerman W-H., Cesnjevar R.: Cardiac Tissue Engineering: Implications for Pediatric Heart Surgery. *Pediatr Cardiol* 30:716-723, 2009.
42. Bursac N., Papadaki M., Cohen R.J., Schoen F.J., Eisenberg S.R., Carrier R., Vunjak-Novakovic G., Freed L.E.: Cardiac muscle tissue engineering: toward an in vitro model for electrophysioligical studies. *Am J Physiol* 27:H433-H444, 1999.

43. Carrier R.L., Papdaki M., Rupnick M., Schoen F.J., Bursac N., Langer R., Freed L.E., Vunjak-Novakovic G.: Cardiac tissue engineering: cell seeding, cultivation parameters and tissue construct characterization. *Biotechnol Bioeng* 64:580-589, 1999.
44. Engelmayr G.C., Cheng M., Bettinger C.J., Borenstein J.T., Langer R., Freed L.E.: Accordion-like honeycombs for tissue engineering of cardiac anisotropy. *Nat Mater* 7:1003-1010, 2008.
45. Leor J., Aboulafia-Etzion S., Dar A., Shapiro L., Barbash I.M., Battler A., Granot Y., Cohen S.: Bioengineered cardiac-grafts a new approach to repair the infarcted myocardium? *Circulation* 102:III56–IIII61, 2000.
46. Radisic M., Park H., Shing H., Consi T., Schoen F.J., Langer R., Freed L.E., Vunjak-Novakovic G.: Functional assembly of engineered myocardium by electrical stimulation of cardiacmyocytes cultured on scaffolds. *Proc Natl Acad Sci USA* 101:18129–18134, 2004.
47. Blan N.R., Birla R.K.: Design and Fabrication of heart muscle using scaffold-based tissue engineering. *J Biomed Mater Res A* 86(1):195-208, 2007.
48. Naito H., Melnychenko I., Didie M., Schneiderbanger K., Schubert P., Rosenkranz S., Eschenhagen T., Zimmermann W-H.: Optimizing engineered heart tissue for therapeutic applications as surrogate heart muscle. *Circulation* 114:I72–I78, 2006.
49. Zimmerman W-H., Fink C., Kralisch D., Remmers U., Weil J., Eschenhagen T.: Three-dimensional engineered heart tissue from neonatal rat cardiac myocytes. *Biotechnol Bioeng* 68:106–114, 2000.
50. Huang Y.C., Khait L., Birla R.K.: Contractile three-dimensional bioengineered heart muscle for myocardial regeneration. *J Biomed Mater Res A* 80:719–731, 2007.
51. Okano T., Yamada N., Okuhara M., Sakai H., Sakurai Y.: Mechanism of cell detachment from temperature-modulated, hydrophilic-hydrophobic polymer surfaces. *Biomaterials* 16:297–303, 1995.
52. Baig M.K., McKenna W.J., Caforio A.L.P., Bonow R.O., Francis G.S., Gheorghiade M.: The pathophysiology of advanced heart failure. *Am Heart J* 135:S216-S230, 1998.

53. Packer M.: The impossible task of developing a new treatment for heart failure. *J Card Fail* 8: 193-196, 2002.
54. Jacobsen G.M., Easter M.D.: Allograft vs. Xenograft: Practical Considerations for Biologic Scaffolds. Musculoskeletal Transplant Foundation, 2008.
55. Eitan Y.P., Sarig U., Dahan N., Macluf M.: Acellular Cardiac Extracellular Matrix as a Scaffold for Tissue Engineering: In Vitro Cell Support, Remodeling and Biocompatibility. *Tissue Engineering: Part C* 16: 671-683, 2010.
56. Potpova I., Doronin S.V., Kelly D.J., Rosen A.B., Schuldt A.J.T., Lu Z., Kochapura P.V., Robinson R.B., Rosen M.R., Brink P.R., Gaudette G.R., Cohen S.: Enhanced Recovery of mechanical function in the canine heart by seeding an extracellular matrix patch with mesnchymal stem cells committed to a cardiac lineage. *Am J Physiol Heart Circ Physiol* 295: H2257-H2263, 2008.
57. Godier-Furnemont A., Martensm T.P., Koeckert M.S., Wan L., Parks J., Arai K., Zhang G., Hudson B., Homma S., Vunjak-Novakovic G.: Composite scaffold provides a cell delivery platform for cardiovascular repair. *PNAS* 108: 7974-7979, 2011.
58. Malchesky P.S.: Artificial Organs 2005: A Year in Review. *Artif Organs* 30: 192–207, 2006.
59. Vara D.S., Kannan R.Y., Bordenave L., Hamilton G., Seifalian A.M.: Cardiovascular tissue engineering: state of the art. *Pathol Biol (Paris)* 53: 599-612, 2005.
60. Soonpaa G.K., Klug M.G., Field L.J.: Formation of nascent intercalated disks between grafted fetal cardiomyocytes and host myocardium. *Science* 264: 98–101, 1994.
61. Jen W.M., Mikos A.G.: Review: Hydrogels for cell immobilization. *Biotechnol Bioeng* 50: 357-64, 1996.
62. Shapiro L.: Novel alginatesponges for cell culture and transplantation. *Biomaterials* 18: 583–590, 1997.
63. Zimmermann W.H., Melnychenko I., Wasmeier G., Didie M., Naito H., Nixdorff U., Hess A., Budinsky L., Brune K., Michaelis B., Dhein S., Schwoerer A., Ehmke H., Eschenhagen T.: Engineered heart tissue grafts improve systolic and diastolic function in infarcted rat hearts. *Nat Med* 12: 452–458, 2006.

64. Gilbert T., Sellaro T.L., Badylak S.F.: Decellulurization of tissues and organs. *Biomaterials* 29: 3675-83, 2006.
65. Kiriazis H.: Effects of aging on the work output and efficiency of rat papillary muscle. *Cardiovasc Res* 48: 111-119, 2000.
66. Mulieri L.A., Leavitt B., Allen P.D., Alpert N.R.: Altered myocardial force-frequency relation in human heart failure. *Circulation* 85: 1743-1750, 1992.
67. Hawkins J.A., Doty D.B.: Aortic atresia: morphologic characteristics affecting survival and operative palliation. *J Thorac Cardiovasc Surg* 88:620-626, 1984.
68. Farrell P.E., Chang A.C., Murdison K.A., Baffa J.M., Norwood W.I., Murphy J.D.: Hypoplastic left heart syndrome. Outcome after initial reconstruction and before modified Fontan procedure. *Circulation* 82: IV 199-207, 1990.
69. Barron D.J., Kilby M.D., Davies B., Wright J.G.C., Jones T.J., Brawn W.J.: Hypoplastic Left Heart Syndrome. *Lancet* 374:551-564, 2009.
70. Aranaz I., Mengíbar M., Harris R., Paños I., Miralles B., Acosta N., Galed G., Heras A.: Functional Characterization of Chitin and Chitosan. *Current Chemical Biology* 3: 203-230, 2009.
71. Solinger R., Elbl F., Minhas K.: Echocardiography in the Normal Neonate. *Circulation* 47:108-118, 1973.
72. Madihally S.V., Matthew H.W.: Porous chitosan scaffolds for tissue engineering. *Biomaterials* 1920: 1133-1142, 1999.
73. Silva S.S., Motta A., Rodrigues M.T., Pinheiro A.F.M., Gomes M.E., Mano J.F., Reis R.L., Migliaresi C.: Novel Genipin-Cross-Linked Chitosan/Silk Fibroin Sponges for Cartilage Engineering Strategies. *Biomacromolecules* 9:2764-2774, 2008.
74. Pflanzer R., McMullen W.: Physiology Lessons for use with the Biopac Student Lab. Biopac Systems Inc. Online. Available from URL: http://www.lavc.edu/kovnatgd/TEC/Electrocardiography%20I.pdf
75. Beinfield W.H., Lehr D.: QRS-T variations in the rat electrocardiogram. *Am J Physiol* 214(1):197-204, 1968.

76. Sobotka P.A., Maver J.H., Bauernfeind R.A., Kanakis C. Jr, Rosen K.M.: Arrhythmias documented by 24-hour continuous ambulatory electrocardiographic monitoring in young women without apparent heart disease. *Am Heart J* 101:753-9, 1981.
77. Hiss R.G., Lamb L.E., Allen M.: Electrocardiographic findings in 67375 asymptomatic subjects: X. Normal Values. *Am J Cardiol* 6: 200, 1960.
78. Spodick D.H.: Differential characteristics of the electrocardiogram in early repolarization and acute pericarditis. *N Engl J Med* 295: 523-7, 1976.
79. Villalona G.A., Udelsman B., Duncan D.R., McGillicuddy E., Sawh-Martinez R.F., Hibino N., Painter C., Mirensky T., Erickson B., Shinoka T., Breuer C.K.: Cell-Seeding Techniques in Vascular Tissue Engineering. *Tissue Eng Part B* 16(3): 341-350, 2010.
80. Papadaki M., Bursac N., Langer R., Merok J., Vunjak-Novakovic G., Freed L.E.: Tissue engineering of functional cardiac muscle: molecular, structural, and electrophysiological studies. *Am J Physiol Heart Circ Physiol* 280(1):H168-78, 2001.
81. Mo X.M., Xu C.Y., Kotaki M., Ramakrishna S.: Electrospun P(LLA-CL) nanofiber: a biomimetic extracellular matrix for smooth muscle cell and endothelial cell proliferation. *Biomaterials* 25(10):1883-90, 2004.
82. Pawlowski K.J., Rittgers S.E., Schmidt S.P., Bowlin G.: Endothelial cell seeding of polymeric vascular grafts. *Front. Biosci* 9:1412-21, 2004.
83. Akins R.E., Boyce R.A., Madonna M.L., Schroedl N.A., Gonda S.R., McLaughlin T.A., Hartzell C.R.: Cardiac organogenesis in vitro: reestablishment of three-dimensional tissue architecture by dissociated neonatal rat ventricular cells. *Tissue Eng* 5(2):103-18, 1999.
84. Sekiya S., Shimizu T., Yamato M., Kikuchi A., Okano T.: Bioengineered cardiac cell sheet grafts have intrinsic angiogenic potential. *Biochem Biophys Res Commun* 341(2):573-82, 2006.
85. Yost M.J., Baicu C.F., Stonerock C.E., Goodwin R.L., Price R.L., Davis J.M., Evans H., Watson P.D., Gore C.M., Sweet J., Creech L., Zile M.R., Terracio L.: A novel tubular scaffold for cardiovascular tissue engineering. *Tissue Eng* 10(1-2):273-84, 2004.

86. Hogan M., Mohamed M.A., Tao Z-W., Gutierrez L., Birla R.: Establishing the Framework to Support Bioartificial Heart Fabrication Using Fibrin-Based Three-Dimensional Artificial Heart Muscle. *Artif Organs* 39(2):165-71, 2015.
87. Shimizu K., Ito A., Arinobe M., Murase Y., Iwata Y., Narita Y., Kagami H., Ueda M., Honda H.: Effective cell-seeding technique using magnetite nanoparticles and magnetic force onto decellularized blood vessels for vascular tissue engineering. *J Biosci Bioeng* 103(5):472-8, 2007.
88. Bowlin G.L., Meyer A., Fields C., Cassano A., Makhoul R.G., Allen C., Rittgers S.E.: The persistence of electrostatically seeded endothelial cells lining a small diameter expanded polytetrafluoroethylene vascular graft. *J Biomater Appl* 16(2):157-73, 2001.
89. Carrier R.L., Rupnick M., Langer R., Schoen F.J., Freed L.E., Vunjak-Novakovic G.: Perfusion improves tissue architecture of engineered cardiac muscle. *Tissue Eng* 8(2):175-88, 2002.
90. Radisic M., Euloth M., Yang L., Langer R., Freed L.E., Vunjak-Novakovic G.: High-density seeding of myocyte cells for cardiac tissue engineering. *Biotechnol Bioeng* 82(4):403-14, 2003.
91. Radisic M., Deen W., Langer R., Vunjak-Novakovic G.: Mathematical model of oxygen distribution in engineered cardiac tissue with parallel channel array perfused with culture medium containing oxygen carriers. *Am J Physiol Heart Circ Physiol* 288(3):H1278-89, 2005.
92. Tao Z-W., Mohamed M.A., Hogan M., Gutierrez L., Birla R.K.: Optimizing a spontaneously contracting heart tissue patch with rat neonatal cardiac cells on fibrin gel. *J Tissue Eng Regen Med*, 2014, doi: 10.1002/term.1895.
93. Freed L.E., Guilak F., Guo X.E., Gray M.L., Tranquillo R., Holmes J.W., Radisic M., Sefton M.V., Kaplan D., Vunjak-Novakovic G.: Advanced tools for tissue engineering: scaffolds, bioreactors and signalling. *Tissue Eng* 12(12):3285-305, 2006.
94. Buschmann M.D., Gluzband Y.A., Grodzinsky A.J., and Hunziker E.B.: Mechanical compression modulates matrix biosynthesis in chondrocyte/agarose culture. *J Cell Sci* 108:1497, 1995.

95. Mauck R.L., Soltz M.A., Wang C.C.B., Wong D.D., Chao P.G., Valhmu W.B., Hung C.T., Ateshian G.A.: Functional tissue engineering of articular cartilage through dynamic loading of chondrocyte-seeded agarose gels. *J Biomech Eng* 122:252, 2000.

96. Seidel J.O., Pei M., Gray M.L., Langer R., Freed L.E., Vunjak-Novakovic G.: Long-term culture of tissue engineered cartilage in a perfused chamber with mechanical stimulation. *Biorheology* 41:445, 2004.

97. Kim B.S., Nikolovski J., Bonadio J., Mooney D.J.: Cyclic mechanical strain regulates the development of engineered smooth muscle tissue. *Nat Biotechnol* 17: 979, 1999.

98. Fink C., Ergun S., Kralisch D., Remmers U., Weil J., Eschenhagen T.: Chronic stretch of engineered heart tissue induces hypertrophy and functional improvement. *FASEB J* 14:669, 2000.

99. Akhyari P., Fedak P.W.M., Weisel R.D., Lee T.Y.J., Verma S., Mickle D.A.G., Li R.K.: Mechanical stretch regimen enhances the formation of bioengineered autologous cardiac muscle grafts. *Circulation* 106:I137, 2002.

100. Niklason L.E., Gao J., Abbott W.M., Hirschi K.K., Houser S., Marini R., Langer R.: Functional arteries grown in vitro. *Science* 284:489, 1999.

101. Krogmann O.N., Rammos S., Jakob M., Corin W.J., Hess O.M., Bourgeois M.: Left Ventricular Diastolic Dysfunction Late After Coarctation Repairin Childhood: Influence of Left Ventricular Hypertrophy. *J Am Coll Cardiol* 21(6):1454-60, 1993.

102. Fletcher P.J., Pfeffer J.M., Pfeffer M.A., Braunwald E.: Left ventricular Diastolic Pressure-Volume Relations in Rats with Healed Myocardial Infarction. *Circ Res* 49(3):618-26, 1981.

103. Liu C.W., Hwang B., Lee B.C., Lu J.H., Meng L.C.; Aortic stenosis in children: 19-year experience. *Zhonghua Yi Xue Za Zhi* (Taipei) 59:107, 1997.

104. Yetman A.T., Rosenberg H.C., Joubert G.I.: Progression of asymptomatic aortic stenosis identified in the neonatal period. *Am J Cardiol* 75(8):636-7, 1995.

105. Egito E.S., Moore P., O'Sullivan J., Colan S., Perry S.B., Lock J.E., Keane J.F.: Transvascular balloon dilation for neonatal critical aortic stenosis: early and midterm results. *J Am Coll Cardiol* 29(2):442-7, 1997.

106. Hoffman J.I.E., Kaplan S., Liberthson R.R.: Prevalence of congenital heart disease. *Am Heart J* 147:425-439, 2004.

107. Grayson A.C., Voskerician G., Lynn A., Anderson J.M., Cima M.J., Langer R.: Differential degradation rates in vivo and in vitro of biocompatible poly(lactic acid) and poly(glycolic acid) homo- and co-polymers for a polymeric drug-deliverymicrochip. *J Biomater Sci Polym Ed* 15:1281–1304, 2004.

108. Albanna M.Z., Bou-Akl T.H., Walters H.L., Matthew H.W.: Improving the mechanical properties of chitosan-based heart valve scaffolds using chitosan fibers. *J Mech Behav Biomed Mater* 5(1):171-80, 2012.

109. Lendlein A., Langer R.: Biodegradable, elastic shape memory polymers for potential biomedical applications. *Science* 296:1673–1676, 2002.

110. Lahann J., Mitragotri S., Tran T.N., Kaido H., Sundaram J., Choi I.S., Hoffer S., Somorjai G.A., Langer R.: A reversibly switching surface. *Science* 299:371–374, 2003.

111. Lutolf M.P., Hubbell J.A.: Synthetic biomaterials as instructive extracellular microenvironments for morphogenesis in tissue engineering. *Nat. Biotechnol* 23:47–55, 2005.

112. Mann B.K., Gobin A.S., Tsai A.T., Schmedlen R.H., West J.L.: Smooth muscle cell growth in photopolymerized hydrogels with cell adhesive and proteolytically degradable domains: synthetic ECM analogs for tissue engineering. *Biomaterials* 22:3045–3051, 2001.

113. Shi Y., Ramamurthi A., Vesely I.: Towards tissue engineering of a composite aortic valve. *Biomed Sci Instrum.* 38:35–40, 2002.

114. Tranquillo R., Girton T., Neidert M.: Tissue Equivalent Approach to a Tissue Engineered Cardiovascular Valve. Minneapolis, Regents of the University of Minnesota, 2003.

115. Ross J.J., Tranquillo R.T.: ECM gene expression correlates with in vitro tissue growth and development in fibrin gel remodeled by neonatal smooth muscle cells. *Matrix Biol* 22:477–490, 2003.

116. Ye Q., Zund G., Benedikt P., Jockenhoevel S., Hoerstrup S.P., Sakyama S., Hubbell J.A., Turina M.: Fibrin gel as a three dimensional matrix in cardiovascular tissue engineering. *Eur J Cardiothorac Surg* 17:587–591, 2000.

117. Ramamurthi A., Vesely I.: Evaluation of the matrix synthesis potential of crosslinked hyaluronan gels for tissue engineering of aortic heart valves. *Biomaterials* 26:999–1010, 2005.

118. Robinson K.A., Li J., Mathison M., Redkar A., Cui J., Chronos N.A., Matheny R.G., Badylak S.F.: Extracellular matrix scaffold for cardiac repair. *Circulation* 112:I135–I143, 2005.

119. Hoerstrup S.P., Sodian R., Daebritz S., Wang J., Bacha E.A., Martin D.P., Moran A.P., Guleserian K.J., Sperling J.S., Kaushal S., Vacanti J.P., Schoen F.J., Mayer J.E.: Functional living trileaflet heart valves grown *in vitro*. *Circulation* 102:SIII-44–SIII-49, 2000.

120. Sutherland F.W.H., Perry T.E., Yu Y., Sherwood M.C., Rabkin E., Masuda Y., Garcia G.A., McLellan D.L., Engelmayr G.C., Sacks M.S., Schoen F.J., Mayer J.E.: From stem cells to viable autologous semilunar heart valves. *Circulation* 111:2783–2791, 2005.

121. Konertz W., Dohmen P.M., Liu J., Beholz S., Dushe S., Posner S., Lembcke A., Erdbrugger W.: Hemodynamic characteristics of the Matrix P decellularized xenograft for pulmonary valve replacement during the Ross operation. *J Heart Valve Dis* 14:78–81, 2005.

122. Mendelson K., Shoen F.J.: Heart Valve Tissue Engineering: Concepts, Approaches, Progress and Challenges. *Ann Biomed Eng* 34(12):1799-1819, 2006.

123. Poutanen T., Tikanoja T., Sairanen H., Jokinen E.: Normal Mitral and Aortic Valve Areas Assessed by Three- and Two-Dimensional Echocardiography in 168 Children and Young Adults. *Pediatr Cardiol* 27:217-225, 2006.